Improving the Foundation Layers for Concrete Pavements

TECHNICAL REPORT:

Pavement Foundation Layer Reconstruction – Pennsylvania US 22 Field Study

June 2016

National Concrete Pavement Technology Center

CP Tech Center

CENTER FOR

CEER

EARTHWORKS ENGINEERING RESEARCH

IOWA STATE UNIVERSITY
Institute for Transportation

About the National CP Tech Center

The mission of the National Concrete Pavement Technology (CP Tech) Center is to unite key transportation stakeholders around the central goal of advancing concrete pavement technology through research, tech transfer, and technology implementation.

About CEER

The mission of the Center for Earthworks Engineering Research (CEER) at Iowa State University is to be the nation's premier institution for developing fundamental knowledge of earth mechanics, and creating innovative technologies, sensors, and systems to enable rapid, high quality, environmentally friendly, and economical construction of roadways, aviation runways, railroad embankments, dams, structural foundations, fortifications constructed from earth materials, and related geotechnical applications.

Disclaimer Notice

Iowa State University Non-Discrimination Statement

Iowa Department of Transportation Statements

Technical Report Documentation Page

1. Report No. DTFH 61-06-H-00011 Work Plan 18	2. Government Accession No.	3. Recipient's Catalog No.	
4. Title and Subtitle Improving the Foundation Layers for Concrete Pavements: Pavement Foundation Layer Reconstruction – Pennsylvania US 22 Field Study		**5. Report Date** June 2016	
		6. Performing Organization Code	
7. Author(s) David J. White, Pavana Vennapusa, Jia Li, Alexander Wolfe, Caleb Douglas		**8. Performing Organization Report No.** InTrans Project 09-352	
9. Performing Organization Name and Address National Concrete Pavement Technology Center and Center for Earthworks Engineering Research (CEER) Iowa State University 2711 South Loop Drive, Suite 4700 Ames, IA 50010-8664		**10. Work Unit No. (TRAIS)**	
		11. Contract or Grant No.	
12. Sponsoring Organization Name and Address Federal Highway Administration U.S. Department of Transportation 1200 New Jersey Avenue SE Washington, DC 20590		**13. Type of Report and Period Covered** Technical Report	
		14. Sponsoring Agency Code TPF-5(183)	
15. Supplementary Notes Visit www.cptechcenter.org or www.ceer.iastate.edu for color PDF files of this and other research reports.			

16. Abstract

This report is one of the field project reports developed as part of the TPF-5(183) and FHWA DTFH 61-06-H-00011:WO18 studies.

The project involved constructing a minimum 457.2 mm thick rock cap over general subgrade fill material as subgrade treatment with geosynthetic separation layer at the interface, a 50.8 mm thick class 2A leveling stone subbase, and a minimum 76.2 mm thick cement or asphalt treated base (CTB or ATB), and a 254 mm thick portland cement concrete (PCC) pavement. Field testing was conducted on three test beds with the leveling subbase layer at the surface, and one test bed each with PCC, ATB/CTB, rock cap, and general subgrade fill material at the testing surface. In situ test methods including nuclear gauge, light weight deflectometer, falling weight deflectometer, dynamic cone penetration, air permeability testing, and intelligent compaction monitoring with 100% coverage, were used. Point testing was conducted by spacing the test measurements about 50 to 100 m apart to capture the variability along the road alignment. The length of the test beds varied between 15 m to 620 m. Testing was conducted along the center line and along left and right of the center line with test point spacing of about 5 to 10 m. In addition, dense grid testing with test spacing between 1 and 4 m was also conducted to capture spatial variability of the measurement values over a small area. Geostatistical semivariogram analysis was performed to analyze the point test data from dense grid pattern testing to characterize and quantify spatial non-uniformity of the PCC surface and foundation layer properties. In situ test results were analyzed and compared with the design assumed modulus and drainage coefficient values. Results indicated that the subgrade layer modulus (E_{SG}) determined on the rock cap layer was on average lower in two test beds and higher in one test bed. The reason for lower E_{SG} values in the two test beds is attributed to a likely weaker underlying general fill subgrade layer. The average subbase layer modulus (E_{SB}) determined for the ATB/CTB layers were higher than the design assumed values. The drainage coefficient values were calculated based on the saturated hydraulic conductivity values measured using the air permeability test device, and the pavement geometry, which showed "good" to "excellent" drainage.

17. Key Words concrete pavement—pavement foundation—quality assurance—quality control— cement treated base—asphalt treated base—subbase—subgrade		18. Distribution Statement No restrictions.	
19. Security Classification (of this report) Unclassified.	**20. Security Classification (of this page)** Unclassified.	**21. No. of Pages** 115	**22. Price** NA

Form DOT F 1700.7 (8-72)   **Reproduction of completed page authorized**

IMPROVING THE FOUNDATION LAYERS FOR CONCRETE PAVEMENTS: PAVEMENT FOUNDATION LAYER RECONSTRUCTION – PENNSYLVANIA US 22 FIELD STUDY

Technical Report
June 2016

Research Team Members
Tom Cackler, David J. White, Jeffrey R. Roesler, Barry Christopher, Andrew Dawson, Heath Gieselman, and Pavana Vennapusa

Report Authors
David J. White, Pavana K. R. Vennapusa,
Jia Li, Alexander J. Wolfe, Caleb Douglas
Iowa State University

**National Concrete Pavement Technology Center and
Center for Earthworks Engineering Research (CEER)**
Iowa State University
2711 South Loop Drive, Suite 4700
Ames, IA 50010-8664
Phone: 515-294-5768
www.cptechcenter.org and www.ceer.iastate.edu

TABLE OF CONTENTS

LIST OF FIGURES

LIST OF TABLES

ACKNOWLEDGMENTS

LIST OF ACRONYMS AND SYMBOLS

A′	Machine acceleration
AF	Area factor
APT	Air permeameter
$A_{2\Omega}$	Acceleration of the first harmonic component of the roller vibration
A_{Ω}	Acceleration of the fundamental component of the roller vibration
ATB	Asphalt treated base material
BCI	Base curvature index
BDI	Base damage index
CBR	California bearing ratio
C	Constant (300) for calculating CMV
C_d	Drainage coefficient
CMV	Compaction meter value
COV	Coefficient of variation
CTB	Cement treated base material
D_0	Deflection measured under the plate
D_1 to D_7	Deflections measured away from the plate at various set distances
D_{SB}	Subbase layer thickness
DCP	Dynamic cone penetration test
DCP-CBR	California bearing ratio calculated from dynamic cone penetration values
DPI	Dynamic penetration index
E	Elastic modulus
E_c	Modulus of elasticity of concrete
E_{sg}	Modulus of elasticity of subgrade
E_{FWD-K3}	Surface modulus determined using 300 mm diameter plate Kuab falling weight deflectometer
E_{LWD-Z2}	Elastic modulus determined from 200 mm diameter plate light weight deflectometer
E_s	Dynamic secant modulus
E_{SB}	Elastic modulus of the subbase
E_{SG}	Elastic modulus of the subgrade
F	Shape factor
FWD	Falling weight deflectometer
F/T	Freeze/thaw
g	Acceleration due to gravity
G_o	Geometric factor
IC	Intelligent compaction
k	Modulus of subgrade reaction
k_{comp}	Composite modulus of subgrade reaction
k_{eff}	Effective modulus of subgrade reaction
$k_{FWD-Dynamic}$	Dynamic modulus of subgrade reaction from FWD test
$k_{FWD-Static-Corr}$	Static modulus of subgrade reaction from FWD test
K_{sat}	Saturated hydraulic conductivity determined using rapid gas permeameter test device
I	Intercept value

J	Load transfer coefficient
L	Radius of relative stiffness
LL	Liquid limit
LI	Plasticity index
LTE	Load transfer efficiency
LS	Loss of support
LWD	Light weight deflectometer
m and b	Machine internal loss coefficients specific to a particular machine
MDP	Machine drive power
MET	Method of equivalent thickness
M_r	Resilient modulus
MV	Measurement value
NG	Nuclear gauge
$P_{o(g)}$	Gauge pressure of the gas at the orifice outlet
P_1	Absolute gas pressure on the soil surface
P_2	Pressure app
P_g	Gross power needed to move the IC machine
PID	Proportional-integral-derivative controller
PL	Plastic limit
R^2	Coefficeint of determination
Q	Volumetric flow rate
r	Plate radius (LWD test)
r	Radius at the outlet (for APT test)
RTK-GPS	Real-time kinematic global positioning system
S_c	PCC modulus of rupture
S	Water saturation
S_e	Effective water saturation
S_r	Residual water saturation
SCI	Surface curvature index
v	Roller velocity
W	Roller weight
α	Slope angle determined from roller pitch from a sensor
$\gamma(h)$	Plot of the average squared differences between data values as a function of separation distance
δ	Depth to impervious layer
γ_d	Dry unit weight determined from Humboldt nuclear gauge
λ	Brooks-Corey pore size distribution index
μ	Statistical mean or average
μ_{air}	Dynamic viscosity of air
μ_{water}	Absolute viscosity of water
η	Poisson's ratio
σ	Statistical standard deviation
σ_0	Applied stress
ρ	Density of water
w	Moisture content determined from Humboldt nuclear gauge
w_{opt}	Optimum moisture content

EXECUTIVE SUMMARY

Quality foundation layers (the natural subgrade, subbase, and embankment) are essential to achieving excellent pavement performance. Unfortunately, many pavements in the United States still fail due to inadequate foundation layers. To address this problem, a research project, Improving the Foundation Layers for Pavements (FHWA DTFH 61-06-H-00011 WO #18; FHWA TPF-5(183)), was undertaken by Iowa State University to identify, and provide guidance for implementing, best practices regarding foundation layer construction methods, material selection, in situ testing and evaluation, and performance-related designs and specifications. As part of the project, field studies were conducted on several in-service concrete pavements across the country that represented either premature failures or successful long-term pavements. A key aspect of each field study was to tie performance of the foundation layers to key engineering properties and pavement performance. In situ foundation layer performance data, as well as original construction data and maintenance/rehabilitation history data, were collected and geospatially and statistically analyzed to determine the effects of site-specific foundation layer construction methods, site evaluation, materials selection, design, treatments, and maintenance procedures on the performance of the foundation layers and of the related pavements. A technical report was prepared for each field study.

This report presents results and analysis from a field study conducted on SR-22 near Clyde in Indiana County, Pennsylvania. The project consisted of reconstruction of pavement foundation layers (subbase and subgrade) of the east and west bound lanes of the highway. The total length of the reconstruction project was about 7.74 km (4.81 miles).

The pavement foundation layers consisted of a minimum 457.2 mm (18 in.) thick rock cap that was placed and compacted on the subgrade and is referred to as subgrade treatment in the project plans. The subgrade beneath the rock cap consisted of general embankment fill consisted of rocky subgrade material obtained from cuts. A geosynthetic separation layer was installed at the subgrade rockcap interface. A 50.8 mm (2 in.) thick Class 2A levelling stone consisting of crushed limestone material was placed as granular leveling course layer over the rock cap. A minimum 76.2 mm (3 in.) thick asphalt treated base (ATB) or cement treated base (CTB) layer was installed over the granular subbase layer. A 254 mm (10 in.) thick new jointed PCC layer was installed over the CTB/ATB layer. The pavement section was designed in accordance with the *AASHTO design guide for design of pavement structures* (AASHTO 1993) rigid pavement design.

The Iowa State University (ISU) research team was present at the project site from July 27 to 29, 2009, during the construction process to conduct a field study on foundation layers and the newly constructed PCC surface layer. Field testing was conducted on seven test beds (TBs). Two test beds consisted of levelling stone subbase layer at the surface, and one test bed each consisted of PCC, CTB, ATB, rock cap layer, and general subgrade fill at the testing surface. Field testing involved falling weight deflectometer (FWD), Zorn and Dynatest light weight deflectometer (LWD), nuclear gauge (NG), dynamic cone penetrometer (DCP), and air permeability test (APT) point testing and intelligent compaction (IC) measurements. Laboratory testing was conducted on the materials collected from the field to characterize the index properties (i.e., gradation,

compaction, specific gravity, soil classification) and frost-heave and thaw-weakening susceptibility of the subgrade general fill materials.

The length of the test beds varied between 15 m to 620 m. Testing was conducted along the center line and along left and right of the center line with test point spacing of about 5 to 10 m. In addition, dense grid testing with test spacing between 1 and 4 m was also conducted to capture spatial variability of the measurement values over a small area. Geostatistical semivariogram analysis was performed to analyze the point test data from dense grid pattern testing to characterize and quantify spatial non-uniformity of the PCC surface and foundation layer properties.

Comparing measured properties from laboratory and in situ testing with the design assumed values revealed the following:

- Average subgrade layer moduli (E_{SG}) was determined based testing on the rock cap layer from three TBs. Average E_{SG} from TBs 1 and 2 from LWD and FWD testing was 71.5 MPa and 120.2 MPa, respectively, which were lower than the design assumed E_{SG} of 206.8 MPa. Average E_{SG} from TB 5 from LWD and FWD measurements were 303.4 and 407.2 MPa, which were higher than the design assumed E_{SG} of 206.8 MPa. Possible reasons for lower E_{SG} values in TBs 1 and 2 can be due to weaker general fill material, as evidenced in TB6 with average moduli of 18.1 MPa. It must be noted that LWD and FWD measurements provide a composite response of materials within its measurement influence depth ranging between 1.5 to 2 times the dimeter of the plate (450 to 600 mm depth).

- Average subbase layer moduli (E_{SB}) values for the CTB and ATB layers were 721 and 4,467 MPa, which are 3.5 to 21.6 times higher than the design assumed E_{SB} of 206.8 MPa. It must be noted that the ATB layer tested in this study was placed one day prior to testing, while the CTB layer was placed several months prior to testing. Additional curing of the ATB material can potentially increase the moduli values of the layer.

- For section with ATB, the composite modulus of subgrade reaction (k_{comp}) values ranged between 196.8 kPa/mm (based on LWD measurements for E_{SG}) and 282.3 kPa/mm (based on FWD measurements for E_{SG}) and were about 1.2 to 1.7 times lower than the design target k_{comp} of 340 kPa/mm. Again, it must be noted that additional curing of the ATB material can potentially increase the E_{SB} values and the resulting k_{comp} values.

- For section with CTB, the estimated k_{comp} value ranged between 252.4 kPa/mm (based on LWD measurements for E_{SG}) and 367.5 kPa/mm (based on FWD measurements for E_{SG}) and were about 1.3 times lower and 1.1 times higher than the design target k_{comp} of 340 kPa/mm.

- The drainage coefficient (C_d) value was assumed in the design as 1.0, which represents that the quality of drainage is rated as "good". Based on the pavement geometry (i.e.,

cross slope, width of the pavement, thickness of the base layer), the measured K_{sat} values from the field, and assuming an effective porosity = 0.3, the time for a target 90% drainage was calculated. Based on APT tests conducted on the CTB layer, the time for 90% drainage was estimated as 1.0 day for $K_{sat} = 0.2$ cm/s (CTB contaminated with fines) to < 1 hour for $K_{sat} = 7$ cm/s (CTB uncontaminated). Based on tests conducted on the ATB layer the time for 90% drainage was estimated < 1 hour for $K_{sat} = 4.6$ cm/s. Based on these estimates, the quality of drainage can be rated as "good" to "excellent" for the ATB and CTB layers and does meet the design requirements.

The findings from the field studies under the Improving the Foundation Layers for Concrete Pavements research project will be of significant interest to researchers, practitioners, and agencies dealing with design, construction, and maintenance of PCC pavements. The technical reports are included in Volume II (Appendices) of the *Final Report: Improving the Foundation Layers for Pavements*. Data from the field studies are used in analyses of performance parameters for pavement foundation layers in the *Mechanistic-Empirical Pavement Design Guide* (MEPDG) program. New knowledge gained from this project will be incorporated into the *Manual of Professional Practice for Design, Construction, Testing and Evaluation of Concrete Pavement Foundations* published in 2016.

CHAPTER 1. INTRODUCTION

This report presents results and analysis from a field study conducted on State Route 22 (SR-22) near Clyde in Indiana County, Pennsylvania. The project consisted of reconstruction of pavement foundation layers (subbase and subgrade) of the east and west bound lanes of the highway. The total length of the reconstruction project was about 7.74 km (4.81 miles).

The existing pavement consisted of bituminous pavement of varying depths along the project and was removed and undercut down to the desired subgrade elevation and in some areas fill was required to build up to the subgrade elevation. General embankment fill consisting of rocky subgrade material was used in the fill areas. A minimum 457.2 mm (18 in.) thick rock cap was placed and compacted on the subgrade and is referred to as subgrade treatment in the project plans. A geosynthetic separation layer was installed at the subgrade rockcap interface. A 50.8 mm (2 in.) thick Class 2A levelling stone consisting of crushed limestone material was placed as granular leveling course layer over the rock cap. A minimum 76.2 mm (3 in.) thick asphalt treated base (ATB) or cement treated base (CTB) layer was installed over the granular subbase layer. A 254 mm (10 in.) thick new jointed PCC layer was installed over the CTB/ATB layer. The pavement section was designed in accordance with the *AASHTO design guide for design of pavement structures* (AASHTO 1993) rigid pavement design.

The Iowa State University (ISU) research team was present at the project site from July 27 to 29, 2009, during the construction process to conduct a field study on foundation layers and the newly constructed PCC surface layer. Field testing involved: Kuab falling weight deflectometer (FWD) to determine elastic modulus and deflection basin parameters; Zorn and Dynatest light weight deflectometer (LWD) to determine elastic modulus; dynamic cone penetrometer (DCP) to estimate California bearing ratio values; Humboldt nuclear gauge (NG) to determine moisture and dry unit weight; rapid air permeameter test (APT) device to measure saturated hydraulic conductivity; and roller-integrated compaction monitoring or intelligent compaction (IC) measurements to obtain 100% coverage of compacted material properties. The spatial northing and easting of all test measurement locations were obtained using a real-time kinematic (RTK) global positioning system (GPS).

Laboratory testing was conducted on the materials collected from the field to characterize the index properties (i.e., gradation, compaction, specific gravity, soil classification) and frost-heave and thaw-weakening susceptibility of the subgrade general fill materials.

Field testing was conducted on seven test beds (TBs). TBs 1 and 2 consisted of class 2A levelling stone subbase placed over the rock cap subgrade treatment, TB3 consisted of ATB, TB4 consisted of CTB, TB5 consisted of rock cap subgrade treatment, TB6 consisted of general subgrade fill, and TB7 consisted of the newly constructed PCC layer at the surface. TB2 was located on SR259, which was also being reconstructed as part of this project, while all remaining TBs were located on SR22 mainline. Except TB3, all other TBs were located just east or west of SR259 near Clyde, PA. TB3 was located on an adjacent project site near Blairsville, PA and was tested to evaluate ATB material properties in comparison with the CTB layer properties.

The length of the test beds varied between 15 m to 620 m. Testing was conducted along the center line and along left and right of the center line with test point spacing of about 5 to 10 m. In addition, dense grid testing with test spacing between 1 and 4 m was also conducted to capture spatial variability of the measurement values over a small area. Geostatistical semivariogram analysis was performed to analyze the point test data from dense grid pattern testing to characterize and quantify spatial non-uniformity of the PCC surface and foundation layer properties.

This report contains six chapters. Chapter 2 provides background information about the project and photographs documenting the construction procedures; and AASHTO (1993) pavement design input parameters. Chapter 3 presents an overview of the laboratory and in situ testing methods followed in this project. Chapter 4 presents results from laboratory testing. Chapter 5 presents results from in situ testing and analysis and compares laboratory and in situ measured values with the design assumed values. Chapter 6 presents key findings and conclusions from the field study.

The findings from this report should be of significant interest to researchers, practitioners, and agencies who deal with design, construction, and maintenance aspects of PCC pavements. This project report is one of several field project reports developed as part of the TPF-5(183) and FHWA DTFH 61-06-H-00011:WO18 studies.

CHAPTER 2. PROJECT INFORMATION AND SPECIFICATIONS

This chapter presents brief background information on the project, photos taken of pavement foundation layer construction during ISU testing, and pavement thickness design parameter selection and assumptions during the design phase of the project.

Project Background

This project is located on SR-22 near Clyde in Indiana County, Pennsylvania, and consisted of reconstruction of pavement foundation layers (subbase and subgrade) of the east and west bound lanes of the highway between Sta. 311+00 and 577+00 (Section 494, Federal Project No. X104-204-L980). The total length of the reconstruction project was about 7.74 km (4.81 miles).

According to the project drawings, the existing pavement consisted of bituminous pavement of varying depths along the project and was removed and undercut down to the desired subgrade elevation and in some areas fill was required to build up to the subgrade elevation. General embankment fill consisting of rocky subgrade material was used in fill areas. A minimum 457.2 mm (18 in.) thick rock cap was placed and compacted on the subgrade and is referred to as subgrade treatment in the project plans. A geosynthetic separation layer was installed at the subgrade rockcap interface. A 50.8 mm (2 in.) thick Class 2A levelling stone consisting of crushed limestone material was placed as granular permeable subbase layer over the rock cap. A minimum 76.2 mm (3 in.) thick asphalt treated base (ATB) or cement treated base (CTB) layer was installed over the granular subbase layer. A 254 mm (10 in.) thick new jointed PCC layer was installed over the CTB/ATB layer. A cross-section profile of the new pavement section is provided in Figure 1.

Photographs documenting the material conditions of the subgrade, rock cap, and subbase layers during construction are shown in Figure 2 to Figure 8.
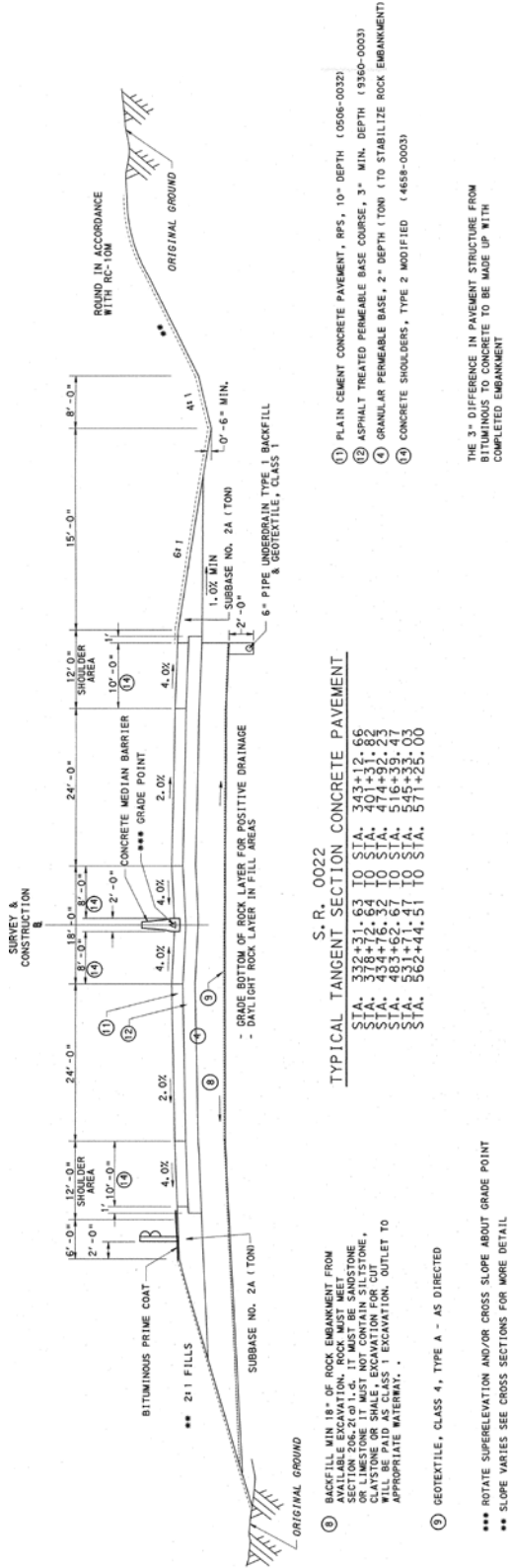
Figure 1. Cross-section profile of the new pavement surface and foundation layers at the SR22 project

Figure 2. Surface of general embankment fill

Figure 3. Surface of rock cap (subgrade treatment) layer

Figure 4. Rock cap material sampled for gradation analysis

Figure 5. Side view of embankment constructed with rock cap over general embankment fill and geosynthetic separation layer between the two layers

Figure 6. Surface of Class 2A leveling stone layer

Figure 7. Surface of ATB layer

Figure 8. Construction of CTB layer

Pavement Design Input Parameter Selection and Assumptions

The pavement design was performed by Penn DOT following the AASHTO (1993) rigid pavement design procedure. The assumptions used in the design are summarized in Table 1. A resilient modulus (M_r) of 206.8 MPa (30 ksi) was assumed for the rock cap layer (subgrade treatment). The subgrade M_r value was assumed to be the same for summer, fall, winter, and spring conditions. An elastic modulus value was assumed for the base layer (E_{SB}), i.e., the ATB layer that varied between 103.4 MPa (15 ksi) and 344.7 MPa (50 ksi) for spring and winter conditions. The assumed E_{SB} for summer and fall conditions was 206.8 MPa (30 ksi). The pavement design information provided by Penn DOT is included in the Appendix.

In the design, an effective modulus of subgrade reaction (k_{eff}) was calculated as 143 kPa/mm (526 pci). In AASHTO (1993) design procedure, the k_{eff} value is calculated from composite modulus of subgrade reaction (k_{comp}) and the anticipated future loss of support (LS) in the subbase layer due to any erosion. The LS is assumed in the design as 0.75. Based on the k_{eff} and LS value provided in the design, k_{comp} was calculated as 340 kPa/mm (1250 pci).

The calculated pavement layer thickness for a jointed PCC layer, based on the assumptions listed in Table 1 was about 251.7 mm (9.91 in.), which was rounded to 254 mm (10 in.).

The original design included ATB, but was reportedly changed to use of CTB on this project due to increase in cost of asphalt at the time of construction (Email communication with Mark Kmetz, PennDOT on 08/20/2009). An adjacent project on SR22 (near Blairsville) consisted of a

similar design and included ATB (Figure 7) and was selected for testing to compare with CTB layer properties measured during this field study.

Table 1. Summary of pavement thickness design input parameters and assumptions (AASHTO 1993 method)

Parameter	Value
General Assumptions	
ESALs over initial performance period	12,822,405
Design period	20 years
Surface Layer Design Assumptions	
Pavement Type	JPCP
Initial serviceability	4.5
Terminal serviceability	3.0
28-day Mean PCC modulus of rupture, S_c	631 psi
28-day Mean Modulus of Elasticity of Concrete, E_c	4,000,000 psi
Reliability level	95%
Overall standard deviation	0.35
Load transfer coefficient, J	2.7
Foundation Layer Design Assumptions*	
Subbase layer thickness, D_{SB}	3 inches minimum of Asphalt Treated Base (ATB)
Subbase elastic modulus, E_{SB}	Winter – E_{SB} = 50,000 psi Spring – E_{SB} = 15,000 psi Summer – E_{SB} = 30,000 psi Fall – E_{SB} = 30,000 psi
Mean Subgrade resilient modulus, M_r	30,000 psi (based on 18 inch rock cap for subgrade treatment, same value for summer, fall, winter, and spring)
Mean Composite modulus of subgrade reaction, k_{comp}	1250 pci (calculated from AASHTO 1993 based on k_{eff} and LS values assumed in design)
Loss of support (due to erosion), LS	0.75
Effective modulus of subgrade reaction, k_{eff} (accounting for LS)	526 pci
Overall drainage coefficient, C_d	1.0
Other	
Pavement Thickness Design	
Calculated design thickness	10 inches (9.91 round up to nearest half inch)

CHAPTER 3. EXPERIMENTAL TESTING METHODS

Experimental testing in this research study involved laboratory testing of foundation layer materials, in situ testing to evaluate the properties of the pavement surface and underlying foundation layers, and in-ground instrumentation to monitor temperatures.

This chapter presents a summary of the laboratory and in situ testing methods, and the statistical analysis methods used in this study.

Laboratory Testing Methods

Particle Size Analysis and Index Properties

Samples from the subgrade, rock cap, and Class 2A levelling subbase layers were collected from the field and were carefully transported to the laboratory for testing. Particle-size analysis tests were performed in accordance with ASTM C136-06 *Standard test method for sieve analysis of fine and coarse aggregates.* Particle-size analysis tests on the sand subbase and subgrade materials were conducted in accordance with ASTM D422-63 *Standard test method for particle-size analysis of soils.* In addition to above, particle-size analysis tests for the rock cap material included manually measuring the particle sizes using rulers due to the rock/boulder size particles in the material (see Figure 4).

Atterberg limit tests (i.e., liquid limit—LL; plastic limit—PL and plasticity index—PI) were performed in accordance with ASTM D4318-10 *Standard test methods for liquid limit, plastic limit, and plasticity index of soils* using the dry preparation method. The results from particle-size analysis and Atterberg limits tests were used to classify the materials on the unified soil classification system (USCS) in accordance with ASTM D2487-10 *Standard practice for classification of soils for engineering purposes (Unified Soil Classification System)* and AASHTO classification system in accordance with ASTM D3282-09 *Standard practice for classification of soils and soil-aggregate mixtures for highway construction purposes.*

Specific gravity tests were performed on the samples in accordance with ASTM D854-10 *Standard test methods for specific gravity of soil solids by water pycnometer.*

Two laboratory compaction tests were used to determine the relationship between dry density and moisture content for the soils obtained from the field. Subgrade soil compaction characteristics were determined using standard and modified Proctor compaction methods in accordance with ASTM D698-07 *Standard test methods for laboratory compaction characteristics of soil using standard effort* and ASTM D1557-07 *Standard test methods for laboratory compaction characteristics of soil using modified effort*, respectively. Maximum and minimum index density tests were performed using a vibratory table on subbase materials in accordance with ASTM D4253-00 *Standard test methods for maximum index density and unit weight of soil using a vibratory table* and ASTM D4254-00 *Standard test methods for minimum index density and unit weight of soils and calculation of relative density.* Moisture-unit weight

relationships of subbase materials were determined by performing maximum index density tests by incrementally increasing the moisture content by approximately 1.5% for each test.

Frost Heave and Thaw Weakening Test

Frost heave and thaw weakening tests were performed in general accordance with ASTM D5918-06 *Standard test methods for frost heave and thaw weakening susceptibility of soils*. The test is used to classify the frost heave and thaw weakening susceptibility of soils based on the heave rate and the thawed CBR values. The heave rate and thawed CBR values are compared with a classification system provided in the standard to determine the susceptibility ratings (Table 2). It must be noted that the test results can only be used to compare the relative frost heave and thaw weakening susceptibility between material types and cannot be used to directly determine the amount of frost heave or thaw weakening in a pavement system.

A cross-sectional view and a three-dimensional view of the custom freeze/thaw (F/T) test setup fabricated at Iowa State University are shown in Figure 9 and Figure 10, respectively. The samples were 146 mm (5.75 in.) in diameter and 152 mm (6 in.) in height and were compacted inside six rings with a rubber membrane between the soil and the rings. The compaction mold setup is shown in Figure 11 and Figure 12. A water supply was made available at a level of 13 mm (0.5 in.) above the bottom of the sample using a Mariotte tube (Figure 9) to saturate the sample. A surcharge weight was applied to the sample to simulate the loading of a typical pavement section. During F/T testing, laser transducers installed on a ring stand and a bracket above the sample obtained measurements of the samples' heave and consolidation, and thermocouples installed in the sample obtained the temperature profile (Figure 9). The laser transducers used in this study had a measurement range of 50 mm and a resolution of 0.75 µm. The lasers and thermocouples were connected to a data acquisition system that recorded the temperature in one-minute intervals.

Table 2. Frost susceptibility classifications (ASTM D5918-06)

Frost Susceptibility Classification	Heave Rate (mm/day)	Thawed CBR (%)
Negligible	<1	>20
Very low	1 to 2	20 to 15
Low	2 to 4	15 to 10
Medium	4 to 8	10 to 5
High	8 to 16	5 to 2
Very High	>16	<2
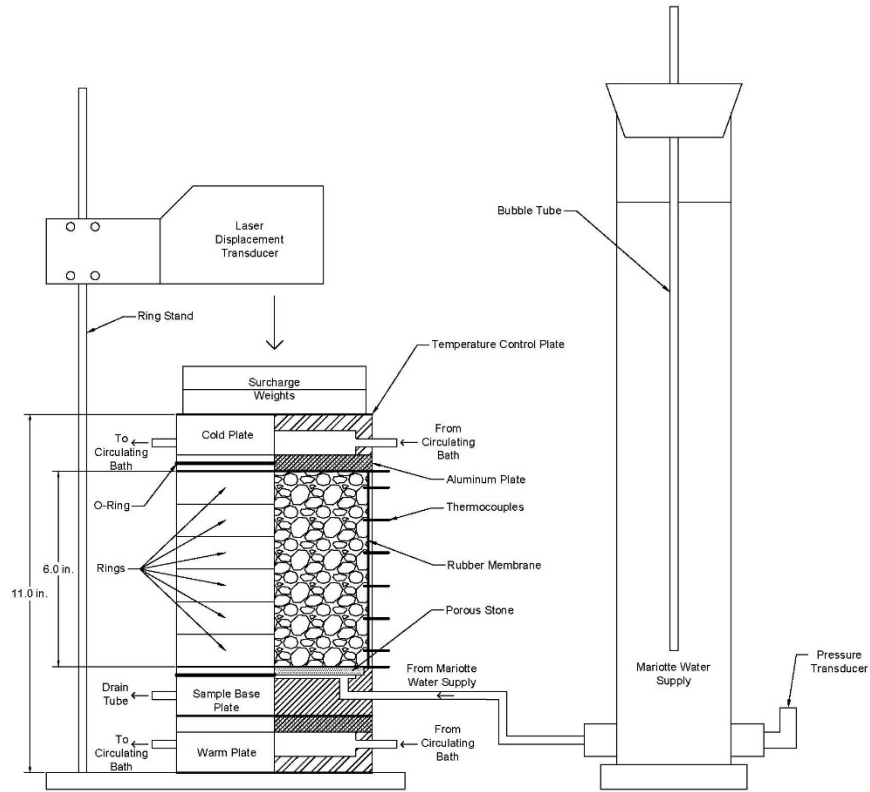
Figure 9. Illustration of frost-heave and thaw-weakening test assembly
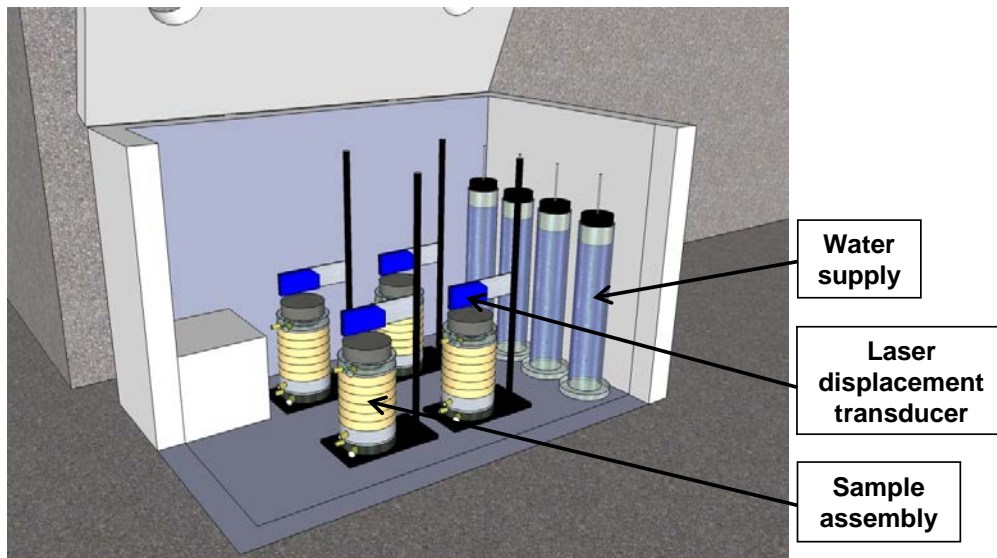
Figure 10. Three-dimensional illustration of frost-heave and thaw-weakening test assembly
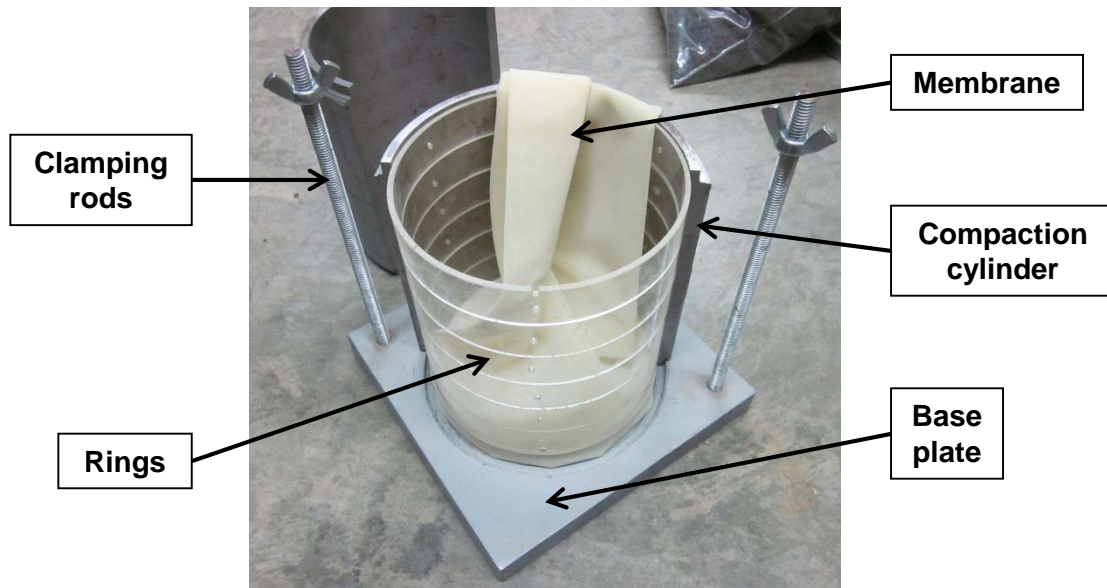
Figure 11. View of frost-heave and thaw-weakening test compaction mold with six rings
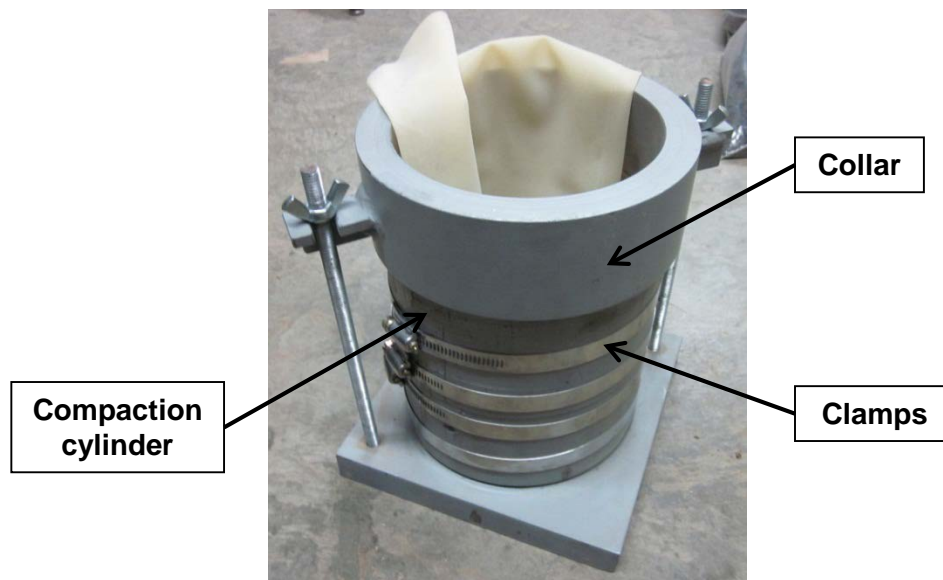
Figure 12. Frost-heave and thaw-weakening test compaction mold setup with collar

The F/T test was carried out by exposing four soil samples to two freeze-thaw cycles over a five day period. The samples were placed in a temperature controlled chest freezer (Figure 10) and then frozen and thawed by changing the temperature at the top and bottom of the samples using temperature controlled water baths (Figure 13). The programmable water baths used in this study had an operating range of -30°C to +200°C and adjustable to ±0.01°C, and were filled with 50% ethylene glycol-water solution. Insulating tape was wrapped around the flexible tubing between the water baths and the temperature control end plates, to help reduce temperature variations in the solution. The target top and bottom of the sample temperatures (Figure 14) were programmed into the water baths and the actual temperatures were measured during the test. An example of

the measured temperatures at the top and bottom of the sample is shown in Figure 15. Results indicated that the measured temperatures were higher during freezing and lower during thawing than the target values. This discrepancy likely occurred because of temperature losses in the glycol solution when transported from the temperature control baths to the temperature control end plates (although care was taken to reduce these variations as indicated above). After the F/T test was completed, a CBR test was performed on the thawed samples in accordance with ASTM D1883-07 and a moisture content profile of the sample was determined by carefully trimming the thawed sample to desired depths.

The heave rate of the sample was determined from the slope of the heave versus time plot as illustrated in Figure 15 for a period of about 24 hours for both the 1st and 2nd freezing cycles. The ASTM D5918 specifies determining heave rate during the first eight hours of each freezing cycle. However, a few samples that were obtained from other research project sites did not heave during the first eight hours, and the samples that did heave during the first eight hours showed similar heave rates over the 8 hour and the 24 hour periods. To be consistent in comparing measurements from different project sites, the research team decided to present the heave rate over the 24 hour period.

Figure 13. Temperature control water baths used to freeze and thaw samples
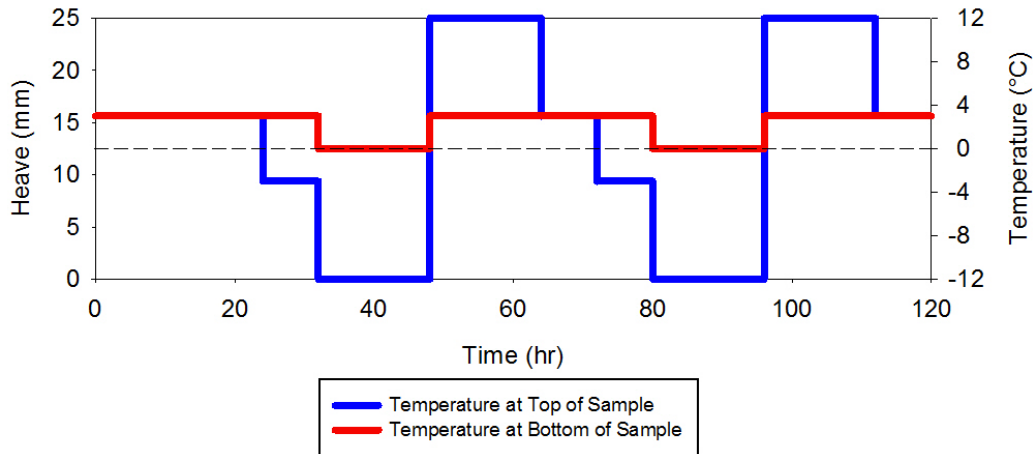
Figure 14. Target top and bottom temperatures with time per ASTM standard during F/T cycles
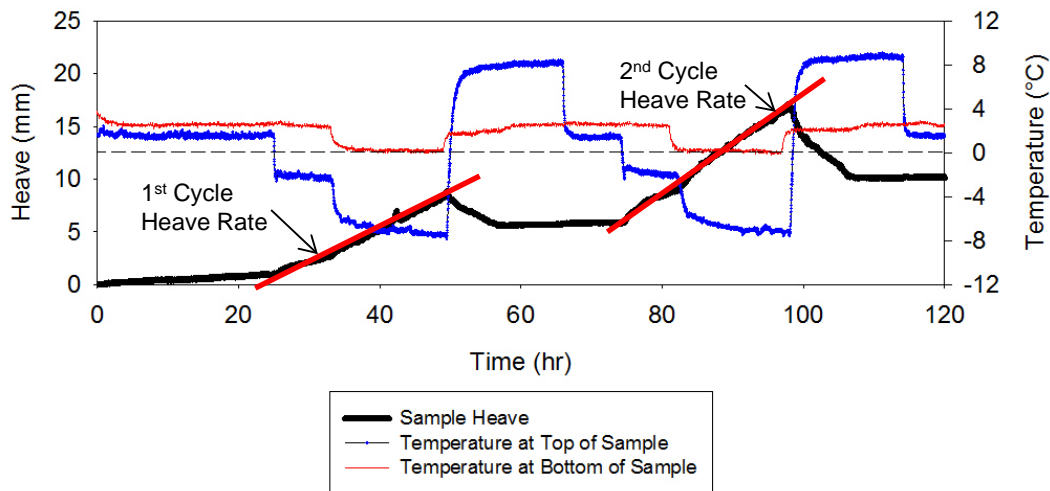
Figure 15. Example of measured top and bottom temperatures during freeze-thaw cycles and determination of heave rate for 1st and 2nd freezing cycles

In Situ Testing Methods

The following in situ test devices were employed on this project: real-time kinematic global positioning system (RTK-GPS) to locate test points; light weight deflectometer (LWD) manufactured by Zorn and Dynatest to determine elastic modulus of the subbase layer; dynamic cone penetrometer (DCP) to determine the California bearing ratio (CBR) of the foundation layers; air permeameter test (APT) device to determine saturated hydraulic conductivity (K_{sat}) of the subbase layer; falling weight deflectometer (FWD) to determine peak deflection under the loading plate (D_0), load transfer efficiency (LTE) at joints and cracks, voids at joints and cracks, foundation composite modulus of subgrade reaction, and deflection basin parameters; and calibrated Humboldt nuclear gauge (NG) to measure in situ moisture and dry density. Brief

15

descriptions of these test procedures are provided below, and equipment used to conduct tests is shown in composite as Figure 6.

Real-Time Kinematic Global Positioning System

An RTK-GPS system was used to obtain the spatial coordinates (x, y, and z) of pavement slabs and test locations. A Trimble SPS881 receiver was used with base station correction provided from a Trimble SPS851 established on site. According to the manufacturer this survey system is capable of horizontal accuracies of < 10 mm and vertical accuracies < 20 mm (Trimble 2013).

Figure 16. In situ test devices: Kuab falling weight deflectometer and Zorn light weight deflectometer (top row left to right); dynamic cone penetrometer, nuclear gauge, and air permeameter (bottom row left to right)

Zorn Light Weight Deflectometer

Zorn LWD tests were performed on granular subbase and subgrade layers. The LWD was set up with a 300 mm diameter plate and 72 cm drop height to provide a calibrated applied stress of 0.1 MPa. The tests were performed following manufacturer recommendations (Zorn 2003) with three seating drops following by three measurement drops, and the elastic modulus values were determined using Equation 3:

$$E = \frac{(1-\eta^2)\sigma_0 r}{D_0} \times F$$

(3)

where E = elastic modulus (MPa); D_0 = measured deflection under the plate (mm); η = Poisson's ratio (0.4); σ_0 = applied stress (MPa); r = radius of the plate (mm); and F = shape factor depending on stress distribution (assumed as 8/3) (see Vennapusa and White 2009). According to the manufacturer, the Zorn LWD has D_0 measurement range of 0.2 mm to 30 mm.

The results are reported as E_{LWD-Z3} (Z represents Zorn LWD and 3 represents 300 mm diameter plate).

Dynatest Light Weight Deflectometer

Dynatest LWD tests were performed on rock cap material using the same procedure as the Zorn LWD. The LWD was set up with a 300 mm diameter plate. The Dynatest LWD measures both applied stress and deformation values, which were measured and used in Eq. 3 to determine the elastic modulus values. According to the manufacturer, the Dynatest LWD has a D_0 measurement range of 0 to 2.2 mm (see Vennapusa and White 2009).

The results are reported as E_{LWD-D3} (D represents Dynatest LWD and 3 represents 300 mm diameter plate).

Dynamic Cone Penetrometer

DCP (Figure 16) tests were performed in accordance with ASTM D6951-03 *Standard Test Method for Use of the Dynamic Cone Penetrometer in Shallow Pavement Applications* to determine dynamic penetration index (DPI) and calculate California bearing ratio (CBR) using Eq. 8. The DCP test results are presented in this report as CBR with depth profiles at each test location. The CBR values were calculation using Equation 5:

$$CBR = \frac{292}{DPI^{1.12}}$$

(4)

Kuab Falling Weight Deflectometer

Falling weight deflectometer (FWD) tests were conducted using a Kuab FWD setup with a 300 mm (11.81 in) diameter loading plate by applying one seating drop and three loading drops. The applied loads varied from about 27 kN (6,000 lb) to 54 kN (12,000 lb) in the three loading drops. The actual applied loads were recorded using a load cell, and deflections were recorded using seismometers mounted on the device, per ASTM D4694-09 *Standard Test Method for Deflections with a Falling-Weight-Type Impulse Load Device.* The FWD plate and deflection sensor setup and a typical deflection basin are shown in Figure 17. To compare deflection values from different test locations at the same applied contact stress, the values at each test location were normalized to a 40 kN (9,000 lb) applied force.
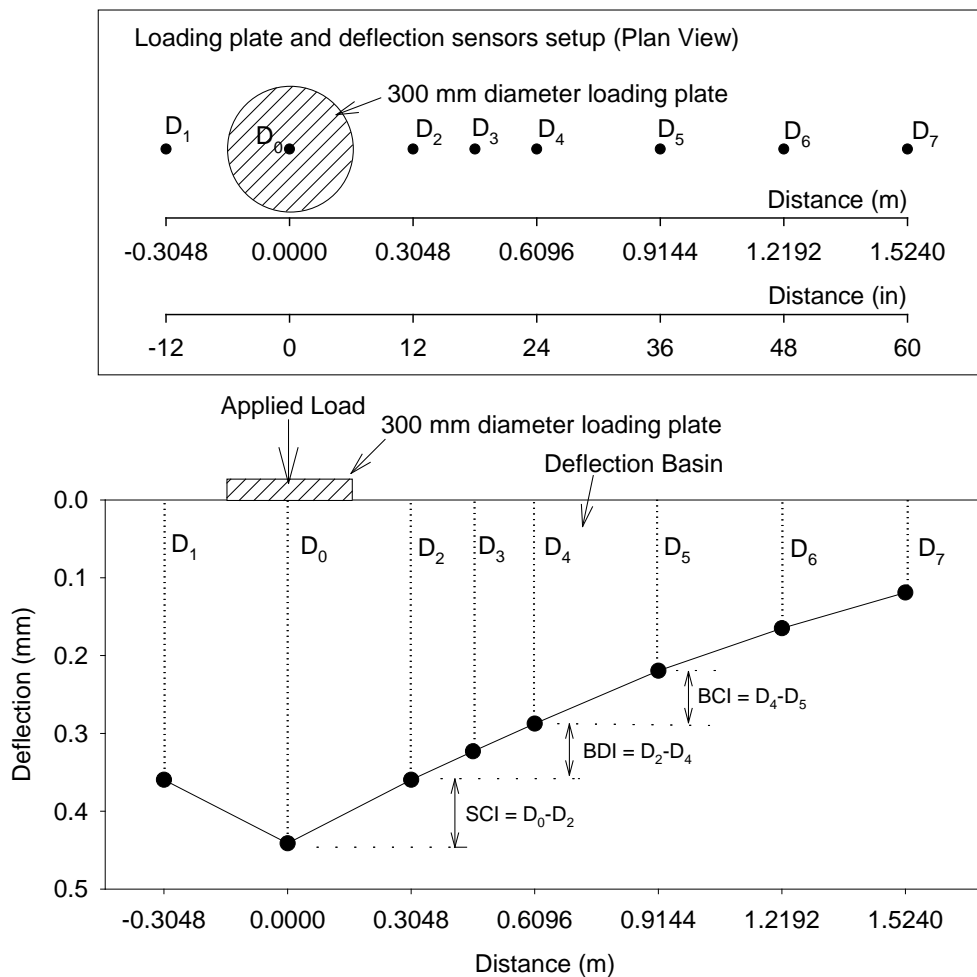
Figure 17. FWD deflection sensor setup used for this study and an example deflection basin

FWD tests were conducted at the center of the PCC slab panels and at the joints. Tests conducted at the joints were used to determine joint load transfer efficiency (LTE) and voids beneath the pavement based on "zero" load intercept values. Tests conducted at the center of the slab panels

18

were used to determine modulus of subgrade reaction (k) values and the intercept values. The procedure used to calculate these parameters are described below.

LTE was determined by obtaining deflections under the plate on the loaded slab (D_0) and deflections of the unloaded slab (D_1) using a sensor positioned about 305 mm (12 in.) away from the center of the plate (Figure 17). The LTE was calculated using Equation 5.

$$LTE(\%) = \frac{D_1}{D_0} \times 100 \tag{5}$$

Voids underneath pavements can be detected by plotting the applied load measurements on the X-axis and the corresponding deflection measurements on the y-axis and plotting a best fit linear regression line, as illustrated in Figure 18, to determine the "zero" load intercept (I) values. AASHTO (1993) suggests I = 0.05 mm (2 mils) as a critical value for void detection. According to Quintus and Simpson (2002), if I = -0.01 and +0.01 mm, then the response would be considered elastic. If I > 0.01 then the response would be considered deflection hardening, and if I < -0.01 then the response would be considered deflection softening.
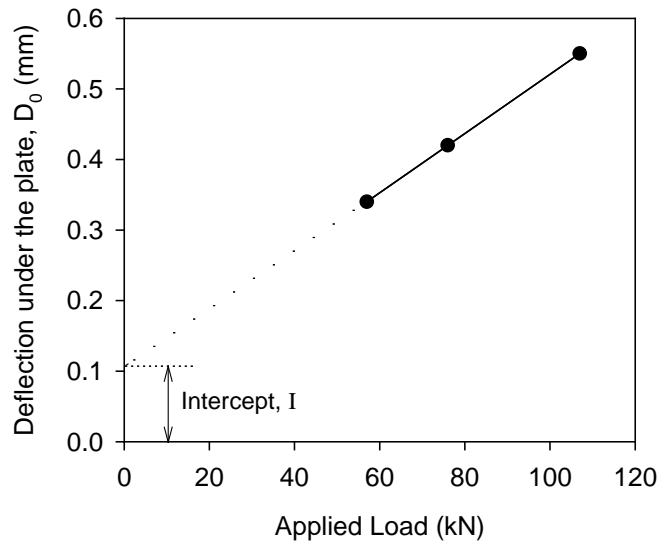
Figure 18. Void detection using load-deflection data from FWD test

Pavement layer temperatures at different depths were obtained during FWD testing, in accordance with the guidelines from Schmalzer (2006). The temperature measurements were used to determine equivalent linear temperature gradients (T_L) following the temperature-moment concept suggested by Jannsen and Snyder (2000). According to Vandenbossche (2005), I-values are sensitive to temperature induced curling and warping affects. Large positive temperature gradients (i.e., when the surface is warmer than the bottom) that cause the panel corners to curl down result in false negative I-values. Conversely, large negative gradients (i.e., when the surface is cooler than the bottom) that cause the panel corners to curl upward result in false positive I-values. Interpretation of I-values therefore should consider the temperature

gradient. Concerning LTE measurements for doweled joints, the temperature gradient is reportedly not a critical factor (Vandenbossche 2005).

The k values were determined using the AREA$_4$ method described in AASHTO (1993). Since the k value determined from FWD test represents a dynamic value, it is referred to here as $k_{\text{FWD-Dynamic}}$. Deflections obtained from four sensors (D_0, D_2, D_4, and D_5 shown in Figure 17) were used in the AREA$_4$ calculation. The AREA method was first proposed by Hoffman and Thompson (1981) for flexible pavements and has since been applied extensively for concrete pavements (Darter et al. 1995). AREA$_4$ is calculated using Equation 6 and has dimensions of length (in inches), as it is normalized with deflections under the center of the plate (D_0):

$$AREA_4 = 6 + 12 \times \left(\frac{D_2}{D_0}\right) + 12 \times \left(\frac{D_4}{D_0}\right) + 6 \times \left(\frac{D_5}{D_0}\right) \tag{6}$$

where D_0 = deflections measured directly under the plate; D_2 = deflections measured at 305 mm (12 in.) away from the plate center ; D_4 = deflections measured at 610 mm (24 in.) away from the plate center; and D_5 = deflections measured at 914 mm (36 in.) away from the plate center. The AREA$_4$ method can also be calculated using different sensor configurations and setups, (i.e., using deflection data from 3, 5, or 7 sensors), and those methods are described in detail in the literature (Substad et al. 2006, Smith et al. 2007)

In early research conducted using the AREA method, the ILLI-SLAB finite element program was used to compute a matrix of maximum deflections at the plate center and the AREA values by varying the subgrade k, the modulus of the PCC layer, and the thickness of the slab (ERES Consultants, Inc. 1982). Measurements obtained from FWD tests were then compared with the ILLI-SLAB program results to determine the k values through back calculation. Barenberg and Petros (1991) and Ioannides (1990) proposed a forward solution procedure based on Westergaard's solution for loading on an infinite plate to replace the back calculation procedure. This forward solution presented a unique relationship between AREA value (for a given load and sensor arrangement) and the dense liquid radius of relative stiffness (L) in which subgrade is characterized by the k value. The radius of relative stiffness (L) is estimated using Equation 7:

$$L = \left[\frac{\ln\left(\frac{x_1 - AREA_4}{x_2}\right)}{x_3} \right]^{x_4} \tag{7}$$

where $x_1 = 36$, $x_2 = 1812.279$, $x_3 = -2.559$, $x_4 = 4.387$. It must be noted that the x_1 to x_4 values vary with the sensor arrangement and these values are only valid for the AREA$_4$ sensor setup. Once, the L value is known, the $k_{\text{FWD-Dynamic}}$ value can be estimated using Equation 8:

$$k_{FWD-Dynamic} \ (pci) = \frac{PD_0^*}{D_0 L^2} \tag{8}$$

where P = applied load (lbs), D_0 = deflection measured at plate center (inches), and D_0^* = non-dimensional deflection coefficient calculated using Equation 9:

$$D_0^* = a \cdot e^{-be^{-cL}} \tag{9}$$

where $a = 0.12450$, $b = 0.14707$, $c = 0.07565$. It must be noted that these equations and coefficients are valid for an FWD setup with an 11.81 in. diameter plate.

The advantages of the $AREA_4$ method are the ease of use without back calculations and the use of multiple sensor data. The disadvantages are that the process assumes that the slab and the subgrade are horizontally infinite. This assumption leads to underestimating the k values of jointed pavements. Crovetti (1993) developed the following slab size corrections for a square slab that is based on finite element analysis conducted using the ILLI-SLAB program and is for use in the $k_{FWD\text{-}Dynamic}$:

$$Adjusted\ D_0 = D_0\left(1 - 1.15085e^{-0.71878\left(\frac{L'}{L}\right)^{0.80151}}\right) \tag{10}$$

$$Adjusted\ L = L\left(1 - 0.89434e^{-0.61662\left(\frac{L'}{L}\right)^{1.04831}}\right) \tag{11}$$

where L' = slab size (smaller dimension of a rectangular slab, length or width). This procedure also has limitations: (1) it considers only a single slab with no load transfer to adjacent slabs, and (2) it assumes a square slab. The square slab assumption is considered to produce sufficiently accurate results when the smaller dimension of a rectangular slab is assumed as L' (Darter et al. 1995). Darter et al. 1995 suggested using $L' = \sqrt{Length \times Width}$ to further refine slab size corrections. However, no established procedures for correcting for load transfer to adjacent slabs have been reported so accounting for load transfer remains as a limitation of this method.

AASHTO (1993) suggests dividing the $k_{FWD\text{-}Dynamic}$ value by a factor of 2 to determine the equivalent $k_{FWD\text{-}Static}$ value. The origin of this factor 2 dates back to Foxworthy's work in the 1980's. Foxworthy (1985) reported comparisons between the $k_{FWD\text{-}Dynamic}$ values obtained using Dynatest model 8000 FWD and the Static k values (Static k_{PLT}) obtained from 30 in. diameter plate load tests (the exact procedure followed to calculate the Static k_{PLT} is not reported in Foxworthy 1985). Foxworthy used the AREA based back calculation procedure using the ILLI-SLAB finite element program. Results obtained from Foxworthy's study (Figure 19) are based on 7 FWD tests conducted on PCC pavements with slab thicknesses varying from about 10 in. to 25.5 in. and plate load tests conducted on the foundation layer immediately beneath the pavement over a 4 ft x 5 ft test area. A few of these sections consisted of a 5 to 12 in. thick base course layer and some did not. The subgrade layer material consisted of CL soil from Sheppard Air Force Base in Texas, SM soil from Seymour-Johnson Air Force Base in North Carolina, and

an unspecified soil type from McDill Air Force base in Florida. No slab size correction was performed on this dataset.

Data from Foxworthy (1985) yielded a logarithmic relationship between the dynamic and the static k values. On average, the $k_{FWD-Dynamic}$ values were about 2.4 times greater than the Static k_{PLT} values. Darter et al. (1995) indicated that the factor 2 is reasonable based on results from other test sites (Figure 19). Darter et al. (1995) also compared FWD test data from eight long-term pavement performance (LTPP) test sections with the static k_{PLT} values and reported factors ranging from 1.78 to 2.16, with an average of about 1.91. The $k_{FWD-Dynamic}$ values used in that comparison were corrected for slab size. For the analysis conducted in this research project, the corrected $k_{FWD-Dynamic}$ values (for finite slab size) were divided by 2 and are reported as $k_{FWD-Static-Corr}$ values.
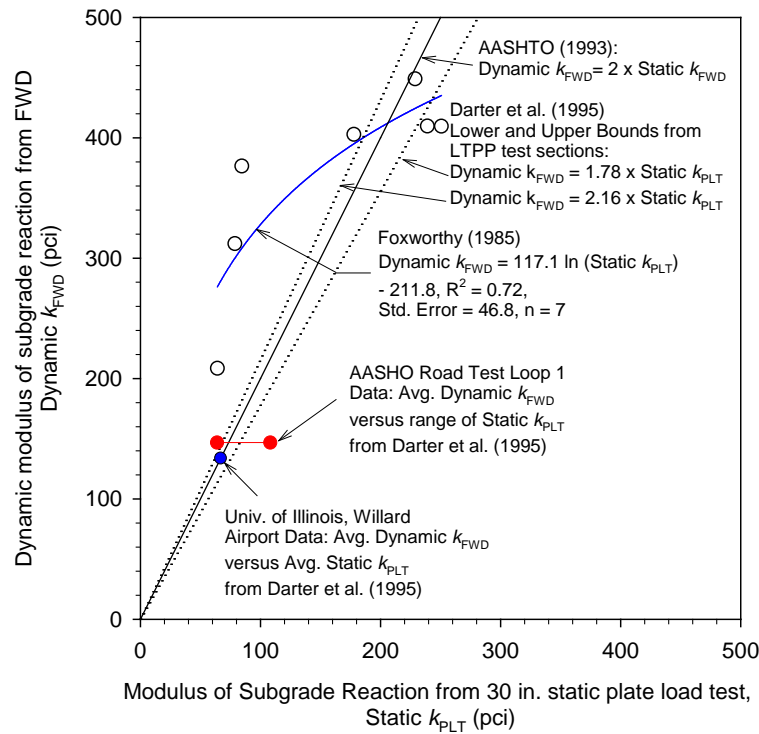
Figure 19. Static k_{PLT} values versus $k_{FWD-Dynamic}$ measurements reported in literature

The SCI, BDI, BCI, and AF measurements are referred to as deflection basin parameters and are determined using the following equations:

$$SCI \text{ (mm)} = D_0 - D_2 \tag{12}$$

$$BDI \text{ (mm)} = D_2 - D_4 \tag{13}$$

$$BCI \text{ (mm)} = D4 - D5 \tag{14}$$

$$AF\ (mm) = \frac{152.4 \times (D_0 + 2D_2 + 2D_4 + D_5)}{D_0}$$
(15)

where, D_0 = peak deflection measured directly beneath the plate, D_2 = peak deflection measured at 305 mm away from the plate center, D_4 = peak deflection measured at 510 mm away from the plate centre, and D_5 = peak deflection measured at 914 mm away from the plate centre.

According to Horak (1987), the SCI parameter provides a measure of the strength/ stiffness of the upper portion (base layers) of the pavement foundation layers (Horak 1987). Similarly, BDI represents layers between 300 mm and 600 mm depth (base and subbase layers) and BCI represents layers between 600 mm and 900 mm depth (subgrade layers) from the surface (Kilareski and Anani 1982). The AF is primarily the normalized (with D_0) area under the deflection basin curve up to sensor D_5 (AASHTO 1993). AF has been used to characterize variations in the foundation layer material properties by some researchers (e.g., Stubstad 2002). Comparatively, lower SCI or BDI or BCI or AF values indicate better support conditions (Horak 1987).

A composite modulus value (E_{FWD-K3}) was calculated using the D_0 corresponding to an applied contact force, and Equation 3. Shape factor F = 2 was used in the calculations assuming a uniform stress distribution (see Vennapusa and White 2009). According to the FWD manufacturer, the segmented plate used results in a uniform stress distribution.

For tests conducted on the CTB or ATB layers, the subgrade layer modulus (E_{SG}) was determined using Equation 16, per AASHTO (1993):

$$E_{SG} = \frac{(1-\eta^2)\sigma_0 r^2}{d_i D_i}$$
(16)

where:
D_i = measured deflection at distance d_i (mm); and
d_i = radial distance of the sensor away from the center of the loading plate.

According to AASHTO (1993), the modulus values estimated from FWD tests exceed the laboratory measured resilient modulus values by a factor of three or more. Therefore an adjustment factor C ≤ 0.33 is recommended to correct E_{SG} determined from Equation 27. In this study, corrected E_{SG} values are calculated using C = 0.33:

$$Corrected E_{SG} = 0.33 \times E_{SG}$$
(17)

AASHTO (1993) suggests that the d_i must be far enough away that it provides a good estimate of the subgrade modulus, independent of the effects of any layers above, but also close enough that it does not result in a too small value. A graphical solution is provided in AASHTO (1993) to

estimate the minimum radial distance based on an assumed effective modulus of all layers above the subgrade and the d_0 value. Salt (1998) indicated that if E_{SG} values are plotted against radial distance, in linear elastic materials such as sands and gravels, the modulus values decrease with increasing distance and then level off after a certain distance. The deformations at the distance at which the modulus values level off can be used to represent E_{SG}. In some cases the modulus values decrease and then increase with distance. Such conditions represent either soils with moderate to high moduli with poor drainage at the top of the subgrade or soft soils with low moduli. In those cases the distance where the modulus is low is represented as E_{SG}.

Ullidtz (1987) described the Odemark's method of equivalent thickness (MET) concept and is used in AASHTO (1993). According to the MET concept, a two-layered system with the top layer modulus higher than the bottom layer, can be transformed into a single layer of equivalent thickness with properties of the bottom layer. Using this concept and the modulus of the bottom layer (E_{SG}), the top layer modulus (E_{SB}) can be back-calculated.

In this study, tests conducted on the ATB and the CTB layer were used to calculate E_{SG} and back-calculate E_{SB} values and compare with the design assumptions.

Humboldt Nuclear Gauge

A calibrated nuclear moisture-density gauge (NG) device (Figure 16) was used to provide rapid measurements of soil dry unit weight (γ_d) and moisture content (w) in the base materials. Tests were performed following ASTM D6938-10 *Standard Test Method for In-Place Density and Water Content of Soil and Soil-Aggregate by Nuclear Methods (Shallow Depth)*. Back-scattering procedure was used in obtaining the measurements. Two measurements of moisture and dry unit weight were obtained at a particular location and the average value is reported.

Rapid Air Permeameter Test (APT Device)

The APT device is a recently developed rapid in situ permeability testing device (White et al. 2014) that uses air as a permeating fluid to determine saturated hydraulic conductivity (K_{sat}). The APT consists of a self-contained pressurized gas system with a self-sealing base plate and uses a theoretical algorithm to determine the K_{sat}. The test involves measuring air pressure on the inlet and outlet sides of a precision orifice, calculating gas flow rate, and assuming material properties (i.e., degree of saturation of the material, residual saturation of the material, and pore-size distribution properties of the material), to determine K_{sat}. The K_{sat} was calculated using Equation 18 (White et al. 2014):

$$K_{sat} = \left[\frac{2\mu_{air}QP_1}{rG_0\left(P_1^2 - P_2^2\right)} \right] \cdot \frac{\rho g}{\mu_{water}(1-S_e)^2(1-S_e^{((2+\lambda)/\lambda)})} \tag{18}$$

where K_{sat} = saturated hydraulic conductivity (cm/s); μ_{air} = dynamic viscosity of air (P_as); Q = volumetric flow rate (cm³/s); P_1 = absolute gas pressure on the soil surface, $P_{o(g)}$ x 9.81 +

101325, (P_a); $P_{o(g)}$ = gauge pressure at the orifice outlet (mm of H_2O); P_2 = atmospheric pressure (P_a); r = radius at the outlet (4.45 cm); G_o= Geometric factor $(4.16e^{(-0.1798\cdot\delta)} + 4.74e^{(-0.0003\cdot\delta)})$; δ = depth to impervious layer (assumed as 100 mm); S_e = effective water saturation $[S_e = (S - S_r)/(1-S_r)]$; λ = Brooks-Corey pore size distribution index; S_r = residual water saturation; S = water saturation; ρ = density of water (g/cm^3); g = acceleration due to gravity (cm/s^2); and μ_{water} = absolute viscosity of water (g/cm-s).

S values of the subbase layer material were determined based on field density and moisture content measurements that varied between 15% and 16%, and $S_r = 0\%$ and $\lambda = 5.0$ were assumed based on a database of typical properties provided in White et al. (2014).

Roller-Integrated Compaction Measurements

A Caterpillar CS683 vibratory smooth drum intelligent compaction (IC) roller was used on the project (Figure 20). The device was equipped with two roller-integrated compaction monitoring measurements: (a) machine drive power (MDP), and (b) compaction meter value (CMV). Brief descriptions of these IC measurement values (MVs) are provided below, and some key features of the roller are summarized in Table 3.

Figure 20. Caterpillar CS683 vibratory smooth drum IC roller

Table 3. Caterpillar CS683 vibratory smooth drum IC roller features

Feature	Description
Drum Geometry	2.13 m width and 1.52 m diameter
Frequency (f)	30 Hz
Amplitude (a) Settings	Static, 0.90 mm (low amplitude), and Static, 1.80 mm (high amplitude)
Compaction Measurement Values (MVs)	MDP_{40} (shown as CCV in the output) and CMV
Display Software	AccuGrade
GPS Coordinates	UTM Zone 15N (NAD83)
Output Documentation	Date/Time; Location (Northing/Easting/Elevation of left and right ends of the roller drum); Speed; CCV; CMV; Frequency; Amplitude; Direction (forward/backward); Vibration (On/Off)

Machine Drive Power (MDP) Value

MDP technology relates mechanical performance of the roller during compaction to the properties of the compacted soil. Detailed background information on the MDP system is provided in White et al. (2005). Controlled field studies documented by White and Thompson (2008), Thompson and White (2008), and Vennapusa et al. (2009) verified that MDP values are empirically related to soil compaction characteristics (e.g., density, stiffness, and strength). MDP is calculated using Equation 19:

$$MDP = P_g - Wv\left(Sin\alpha + \frac{A'}{g}\right) - (mv + b)$$

(19)

where MDP = machine drive power (kJ/s), P_g = gross power needed to move the machine (kJ/s), W = roller weight (kN), A' = machine acceleration (m/s^2), g = acceleration of gravity (m/s^2), α = slope angle (roller pitch from a sensor), v = roller velocity (m/s), and m (kJ/m) and b (kJ/s) = machine internal loss coefficients specific to a particular machine (White et al. 2005).

MDP is a relative value referencing the material properties of the calibration surface, which is generally a hard compacted surface (MDP = 0 kJ/s). Positive MDP values therefore indicate material that is less compact than the calibration surface, while negative MDP values indicate material that is more compacted than the calibration surface (i.e., less roller drum sinkage). The MDP values obtained from the machine were recalculated to range between 1 and 150 using Equation 20 (referred to as MDP_{40}).

$$MDP_{40} = 54.23 - 0.355(MDP)$$

(20)

In Equation 13, the calibration surface with MDP = 0 kJ/s was scaled to $MDP_{40} = 150$ and a soft surface with MDP = 54.23 kJ/s (40000 lb-ft/s) was scaled to $MDP_{40} = 1$.

Compaction Meter Value (CMV)

CMV is a dimensionless compaction parameter developed by Geodynamik that depends on roller dimensions, (i.e., drum diameter and weight) and roller operation parameters (e.g., frequency, amplitude, speed), and is determined using the dynamic roller response (Sandström 1994). CMV is calculated using Equation 21:

$$CMV = C \cdot \frac{A_{2\Omega}}{A_{\Omega}}$$

(21)

where, C is a constant (300); $A_{2\Omega}$ = the acceleration of the first harmonic component of the vibration; and A_{Ω} = the acceleration of the fundamental component of the vibration (Sandström and Pettersson 2004).

Correlation studies relating CMV to soil dry unit weight, strength, and stiffness are documented in the literature (e.g., Floss et al. 1983, Samaras et al. 1991, Brandl and Adam 1997, Thompson and White 2008, White and Thompson 2008).

Geostatistical Data Analysis

Spatially referenced in situ point measurements in a dense grid pattern were obtained in some of the test beds in this study. These data sets provide an opportunity to quantify "non-uniformity" of compacted fill materials. Non-uniformity can be assessed using conventional univariate statistical methods (i.e., by statistical standard deviation (σ) and coefficient of variation (COV)), but they do not address the spatial aspect of non-uniformity. Vennapusa et al. (2010) demonstrated the use of semivariogram analysis in combination with conventional statistical analysis to evaluate non-uniformity in QC/QA during earthwork construction. A semivariogram is a plot of the average squared differences between data values as a function of separation distance, and is a common tool used in geostatistical studies to describe spatial variation. A typical semivariogram plot is presented in Figure 21. The semivariogram $\gamma(h)$ is defined as one-half of the average squared differences between data values that are separated at a distance h (Isaaks and Srivastava 1989). If this calculation is repeated for many different values of h (as the sample data will support) the result can be graphically presented as experimental semivariogram, shown as circles in Figure 21. More details on experimental semivariogram calculation procedure are available elsewhere in the literature (e.g., Clark and Harper 2002, Isaaks and Srivastava 1989).

27

Spherical Semivariogram

$$\gamma(0) = 0$$

$$\gamma(h) = C_0 + C\left[\frac{3h}{2R} - \frac{h^3}{2R^3}\right] ----> 0 < h < R$$

$$\gamma(h) = C_0 + C ----> h > R$$

Range (R)

Semivariogram, γ(h)

Experimental Semivariogram (circles)

Scale, C

Sill C + C_0

Nugget, C_0

Separation Distance, h
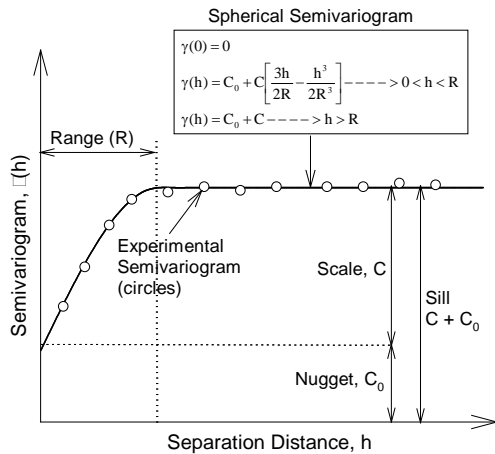
Range, R: As the separation distance between pairs increase, the corresponding semivariogram value will also generally increase. Eventually, however, an increase in the distance no longer causes a corresponding increase in the semivariogram, i.e., where the semivariogram reaches a plateau. The distance at which the semivariogram reaches this plateau is called as range. Longer range values suggest greater spatial continuity or relatively larger (more spatially coherent) "hot spots".

Sill, C+C_0: The plateau that the semivariogram reaches at the range is called the sill. A semivariogram generally has a sill that is approximately equal to the variance of the data.

Nugget, C_0: Though the value of the semivariogram at h = 0 is strictly zero, several factors, such as sampling error and very short scale variability, may cause sample values separated by extremely short distances to be quite dissimilar. This causes a discontinuity at the origin of the semivariogram and is described as nugget effect. (Isaaks and Srivastava, 1989)

Figure 21. Description and parameters of a typical experimental and spherical semivariogram

To obtain an algebraic expression for the relationship between separation distance and experimental semivariogram, a theoretical model is fit to the data. Some commonly used models include linear, spherical, exponential, and Gaussian models. A spherical model was used for data analysis in this report. Arithmetic expression of the spherical model and the spherical variogram are shown in Figure 21. Three parameters are used to construct a theoretical semivariogram: sill (C+C_0), range (R), and nugget (C_0). These parameters are briefly described in Figure 21.

Additional discussion on the theoretical models can be found elsewhere in the literature (e.g., Clark and Harper 2002, Isaaks and Srivastava 1989). For the results presented in this report, the sill, range, and nugget values during theoretical model fitting were determined by checking the models for "goodness" using the modified Cressie goodness fit method (see Clark and Harper 2002) and cross-validation process (see Isaaks and Srivastava 1989). From a theoretical semivariogram model, a low sill and longer range of influence values represent the best conditions for uniformity, while the opposite represents an increasingly non-uniform condition.

CHAPTER 4. LABORATORY TEST RESULTS

Soil Index Properties

The following laboratory tests were conducted on pavement foundation material samples collected from the project site: particle size analysis, Atterberg limits tests, standard and modified Proctor tests, relative density tests, and specific gravity. The results for each of the materials are summarized in Table 5.

Table 4. Summary of material index properties

Parameter	TS6 Subgrade	TS5 Rock Cap	TS2 Class 2A Subbase
Standard Proctor γ_{dmax} (kN/m³)	17.70	—	—
Standard Proctor w_{opt} (%)	16.3	—	—
Modified Proctor γ_{dmax} (kN/m³)	19.10	—	—
Modified Proctor w_{opt} (%)	12.1	—	—
Relative Density Test* γ_{dmin} (kN/m³)	—	—	—
Relative Density Test* γ_{dmin} (pcf)	—	—	—
Relative Density Test* γ_{dmax} (kN/m³)	—	—	14.94
Relative Density Test* γ_{dmax} (pcf)	—	—	18.14
Gravel Content (%) (> 4.75mm)	11	63	55
Sand Content (%) (4.75mm – 75μm)	31	32	34
Silt Content (%) (75μm – 2μm)	36	5	12
Clay Content (%) (< 2μm)	22		
Liquid Limit, LL (%)	37	NP	NP
Plastic Limit, PL (%)	22	NP	NP
Plasticity Index, PI (%)	15	NP	NP
AASHTO Classification	A-6 (6)	A-1-a	A-1-a
USCS Classification	CL	GW	GP-GM
Specific Gravity, G_s	2.78	2.70	2.82

— Not measured
* at oven-dry moisture content

Particle size distributions curves for the three materials are provided in Figure 22 to Figure 24. Relative density tests provided moisture-dry unit weight relationships for the Class 2A subbase material (Figure 25). Standard and modified Proctor tests provided the moisture-dry unit weight relationships for the TS6 subgrade material (Figure 26).

Figure 22. Particle size distribution of TS6 subgrade material

Figure 23. Particle size distribution of TS5 rock cap material
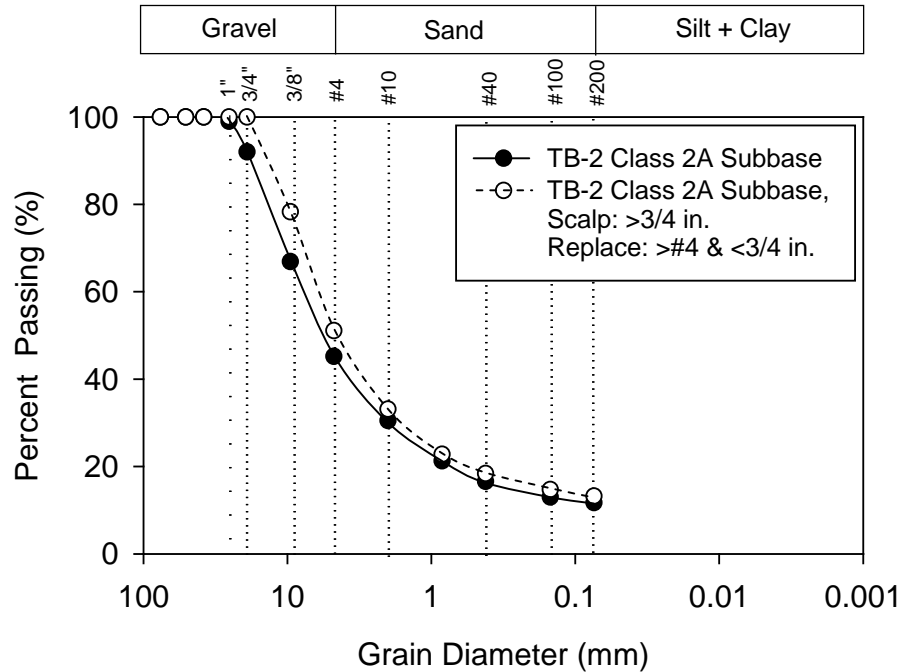
Figure 24. Particle size distribution of TS2 Class A subbase material

The moisture-dry unit weight figures for the class 2A subbase material included both in situ and laboratory values. In situ dry unit weights for the class 2A subbase were larger than the laboratory values. In situ class 2A relative density values ranged from 168–235%. In situ moisture contents ranged from 3.4–9.1%. Possible reasons for the higher in situ dry unit weight values include segregation and gradation variations.

The moisture-dry unit weight figures for the TS6 subgrade material included both in situ and laboratory values. In situ TS6 subgrade relative compaction values ranged from 91–105% of the maximum standard Proctor dry unit weight. In situ TS6 subgrade moisture values ranged from 3.7% below to 5.6% above standard Proctor optimum moisture content.
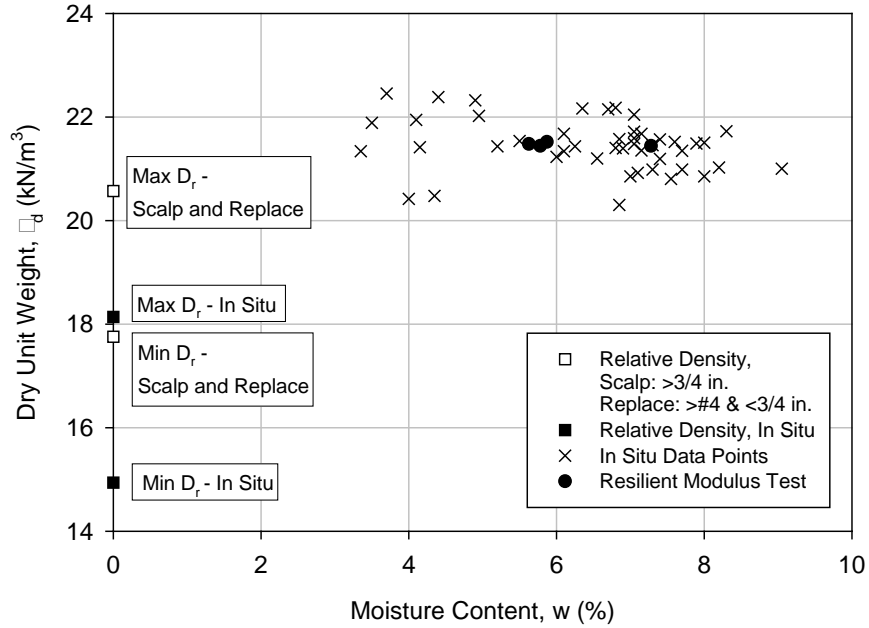
Figure 25. Laboratory moisture-density relationships of TS2 Class 2A subbase material
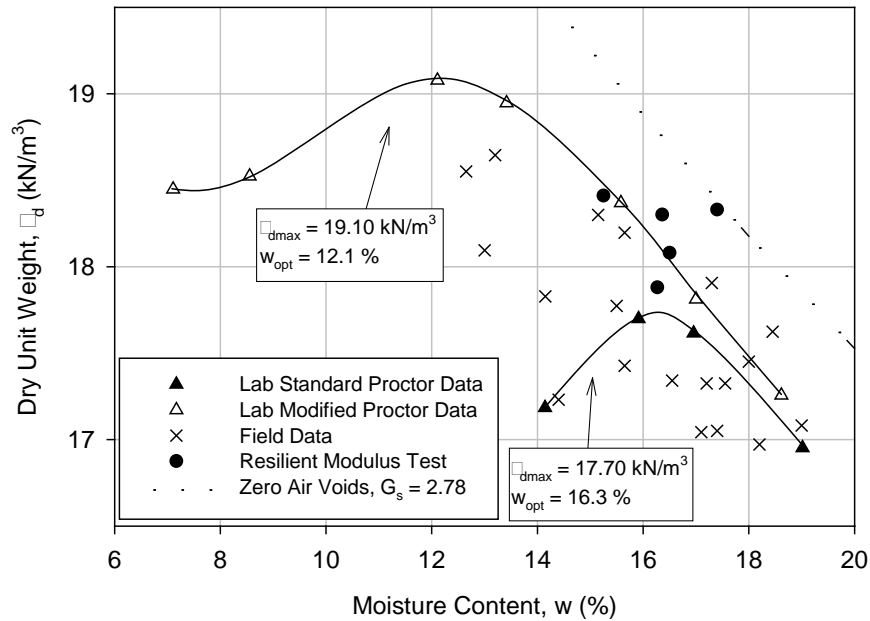
Figure 26. Laboratory moisture-density relationships of TS6 subgrade material

Frost-Heave and Thaw-Weakening Susceptibility

Frost-heave and thaw-weakening susceptibility tests were conducted on TS6 subgrade material. The frost-heave time plots for the four replicate samples prepared are presented in Figure 27. The results were similar for all four samples. The slope of the heave versus time line is approximately the same for the first and second freeze; however the total heave is higher during the second

freeze because the samples did not return to their original height after the first freeze-thaw cycle. The samples reached a peak heave after the first freeze and never consolidated during thawing. The sample height also increased after the second freeze-thaw cycle.

The moisture content profiles after thawing are presented in Figure 28.The moisture content increased after freeze-thaw cycling compared to the initial moisture content. There are no trends showing redistribution of water in the samples, which would indicate that there was no sufficient capillary action to draw water to the top of the sample.

The frost-heave and thaw-weakening results are summarized in Table 5. The CBR after freeze-thaw cycling was lower than the standard CBR. The thaw-weakening susceptibility rating is high for the material. The frost-heave rate increased slightly from the first to the second freeze cycle. The frost-susceptibility rating for the first freeze is low and medium for the second freeze.
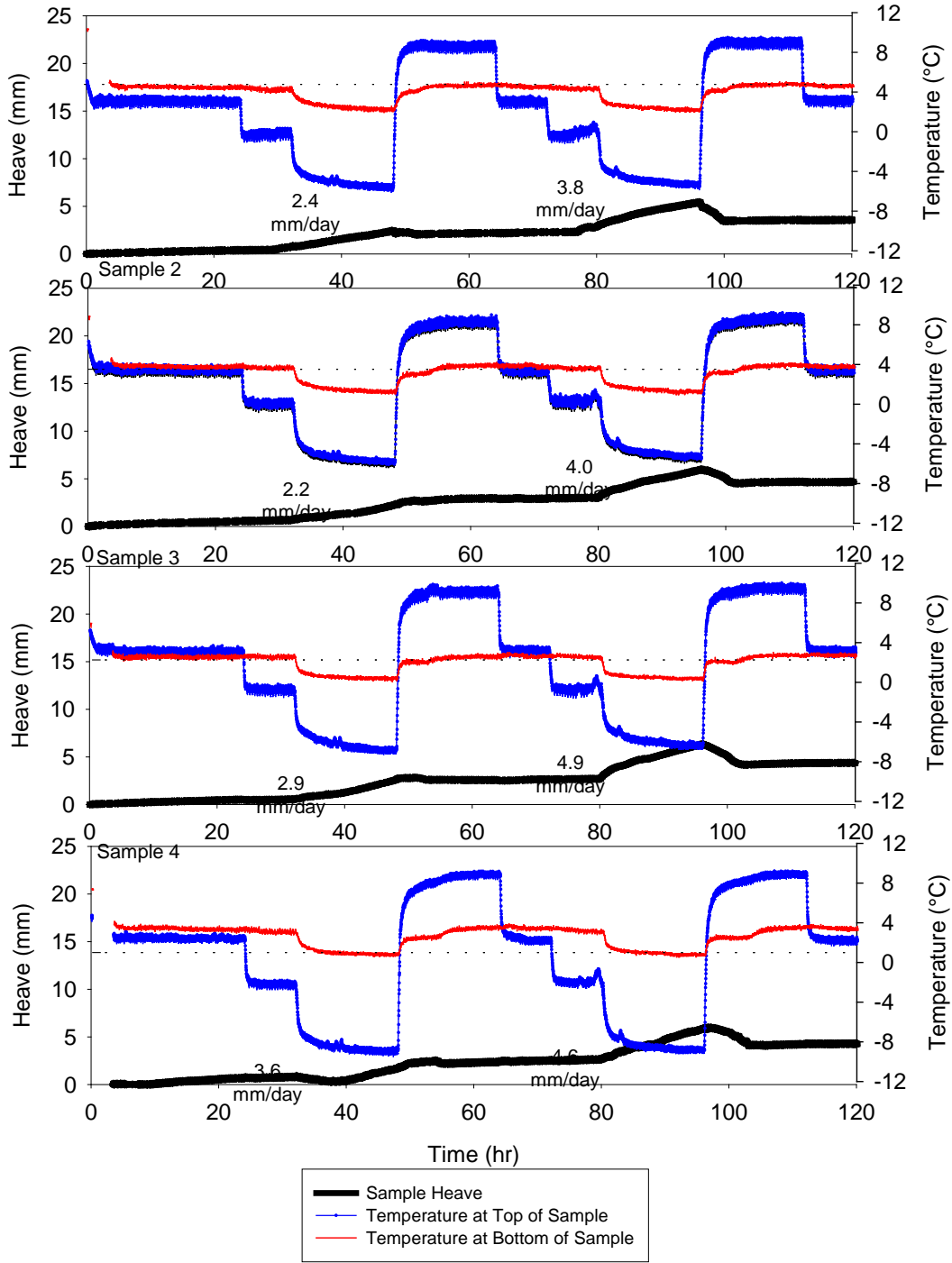
Figure 27. Frost heave time plots for TS6 subgrade material
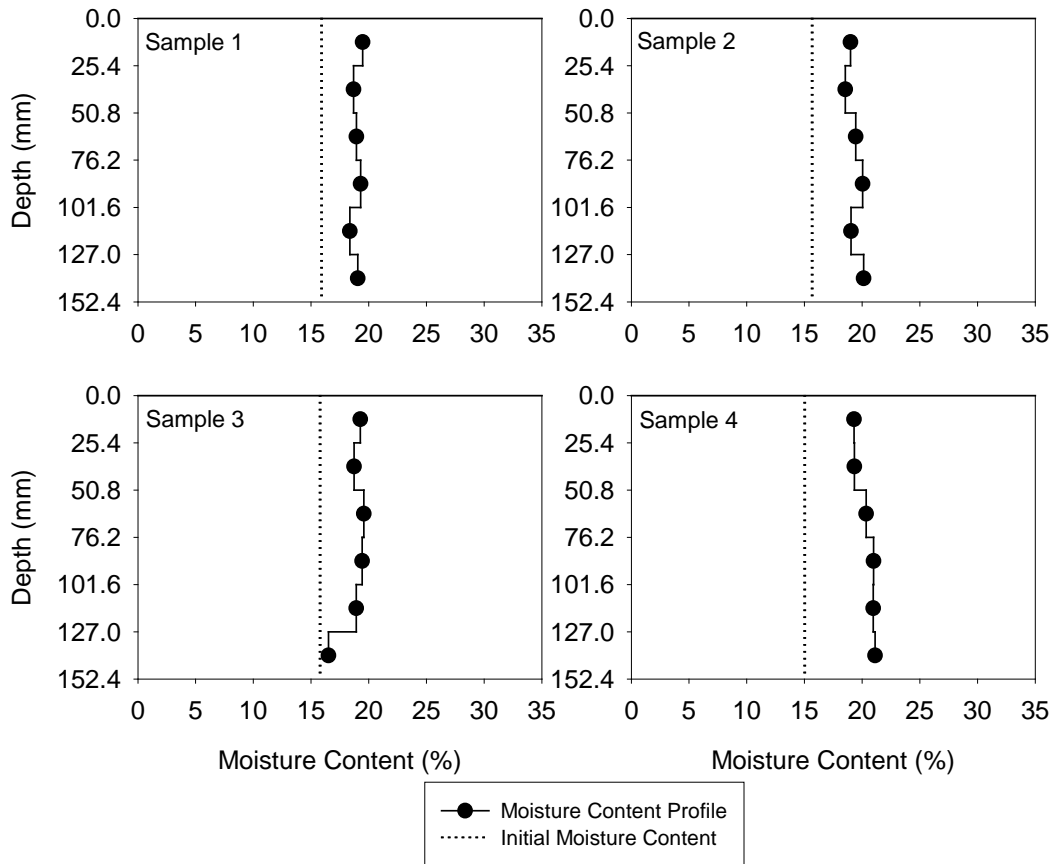
Figure 28. Moisture content profiles of TS6 subgrade material

Table 5. Frost-heave and thaw-weakening test results of TS6 subgrade

Property	μ	σ	COV (%)	# of samples
CBR (%) (standard test)	21.1			1
CBR (%) (after frost-susceptibility test)	3.0	0.3	12.8	4
1st Frost-heave rate (mm/day)	2.8	0.5	18.8	
2nd Frost-heave rate (mm/day)	4.3	0.5	11.4	
1st Frost-heave susceptibility rating	Low	—	—	
2nd Frost-heave susceptibility rating	Medium	—	—	
Thaw-weakening susceptibility rating	High	—	—	

35

CHAPTER 5. IN-SITU TEST RESULTS

Description of Test Beds

Table 8 summarizes date of testing, location of each test bed (TB), in situ test measurements performed on each test bed, and field notes. In situ testing was conducted on seven TBs as part of this field study. TBs 1 and 2 consisted of class 2A levelling stone subbase placed over the rock cap subgrade treatment, TB3 consisted of ATB, TB4 consisted of CTB, TB5 consisted of rock cap subgrade treatment, TB6 consisted of general subgrade fill, and TB7 consisted of the newly constructed PCC layer at the surface. TB2 was located on SR259, which was also being reconstructed as part of this project, while all remaining TBs were located on SR22 mainline. Except TB3, all other TBs were located just east or west of SR259 near Clyde, PA. TB3 was located on an adjacent project site near Blairsville, PA.

Table 6. Summary of test beds and in situ testing

TB	Date	Location	Material	In-situ Test Measurement	Comments
1	7/27/2009	SR22 Sta. 566+50 to 570+50	Class 2A leveling stone	NG, DCP, Zorn LWD, and FWD	Approximately 51 mm thick Class 2A leveling stone over 457 mm thick rock cap
2	7/27/2009	SR259 Sta.12+00 to 15+50	Class 2A leveling stone	NG, DCP, Zorn LWD, FWD, APT, and IC Roller	
3	7/30/2009	SR22 B09 Project	Asphalt Treated Base	FWD and APT	Approximately 100 mm thick ATB over Class 2A leveling stone and rock cap
4	7/28 – 7/29/2009	SR22 Sta. 475+00 to 481+00	Cement Treated Base	FWD, APT, and DCP	Approximately 100 mm thick CTB over Class 2A leveling stone and rock cap
5	7/28/2009	SR22 Sta. 409+90 to 417+00	Rock cap	Dynatest LWD, FWD, and IC roller	Rock cap subgrade treatment over general subgrade fill (prior to placement of leveling stone)
6	7/28/2009	SR22 Sta. 377+00 to 397+00	General Fill	NG, DCP, Zorn LWD, and IC Roller	General subgrade fill (relatively soft and wet). Reworked after testing, but no testing after rework.
7	7/28 – 7/29/2009	SR22 Sta. 475+00 to 481+00	JCPC Pavement Surface	FWD	PCC pavement over CTB, class 2A leveling stone, and rock cap. Testing at joints and center panel.

Note: NG – nuclear gauge, DCP – dynamic cone penetrometer, FWD – falling weight deflectometer, LWD – light weight deflectometer, IC roller – intelligent compaction roller, APT – air permeameter test.

In the following sections of this chapter, results are presented separately for each test bed. In addition, comparisons between the test beds with the design assumed values and correlations between IC roller measurements and in situ test measurement values are presented.

TB1: Class 2A Leveling Stone Subbase

TB1 consisted of testing the final compacted surface of the nominal 50 mm thick granular subbase layer with Class 2A leveling stone material over nominal 457 mm thick rock cap (Figure 29). The test area limits for this TB were between Sta. 566+50 and 570+50. The plan area of the test bed was about 12 m x 125 m. NG, DCP, Zorn LWD, and FWD tests were conducted. Tests were conducted along 4 testing lanes across width of the pavement in a grid pattern as shown in Figure 30 at a total of 81 locations. The center line of the test area corresponded to the centerline of the pavement. In the middle of the TB (from Sta. 568+50 to 569+00), the test points were located in a dense grid pattern at about 1.5 m apart along five lanes, while the points were spaced at about 12 m elsewhere. The spacing pattern was laid out to assess both short-term and long-term spatial relationships in geostatistical analysis.

**Figure 29. TB 1: Picture of the test area**
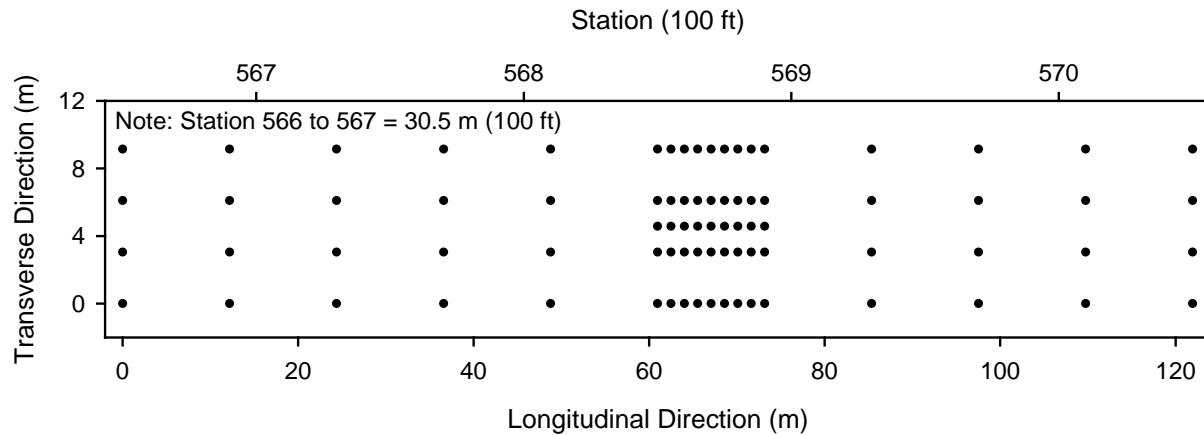
Figure 30. TB 1: Local coordinates of in situ test locations

LWD and FWD tests were conducted at all test locations, while NG and DCP tests were conducted at only 44 test locations. NG and DCP tests were not conducted in densely spaced locations due to time constraints.

The data obtained from this TB were analyzed using geostatistical analysis to characterize the spatial characteristics of the measurements. Kriged spatial contour maps, linear plots with actual measurement values along the pavement profile, semivariograms, and histograms of each in situ point measurement are presented in Figure 31 and Figure 34. The spatial statistical parameters (i.e., scale (sill minus nugget), range, and nugget) are provided in the semivariogram plot of each figure.

The DCP-CBR profiles are shown in Figure 35 at all test locations. The DCPs were terminated at 22 out of the 44 test locations due to refusal with presence of rock. The results were not sufficient to conduct spatial analysis, but showed variable conditions with CBR varying between 8 and 100+ within the rock cap layer.

The LWD and FWD test results were used to measure the elastic moduli values and compare with the design assumed E_{SG} values (206.8 MPa or 30 ksi for rock cap). Results showed that moduli values obtained from the FWD test (E_{FWD-K3}) at 0.57 MPa applied stress, were on average 1.6 times higher moduli values obtained from the Zorn LWD test at 0.1 MPa applied stress. Moduli values obtained from both tests were lower than the design assumed E_{SG} of 206.8 MPa at all test locations except one.

The NG test measurements were obtained in backscatter mode. Dry density measurements showed high relative density values. This is likely because of variations in gradation in the laboratory sample versus field material. The moisture content of the material varied between 3.5 and 8.5%.

Spatial contours of all test measurements (except moisture content) showed concentrated circles around the test points, especially for test locations that are spaced 12 m apart. The variograms

38

showed range values for these test measurements were < 12 m, which indicates that there should be at least a few test points at distances < 12 m to be able to capture the short-scale variability for these measurement values on this material.
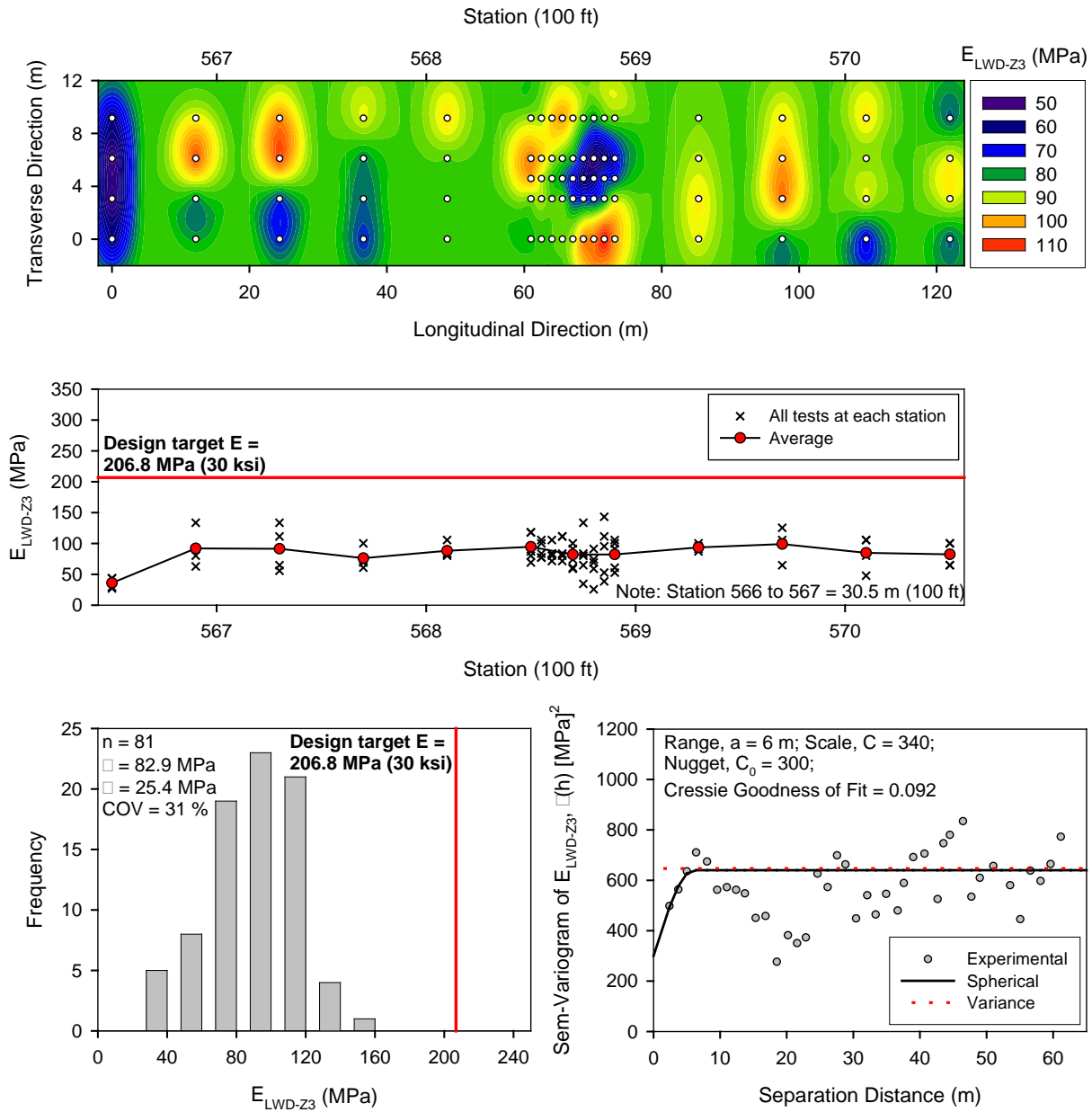
Figure 31. TB1: Kriged spatial contour map (top), measurements longitudinally along the test section (middle), histogram (bottom left), and semivariogram (bottom right) of E_{LWD-Z3} measurements
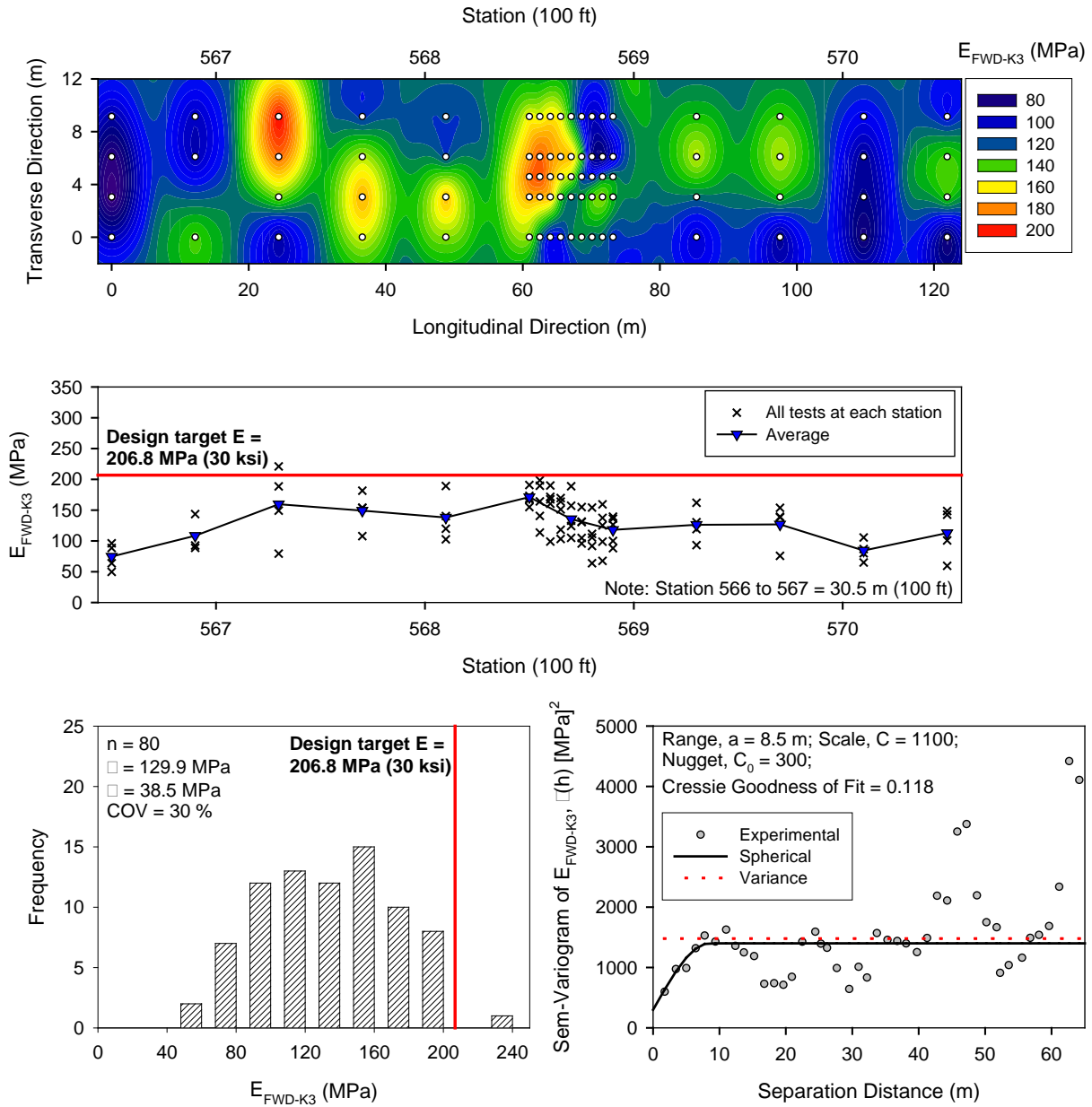
Figure 32. TB1: Kriged spatial contour map (top), measurements longitudinally along the test section (middle), histogram (bottom left), and semivariogram (bottom right) of E_{FWD-K3} measurements
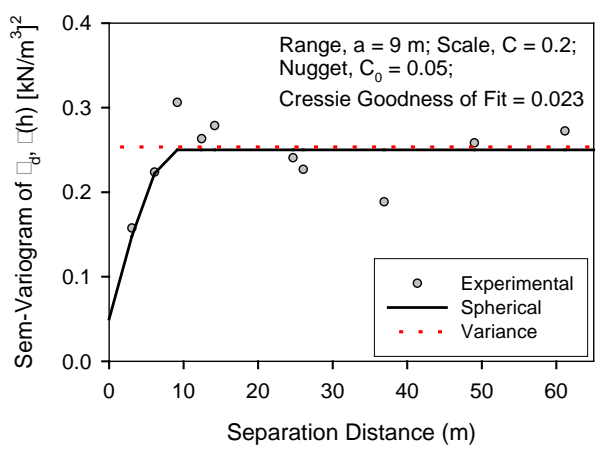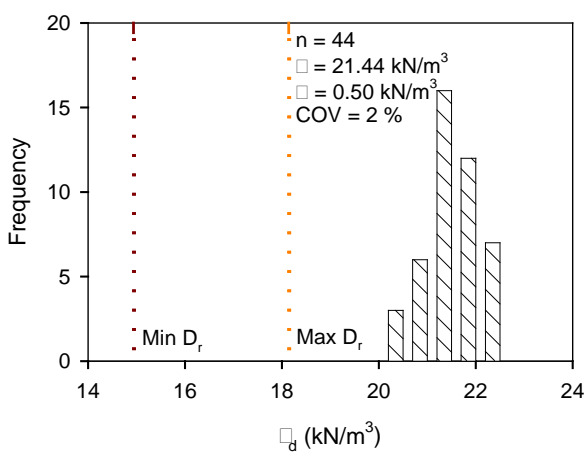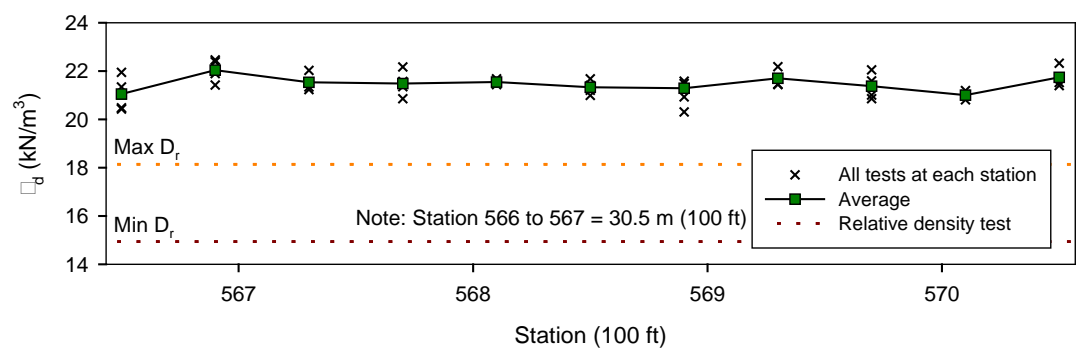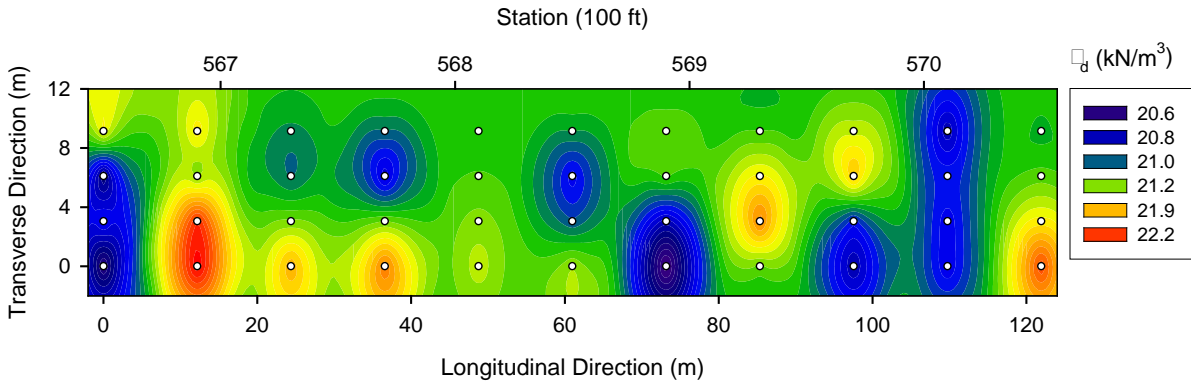
Figure 33. TB1: Kriged spatial contour map (top), measurements longitudinally along the test section (middle), histogram (bottom left), and semivariogram (bottom right) of γ_d
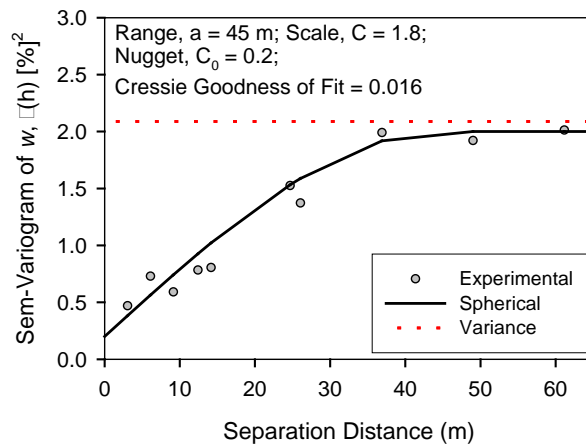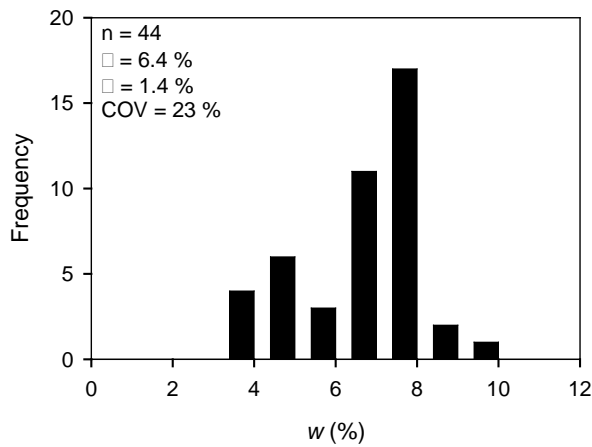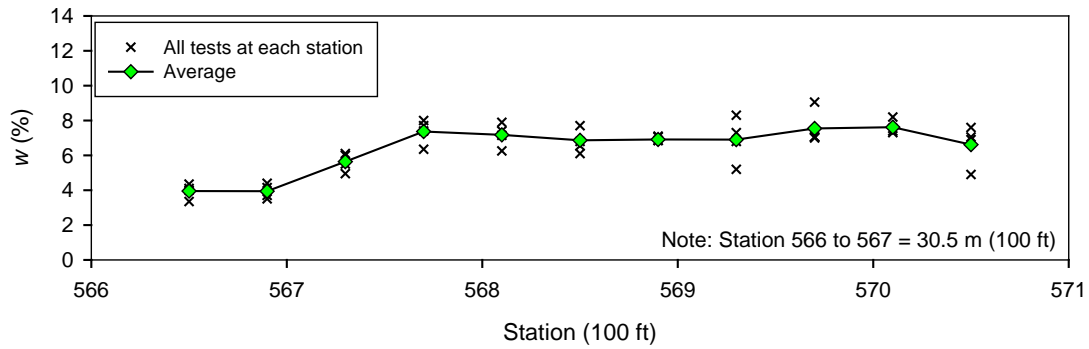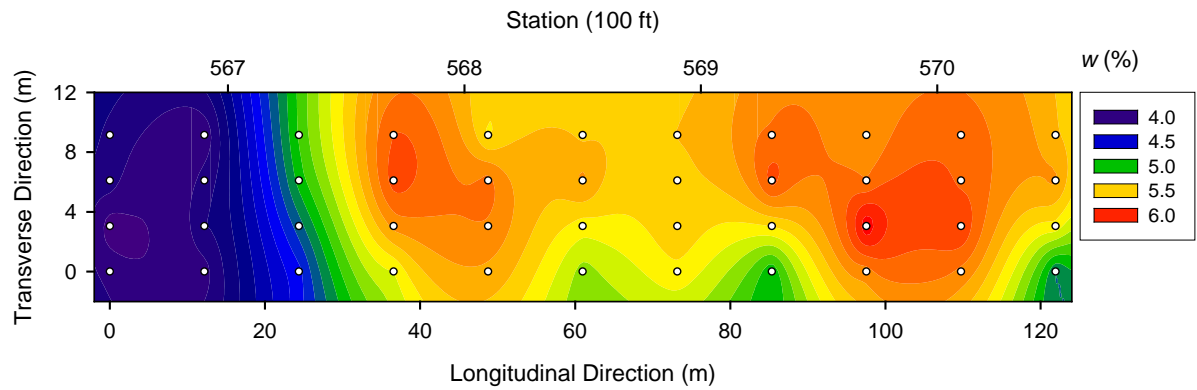
Figure 34. TB1: Kriged spatial contour map (top), measurements longitudinally along the test section (middle), histogram (bottom left), and semivariogram (bottom right) of *w*
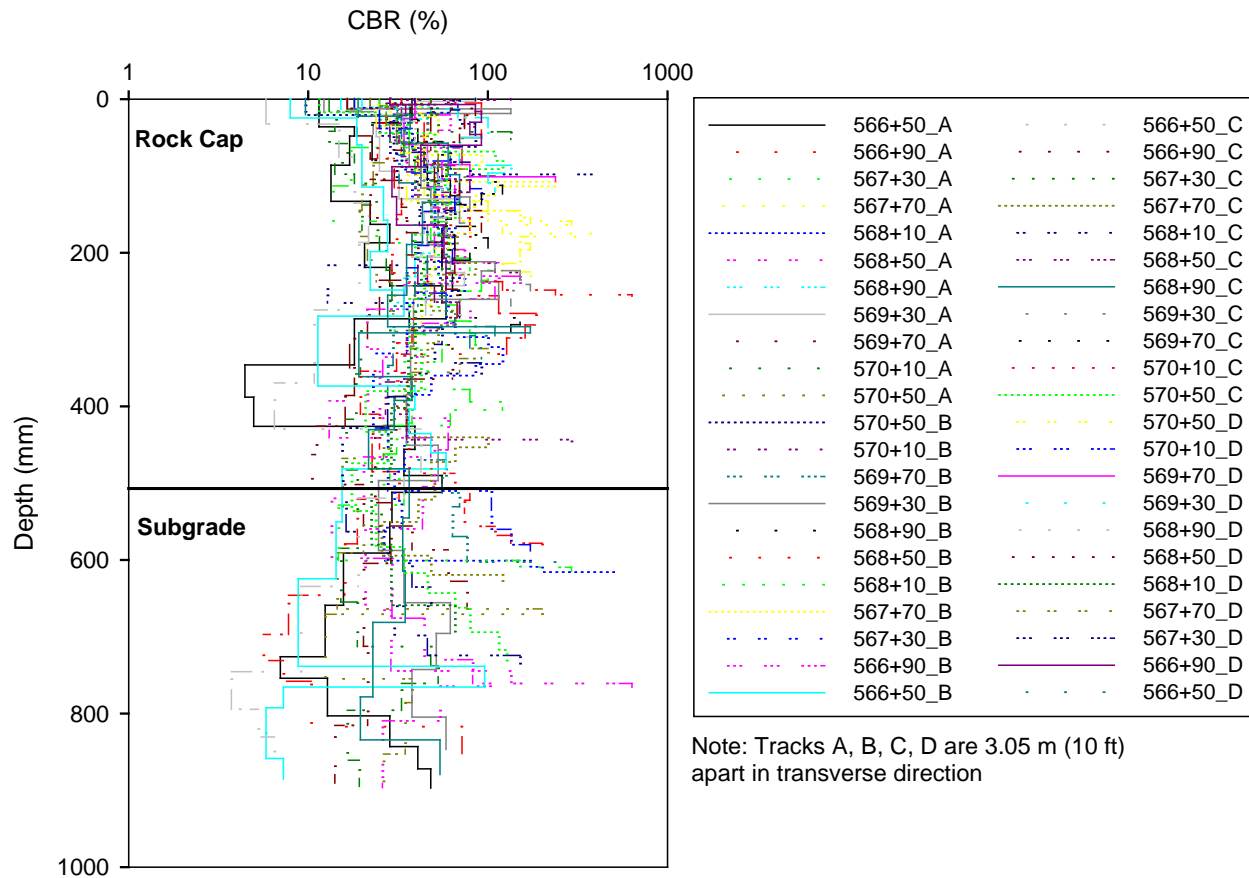
Figure 35. TB1: DCP-CBR profiles along all four tracks in longitudinal direction from Sta. 566+50 to Sta. 570+10

TB2: Class 2A Leveling Stone Subbase

Similar to TB1, TB2 consisted of testing the final compacted surface of the nominal 50 mm thick granular subbase layer with Class 2A leveling stone material over nominal 457 mm thick rock cap (Figure 36). The test area limits for this TB were between Sta. 12+00 and 15+50 on SR259, just north of SR22. The plan area of the test bed was about 6 m x 120 m. IC roller was first used on this TB to map the area with two roller passes and record CMV and MDP* values. After the mapping passes, NG, DCP, APT, Zorn LWD, and FWD point tests were conducted. Tests were conducted along 4 testing lanes across width of the pavement as shown in Figure 37 at a total of 32 test locations. The center line of the test area corresponded to the centerline of the pavement.

Figure 36. TB 2: Picture of the test bed area
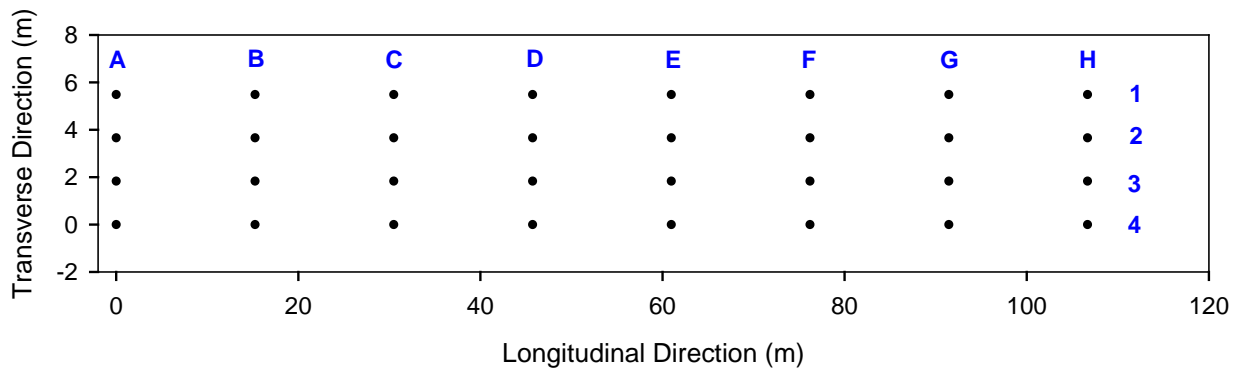
Figure 37. TB 2: Local coordinates of in situ test locations

The CMV and MDP* color-coded georeferenced maps are shown in Figure 38 and Figure 39. A histogram plot of the measurements is also included in the figures. The results showed an average CMV of about 24 with coefficient of variation (COV) of about 60%, and average MDP* of about 117 with COV of about 8%. The CMV value is generally considered to have deeper influence depths (up to 1.5 m) than the MDP* value (< 0.5 m).

The CMV and MDP* maps both identified stiff zones with higher values near locations marked as A, B, and F on the maps.
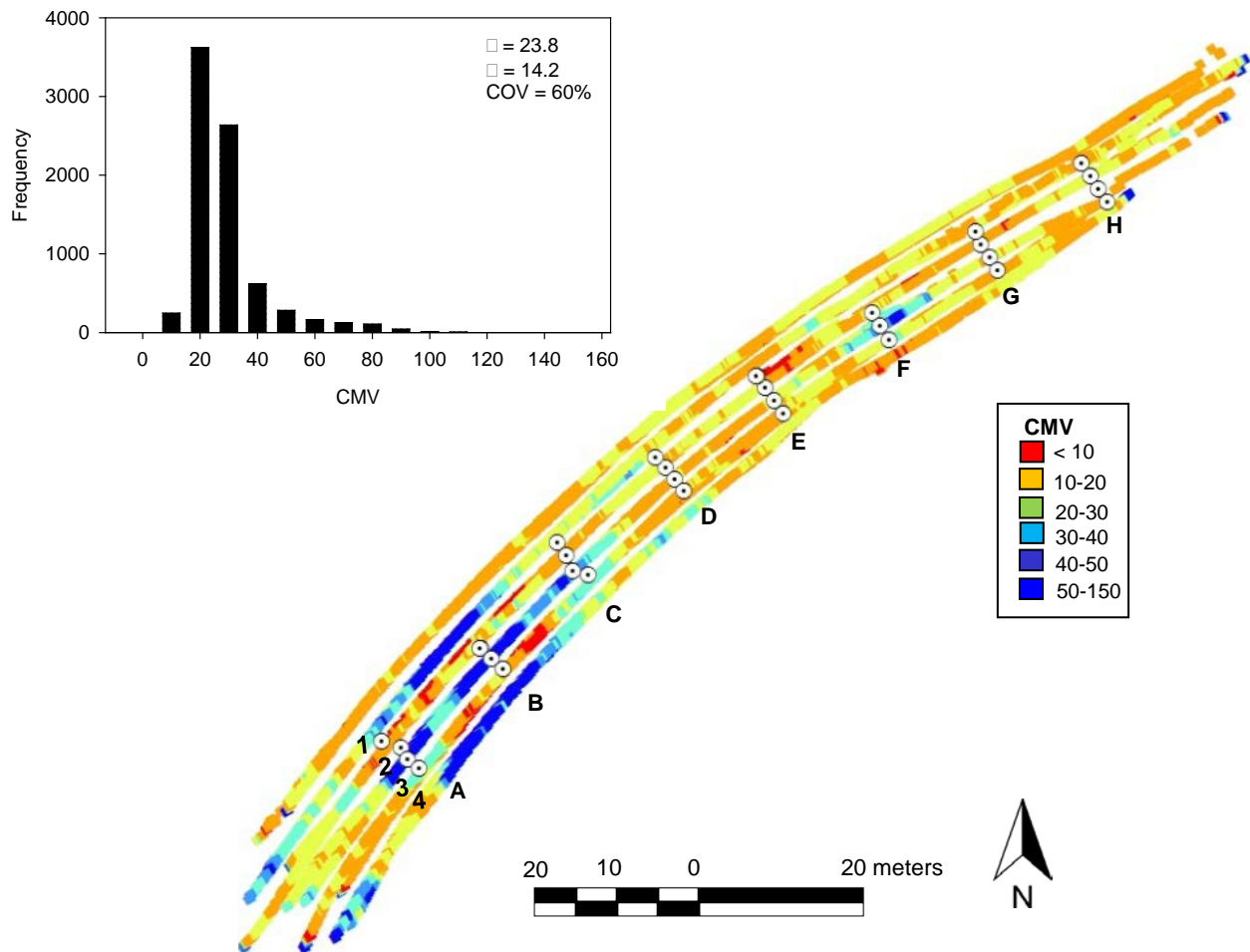
Figure 38. TB 2: Color-coded map of georeferenced CMV map

Results from LWD, FWD, NG, and APT tests are presented as linear plots with distance in Figure 40 and histograms of each measurement value with univariate statistics are presented in Figure 41.

DCP-CBR profiles are shown in Figure 42 for all test locations. At 17 out of the 32 test locations, the DCPs were terminated within the rock cap layer due to refusal with presence of rock. DCPs at three select locations were extended down to about 2 m.
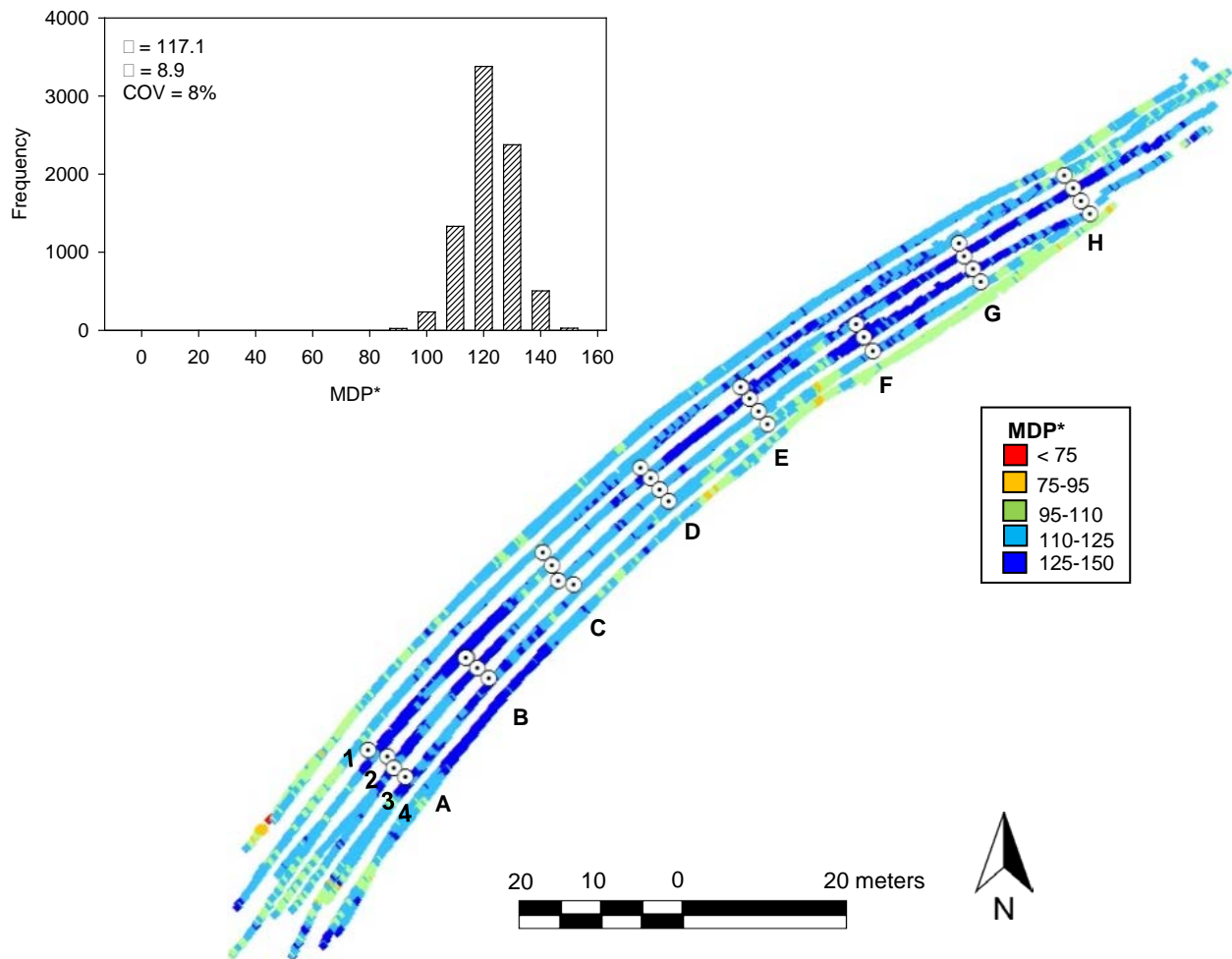
Figure 39. TB 2: Color-coded map of georeferenced MDP* map

The LWD and FWD test results were used to measure the elastic moduli values and compare with the design assumed E_{SG} values (206.8 MPa or 30 ksi for rock cap). Results showed that moduli values obtained from the FWD test (E_{FWD-K3}) at 0.57 MPa applied stress, were on average 2.3 times higher moduli values obtained from the Zorn LWD test at 0.1 MPa applied stress. Moduli values obtained from both tests were lower than the design assumed E_{SG} of 206.8 MPa at all test locations except two.

The NG test measurements were obtained in backscatter mode. Dry density measurements showed high relative density values. This is likely because of variations in gradation in the laboratory sample versus field material. The moisture content of the material varied between 3.5 and 5.0%.

The K_{sat} of the material varied between 0.1 and 1 cm/s, with an average of 0.9 cm/s at COV of about 80%.
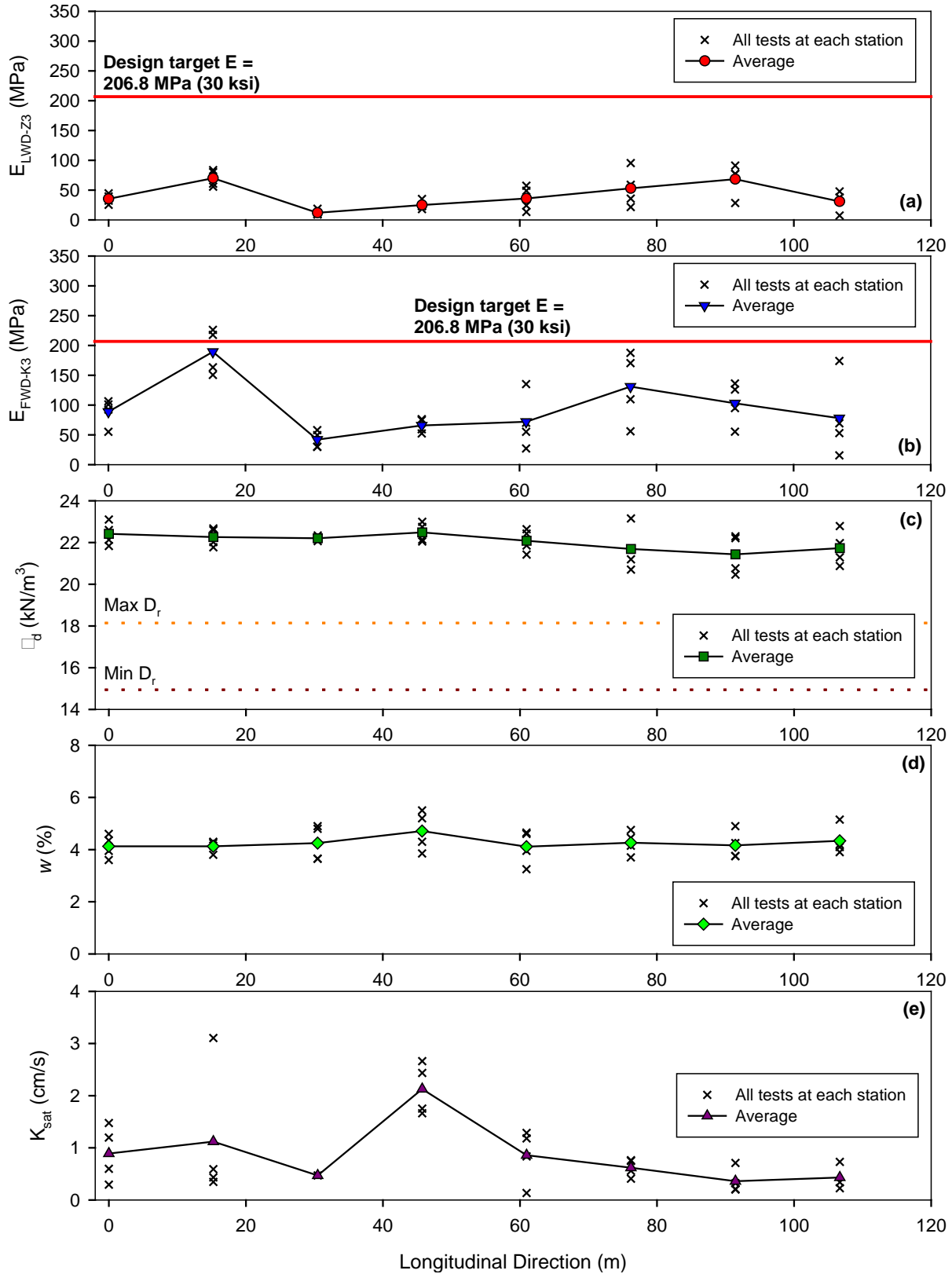
Figure 40. TB 2: In situ test results (a) E_{LWD-Z3}, (b) E_{FWDK3}, (c) γ_d, (d) w, and (e) K_{sat} along an about 107 m test section in longitudinal direction
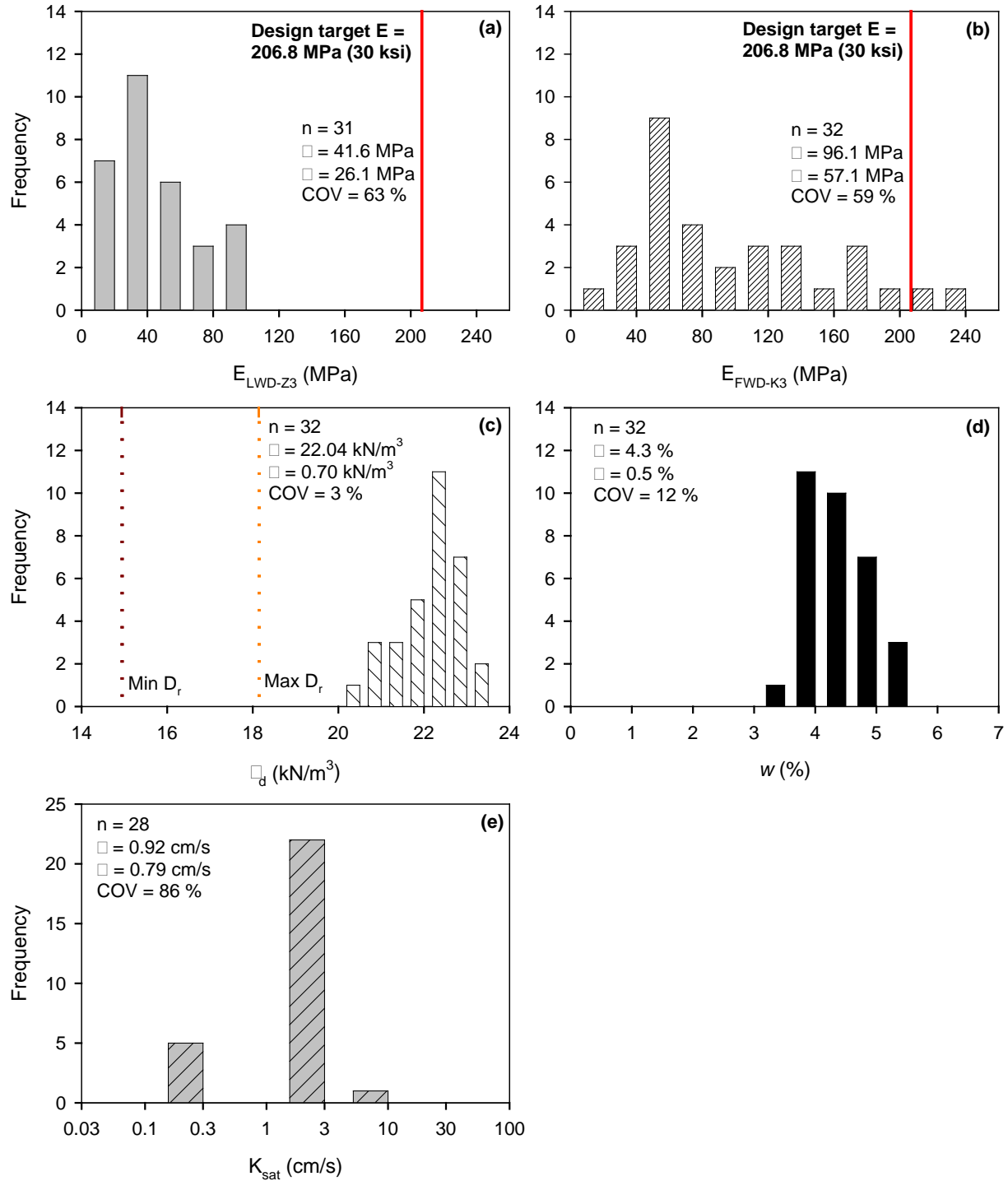
Figure 41. TB 2: Histograms of in situ test measurements (a) E_{LWD-Z3}, (b) E_{FWDK3}, (c) γ_d, (d) w, and (e) K_{sat}
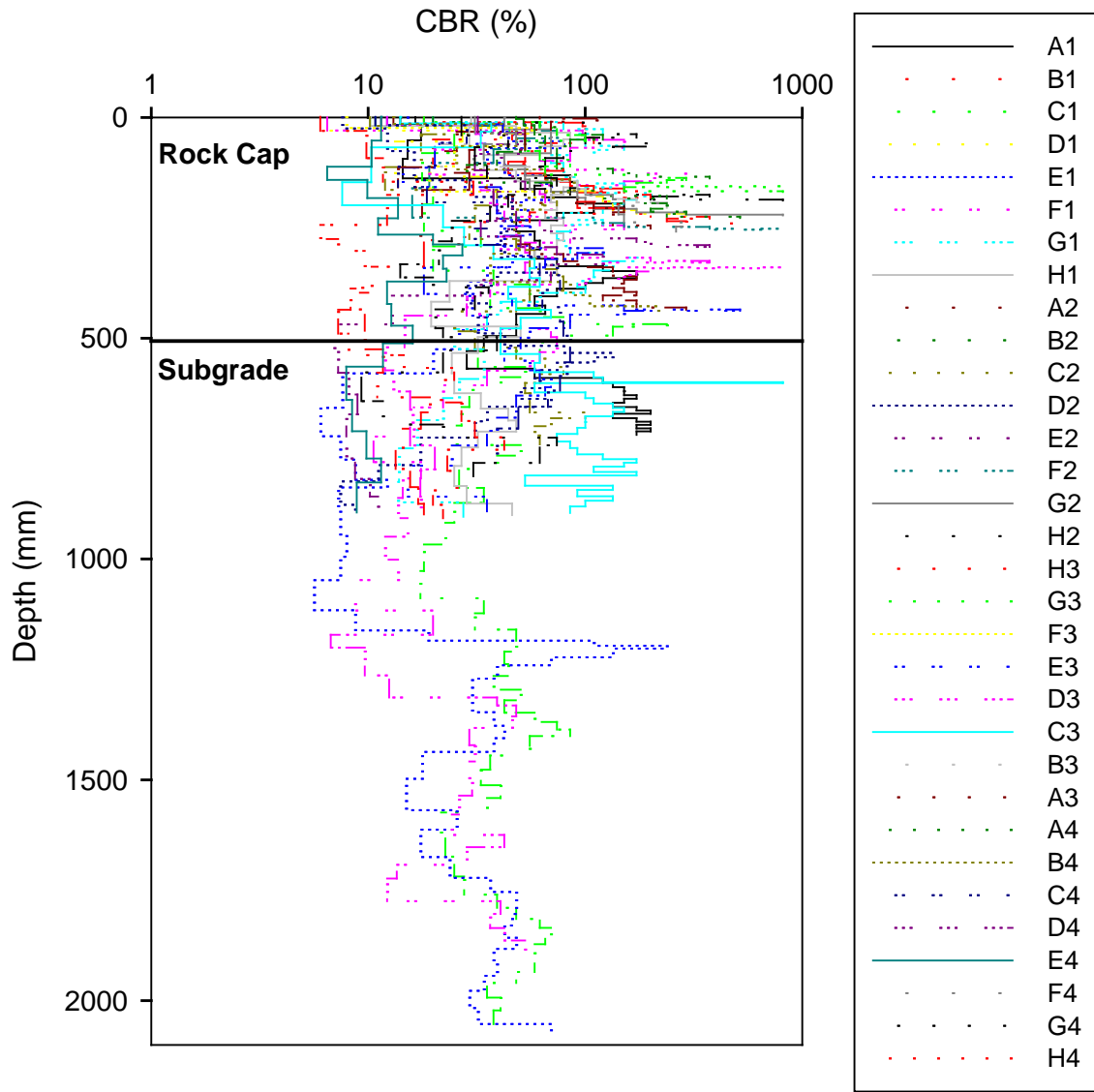
Figure 42. TB 2: DCP-CBR profiles along all four tracks in longitudinal direction

TB3: Asphalt Treated Base

The test bed area tested consisted of ATB subbase layer at the surface on the mainline and exposed leveling subbase layer in the shoulder Figure 43. This test bed was located on SR22 but at an adjacent project site near Blairsville, with similar design as in the Clyde project. The ATB layer was reportedly placed one day prior to testing. Field testing involved APT testing at 99 test locations in a dense grid pattern in an area of about 14 m by 14 m covering both ATB and the subbase layer in the shoulder. FWD tests were conducted at 48 test locations covering only a portion of the ATB layer across the pavement width and a portion of the shoulder area. The test point locations are identified in Figure 44.

Figure 43. TB 3: Picture of the test bed area
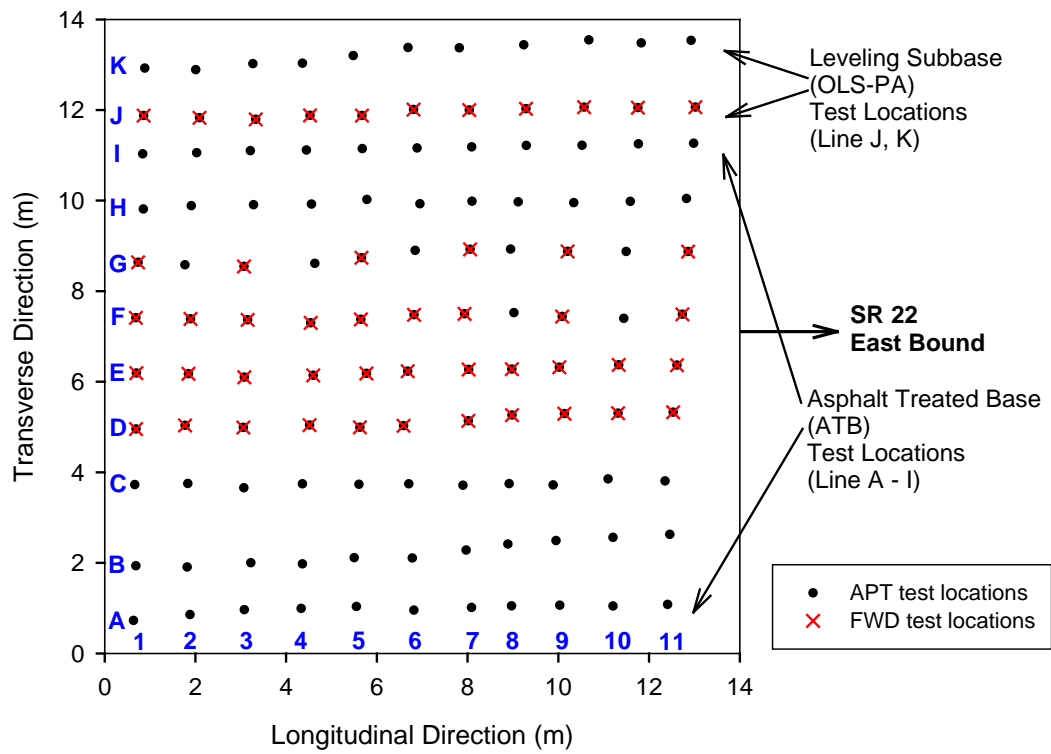
Figure 44. TB 3: Local coordinates of in situ test locations

Results from FWD testing with composite elastic moduli values (E_{FWD-K3}), and back-calculated subgrade (E_{SG}) and subbase layer (E_{SB}) moduli values are shown in Figure 45. Histogram plots of these measurement values along with univariate statistics are included in Figure 46. Both corrected and uncorrected E_{SG} values are included in the figures. The design target moduli values are included the figure for comparison. Note that the composite modulus values also equals 206.8 MPa because both E_{SB} and E_{SG} layers are assumed as 206.8 MPa. The back-calculation was performed to calculate the E_{SB} values for the 76. 2 mm (3 in.) thick ATB layer.
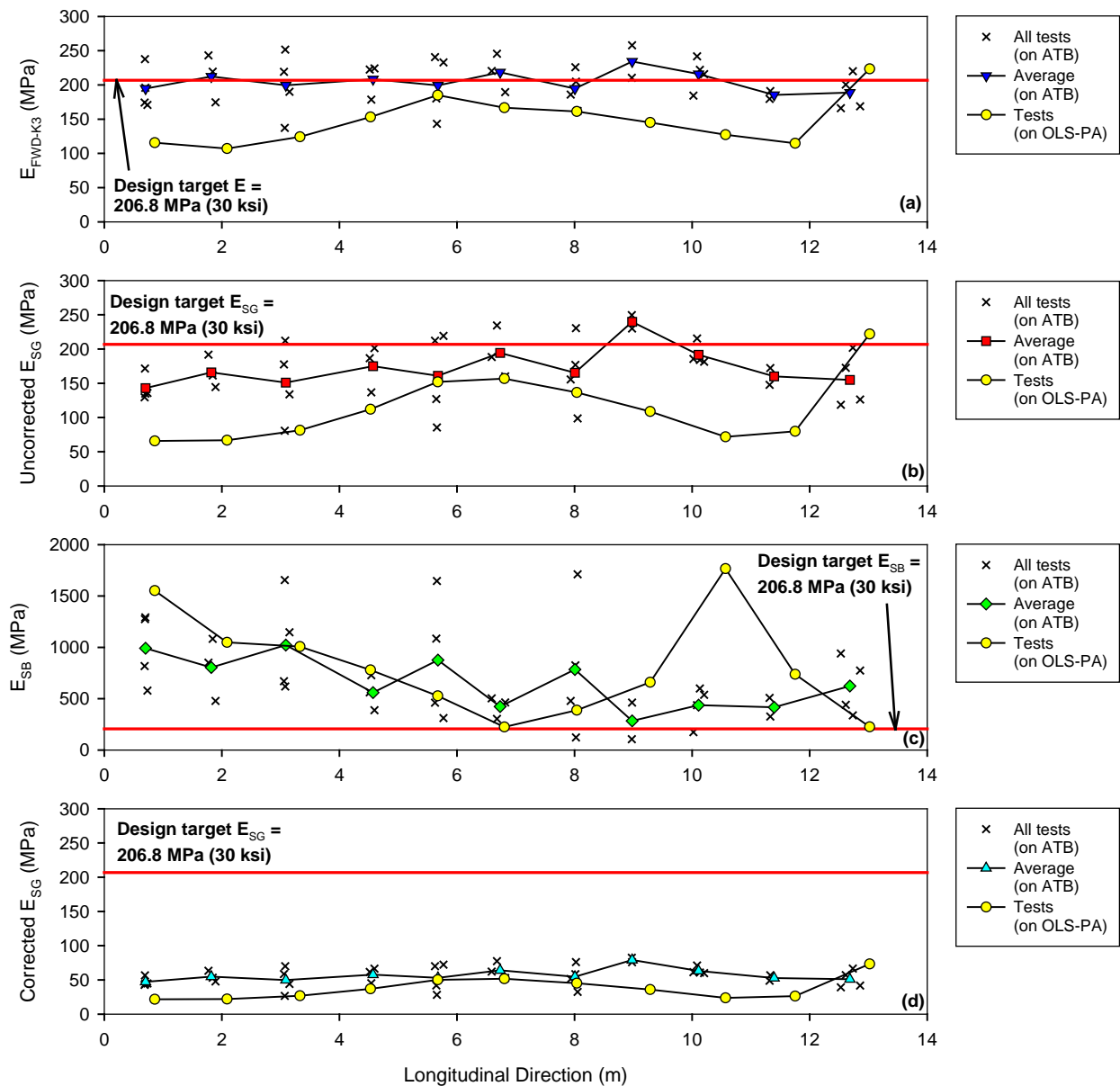
Figure 45. TB 3: In situ test results (a) E$_{FWDK3}$, (b) Uncorrected E$_{SG}$, (c) E$_{SB}$, and (d) Corrected E$_{SG}$ along an about 13 m test section in longitudinal direction
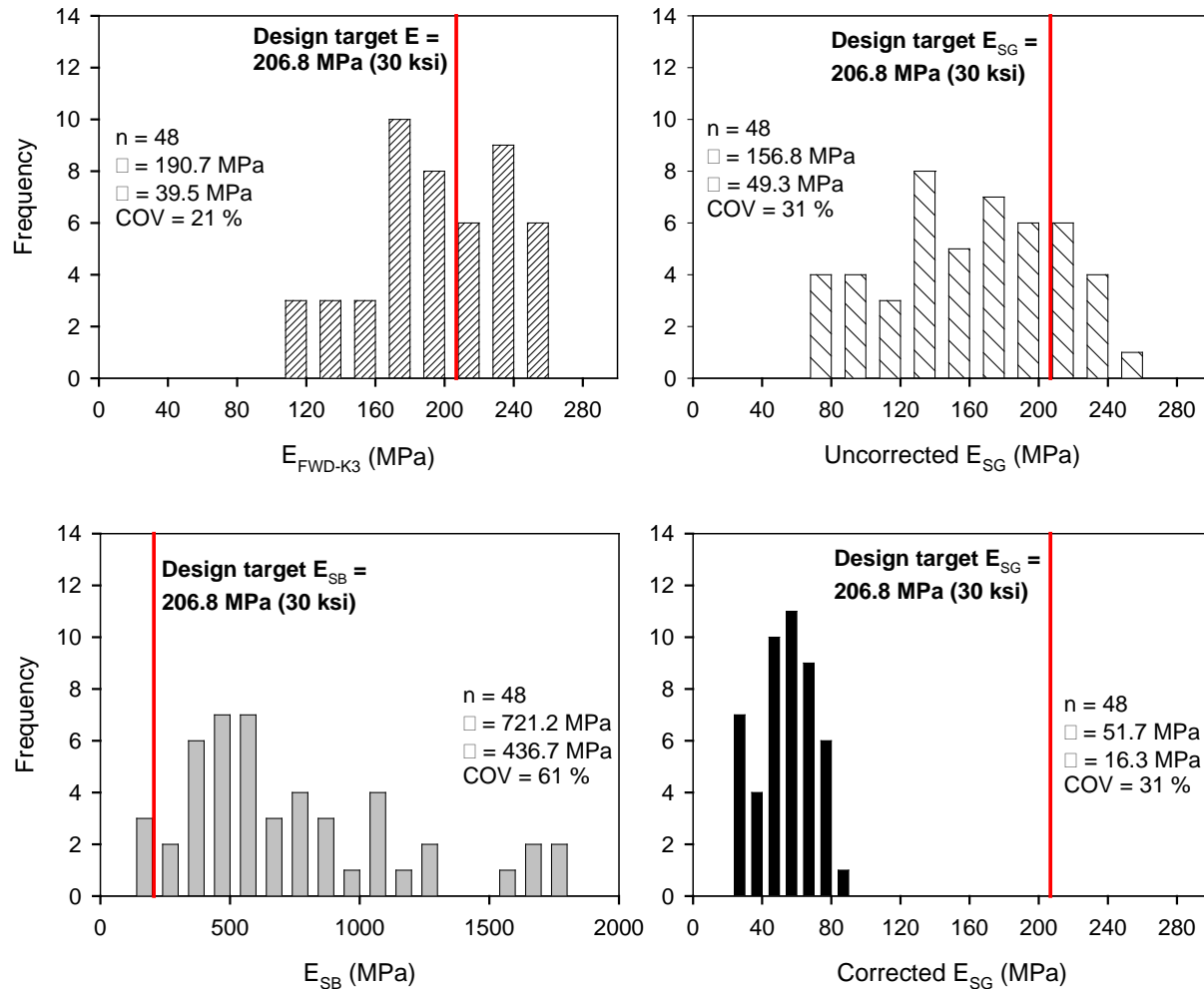
Figure 46. TB 3: Histograms of in situ test measurements (a) E$_{FWDK3}$, (b) Uncorrected E$_{SG}$, (c) E$_{SB}$, and (d) Corrected E$_{SG}$

The FWD test results indicated that the composite modulus values showed an average of about 191 MPa, which is about 1.1 times lower than the design assumed value of 206.8 MPa. The back-calculated uncorrected E$_{SG}$ showed an average of about 157 MPa, which is about 1.3 times lower than the design assumed E$_{SG}$ of 206.8 MPa. The back-calculated E$_{SB}$ of the ATB layer, however, was 3.5 times higher than the design E$_{SB}$ of 206.8 MPa.

The corrected E$_{SG}$ value is more representative of a future saturated condition and is not representative of the current conditions, so therefore is only shown here as a reference and is not used in comparison. Also, the rock cap layer consisted of granular material and is not anticipated to have such a reduction as was assumed in the case of cohesive soils in AASHTO (1993) in developing the corrections.

APT measurements were obtained at various combinations of $P_{o(g)}$ and Q measurements over a range of 5 to 75 mm of H_2O and 200 to 7500 cm^3/s, respectively. An average K_{sat} was calculated for different combinations of $P_{o(g)}$ and Q at each test location.

Using APT test results on the ATB layer and the granular subbase layer from a dense grid pattern, spatial contour maps, semivariogram plots with spatial statistics, histogram plots with univariate statistics of K_{sat} are included in Figure 47. A summary of univariate and spatial statistics of K_{sat} measurements are also summarized in Figure 47.

The ATB layer and leveling base layer contained different ranges of K_{sat} thus presenting non-stationary conditions; therefore, the two areas were separately modeled in the semivariogram analysis. Kriged contours are generated separately for the two areas using the respective semivariogram models and then combined as presented in Figure 47.

APT tests yielded an average K_{sat} of about 4.6 cm/s in the ATB layer and 0.16 cm/s in the leveling subbase layer.
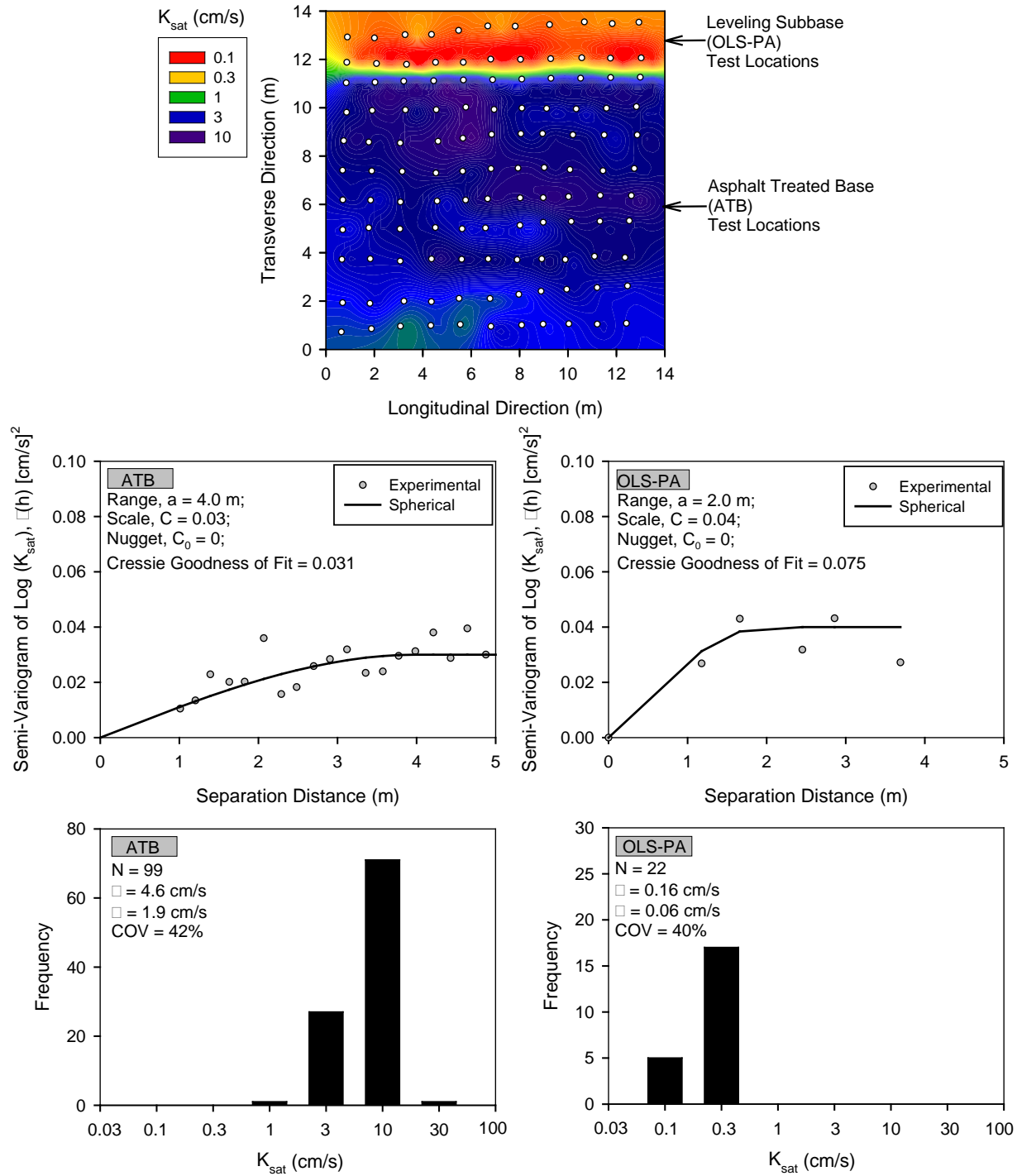
Figure 47. TB3: Kriged spatial contour map (top), semivariogram (middle), and histogram (bottom) plots of K$_{sat}$ measurements [left semi-varaiogram and histogram plots represent measurements on the ATB layer and the right plots represent measurements on the granular subbase layer]

TB4: Cement Treated Base

The test bed area consisted of CTB layer at the surface on connected shoulder lanes of the eastbound and westbound lanes (Figure 48), between Sta. 475+00 and 481+00. The eastbound lane CTB on the left side of the picture in Figure 48 was constructed in summer 2009 while the westbound lane base layer on the right side of the picture in Figure 48was constructed in fall of 2008. A portion of the westbound lane base layer was contaminated with washed out fines as can be seen in the bottom portion of Figure 48.

Figure 48. TB 4: Picture of the test bed area (left side of the black line shows the N [North] area and the right side shows the S [South] area of the test bed)

Field testing involved obtaining FWD and nuclear gauge moisture and dry density tests approximately every 8 m along the middle of both eastbound and west bound shoulder lanes at 20 locations along each lane. The test point locations are identified in Figure 49 and this testing is identified as TB4A. In addition, a 5 m x 9 m portion near the middle of this test bed, APT

measurements and moisture-dry unit weight measurements using nuclear gauge were obtained at 63 test locations. The test area with APT testing is referred to as TB4B.
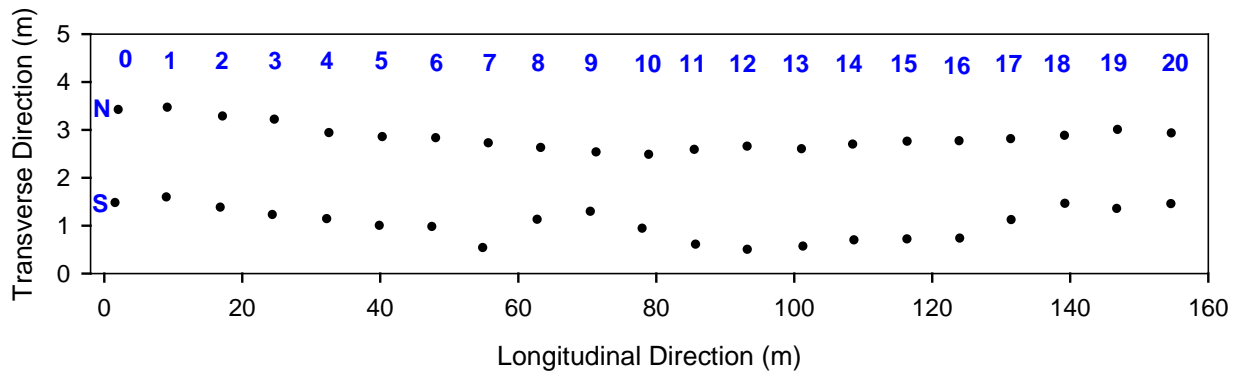
Figure 49. TB 4A: Local coordinates of in situ test locations on CTB

Results from FWD testing with composite elastic moduli values (E_{FWD-K3}) and moisture and dry desnity from NG are presented in Figure 50. The back-calculated subgrade (E_{SG}) and subbase layer (E_{SB}) moduli values are shown in Figure 51. Histogram plots of these measurement values along with univariate statistics are included in Figure 52. Both corrected and uncorrected E_{SG} values are included in the figures. The design target moduli values are included the figure for comparison. The back-calculation was performed to calculate the E_{SB} values for the 76.2 mm (3 in.) thick CTB layer.

Results from DCP testing are shown in Figure 53. DCP tests were conducted by drilling a hole in the CTB layer down to the top of the underlying leveling subbase layer. Results indicated that the CBR of the subbase layer/rock cap layer and the subgrade layer was variable. CBR in these layers ranged between 8 and 100.

The FWD test results indicated that the composite modulus values showed an average of about 153 MPa, which is about 1.35 times lower than the design assumed value of 206.8 MPa. The back-calculated uncorrected E_{SG} showed an average of about 70 MPa, which is about 3.0 times lower than the design assumed E_{SG} of 206.8 MPa. The back-calculated E_{SB} of the CTB layer, however, was 22 times higher than the design E_{SB} of 206.8 MPa.

The corrected E_{SG} value is more representative of a future saturated condition and is not representative of the current conditions, so therefore is only shown here as a reference and is not used in comparison. Also, the rock cap layer consisted of granular material and is not anticipated to have such a reduction as was assumed in the case of cohesive soils in AASHTO (1993) in developing the corrections.
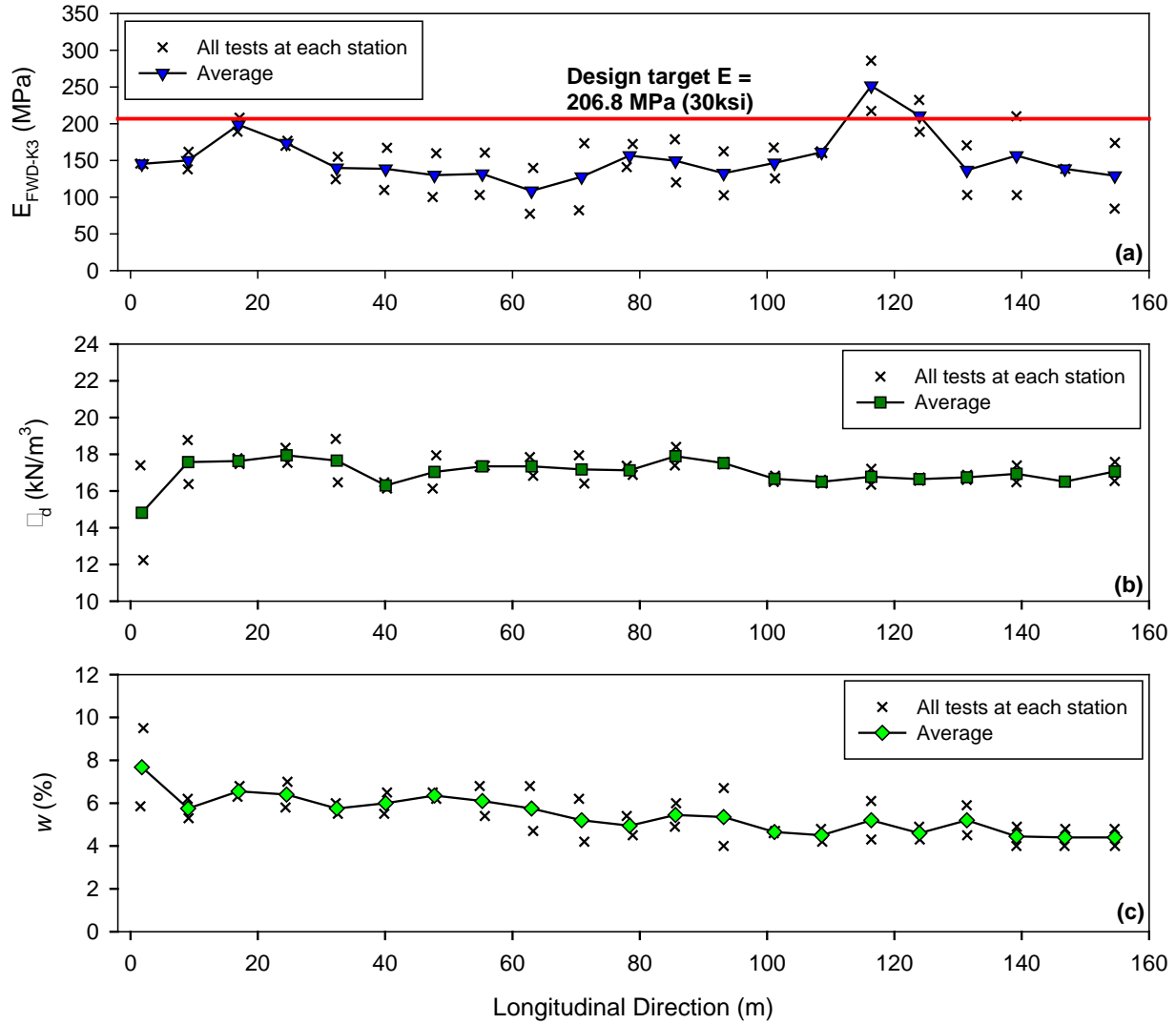
Figure 50. TB 4A: In situ test results (a) E$_{FWDK3}$, (b) γ_d, and (c) w along an about 160 m test section in longitudinal direction on CTB
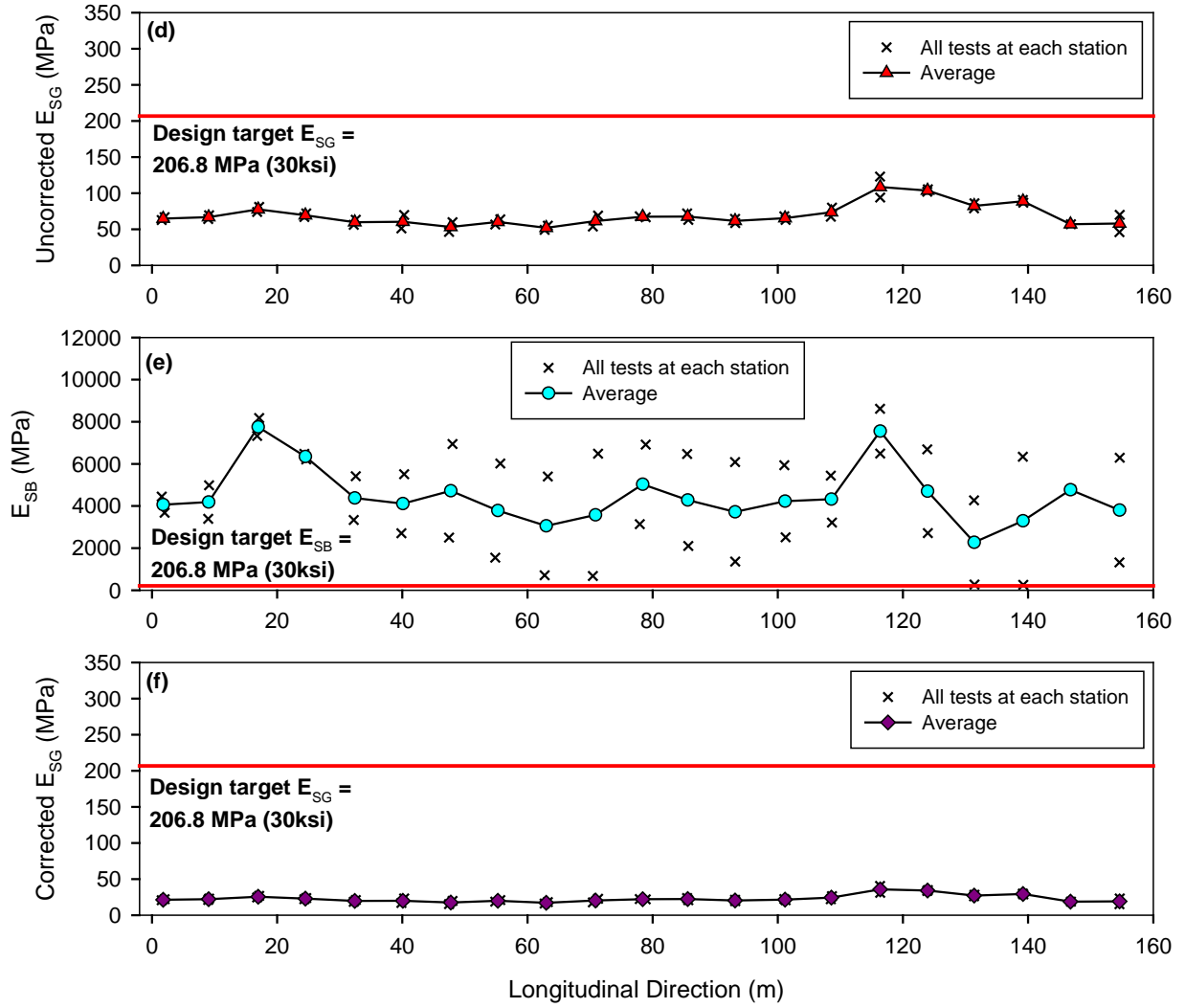
Figure 51. TB 4A: In situ test results (d) Uncorrected E$_{SG}$, (e) E$_{SB}$, and (f) Corrected E$_{SG}$ along an about 160 m test section in longitudinal direction on CTB
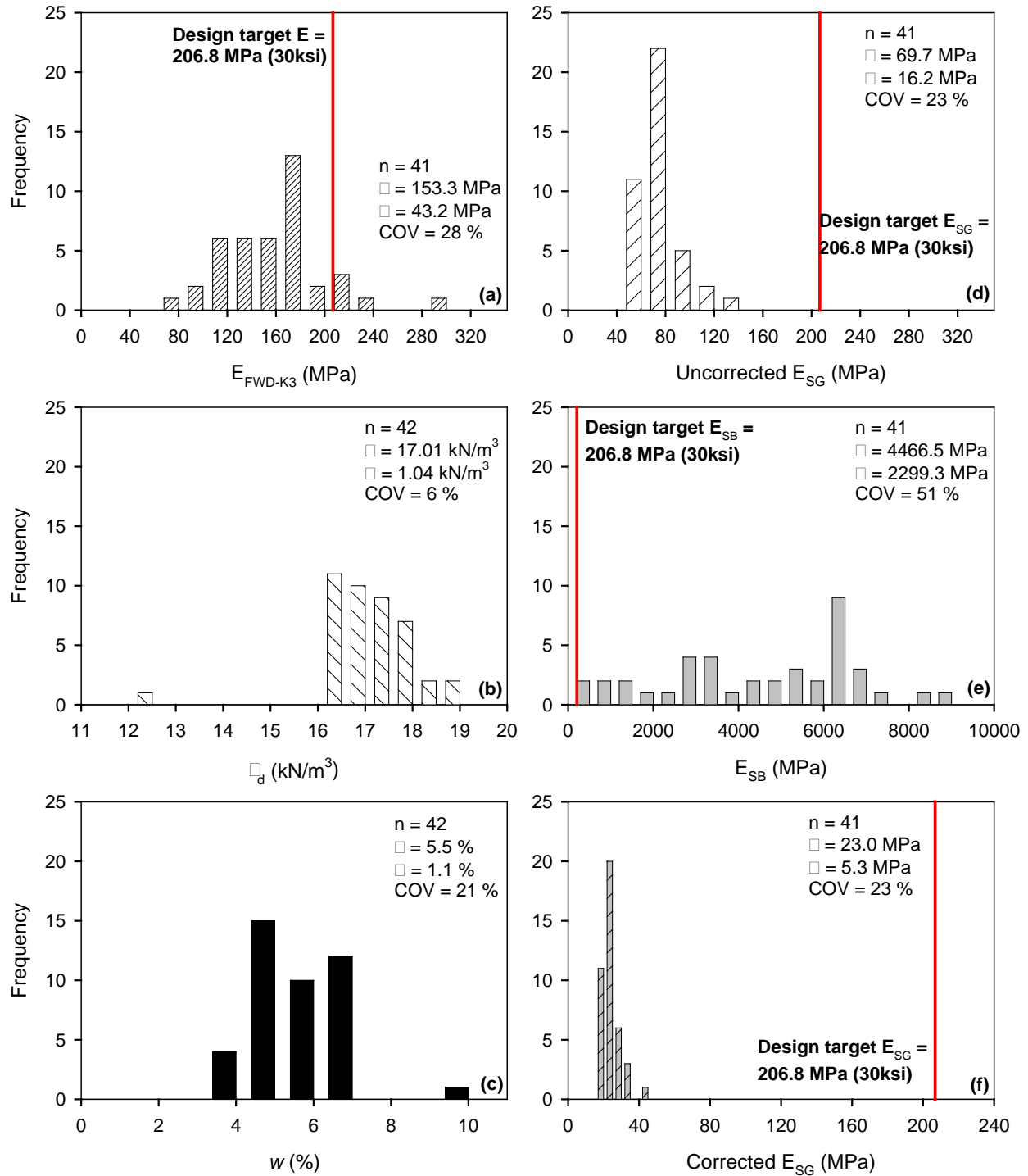
Figure 52. TB 4A: Histograms of in situ test measurements (a) E_{FWDK3}, (b) γ_d, (c) w, (d) Uncorrected E_{SG}, (e) E_{SB}, and (f) Corrected E_{SG}
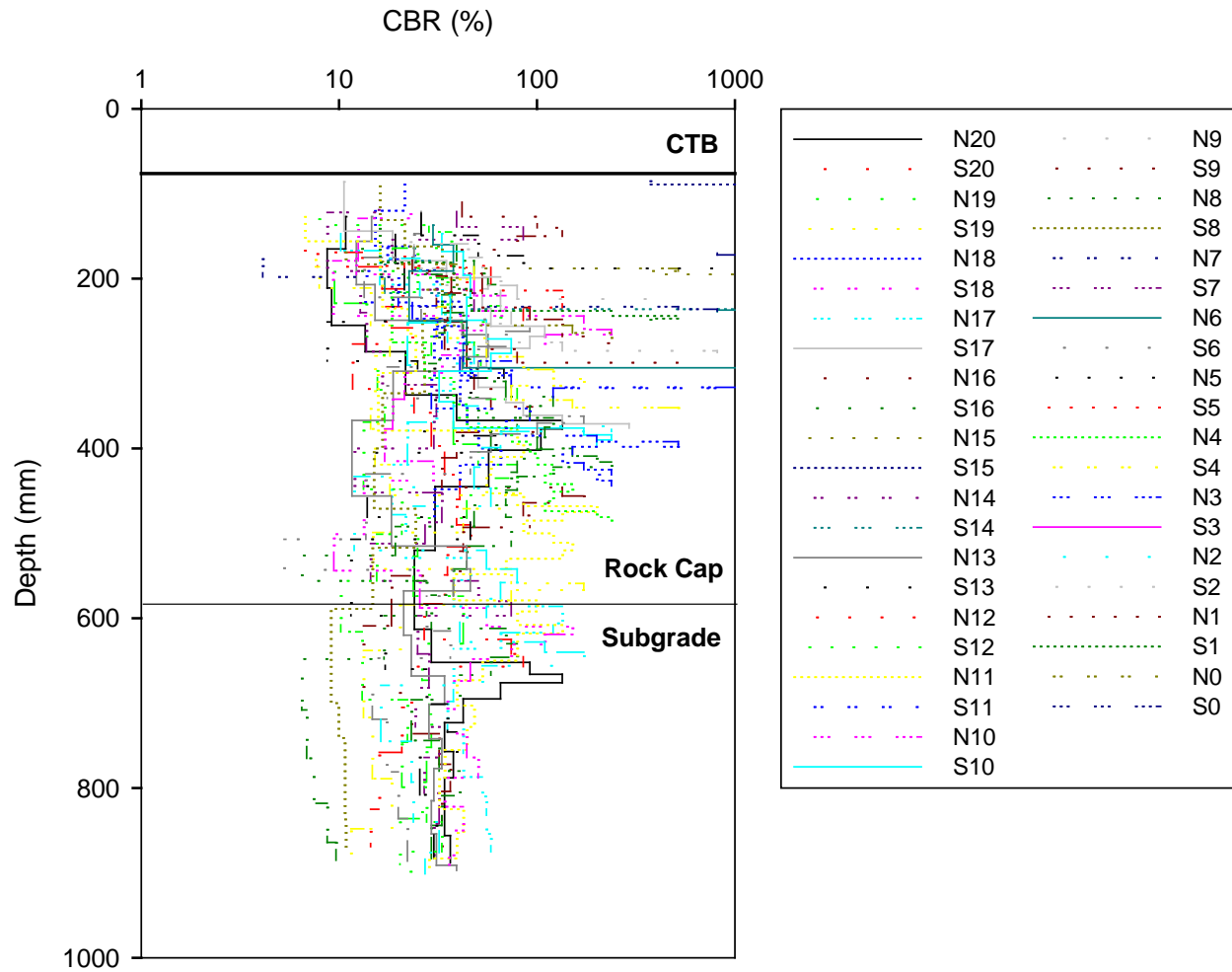
Figure 53. TB 4A: DCP-CBR profiles along two tracks in longitudinal direction

APT measurements were obtained in the TB4B area at various combinations of $P_{o(g)}$ and Q measurements over a range of 5 to 75 mm of H_2O and 250 to 7500 cm^3/s, respectively. An average K_{sat} was calculated for different combinations of $P_{o(g)}$ and Q at each test location. The 5 m x 9 m test area was divided in to Areas A and B. Area B consisted of CBT layer that was contaminated with fines, while Area A was relatively clean.

Spatial contour maps, semivariogram plots with spatial statistics, histogram plots with univariate statistics of K_{sat} are presented in Figure 54. Since the combined K_{sat} data obtained from Areas A and B is non-stationary, i.e., binomially distributed, the two areas were separately modeled in the semivariogram analysis. Kriged contours are generated separately for the two areas using the respective semivariogram models and then combined as presented in Figure 54.

APT tests in the ATB layer yielded an average K_{sat} of about 7.0 cm/s in Area A and 0.2 cm/s in Ara B.
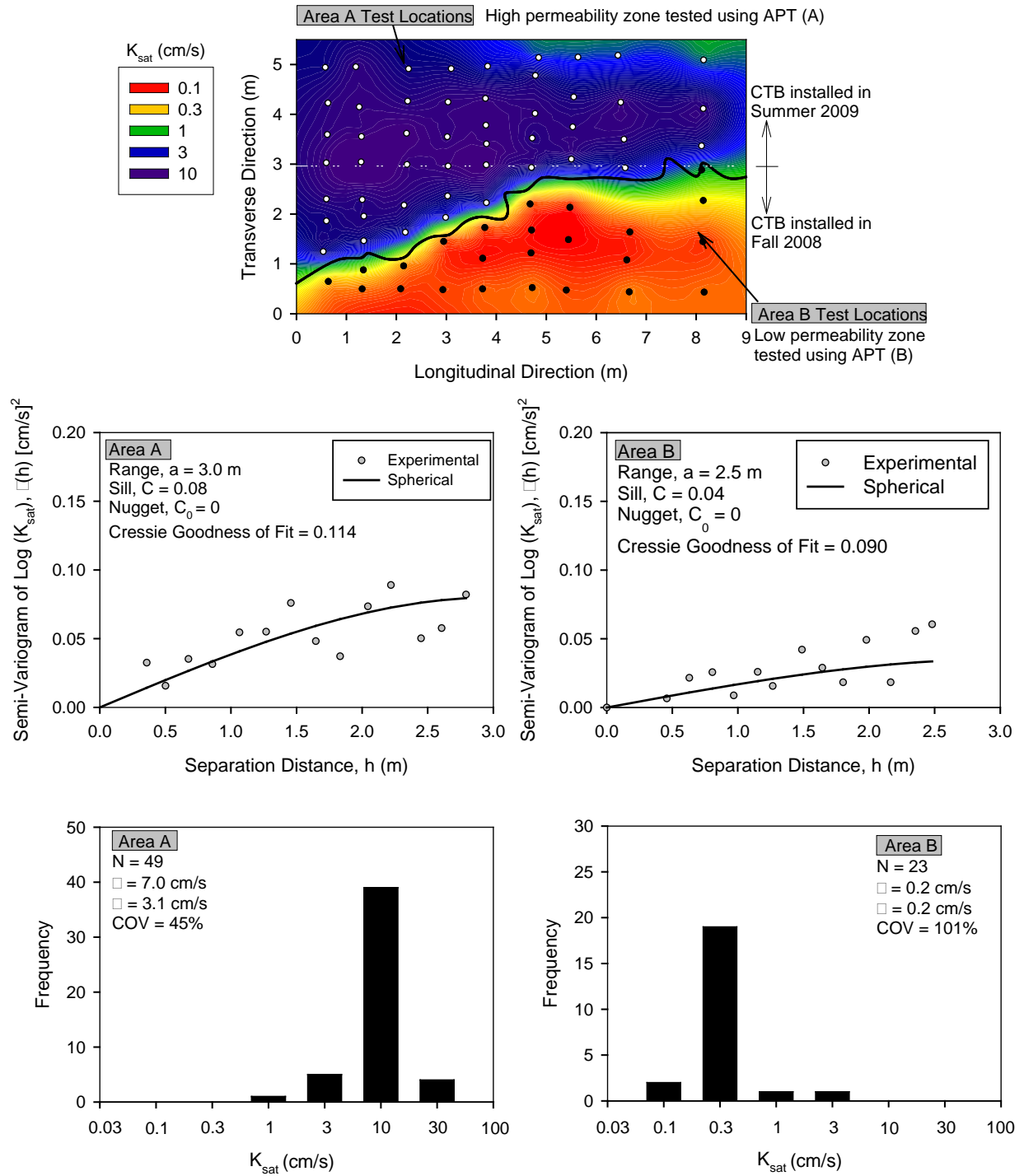
Figure 54. TB4B: Kriged spatial contour map (top), semivariogram (middle), and histogram (bottom) plots of K$_{sat}$ measurements

TB5: Rock Cap (Subgrade Treatment)

The test bed area was located between Sta. 377+00 and 379+00 and consisted of nominal 457 mm thick rock cap subgrade treatment layer placed over natural subgrade (Figure 55). The rock cap layer was placed and compacted prior to ISU testing. IC roller was first used on this TB to map the area with one roller pass and record CMV and MDP* values. After the mapping passes, NG, Dynatest LWD and FWD tests were conducted. Tests were conducted along three test lanes across width of the pavement as shown in Figure 56 at a total of 45 test locations. The center line of the test area corresponded to the centerline of the pavement.

Figure 55. TB 5: Picture of the test bed area
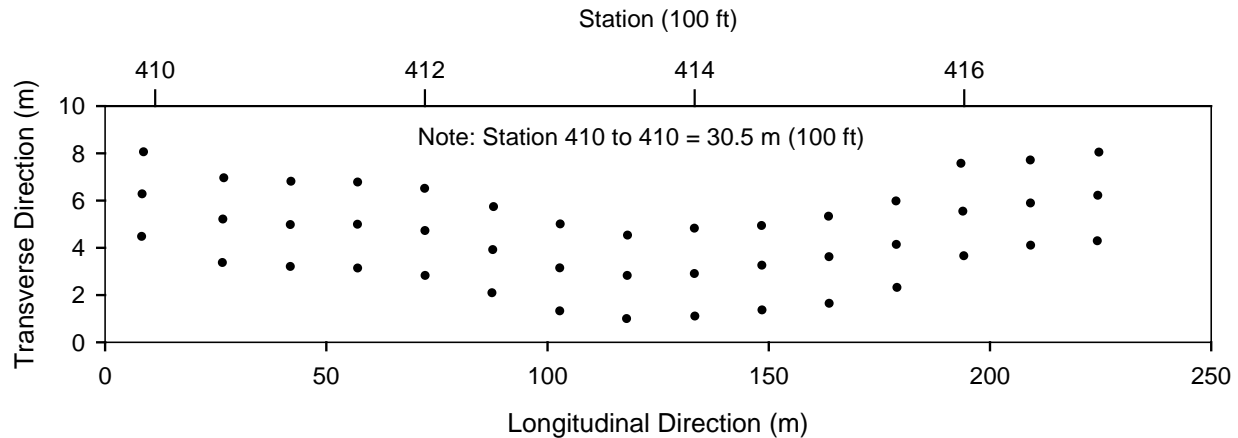
Figure 56. TB 5: Local coordinates of in situ test locations

The CMV and MDP* color-coded georeferenced maps are shown in Figure 57 and Figure 58, respectively. The GPS on the machine did not receive continuously receive RTK near this TB, because of presence of tall trees, which resulted in spotty data in the figures. A histogram plot of the measurements is also included in the figures. The results showed an average CMV of about 130 with coefficient of variation (COV) of about 17%, and average MDP* of about 137 with COV of about 4%. Both CMV and MDP* maps indicate higher values than observed on TB2.

Results from Dynatest LWD and FWD tests are presented as linear plots with distance in Figure 59 along with histograms of the measurement values and univariate statistics.

The LWD and FWD test results were used to measure the elastic moduli values and compare with the design assumed E_{SG} values (206.8 MPa or 30 ksi for rock cap). Results showed that moduli values obtained from the FWD test (E_{FWD-K3}) at 0.57 MPa applied stress, were on average 1.3 times higher moduli values obtained from the Dynatest LWD test at about 0.1 MPa applied stress. Moduli values obtained from both tests were on average higher than the design assumed E_{SG} of 206.8 MPa.
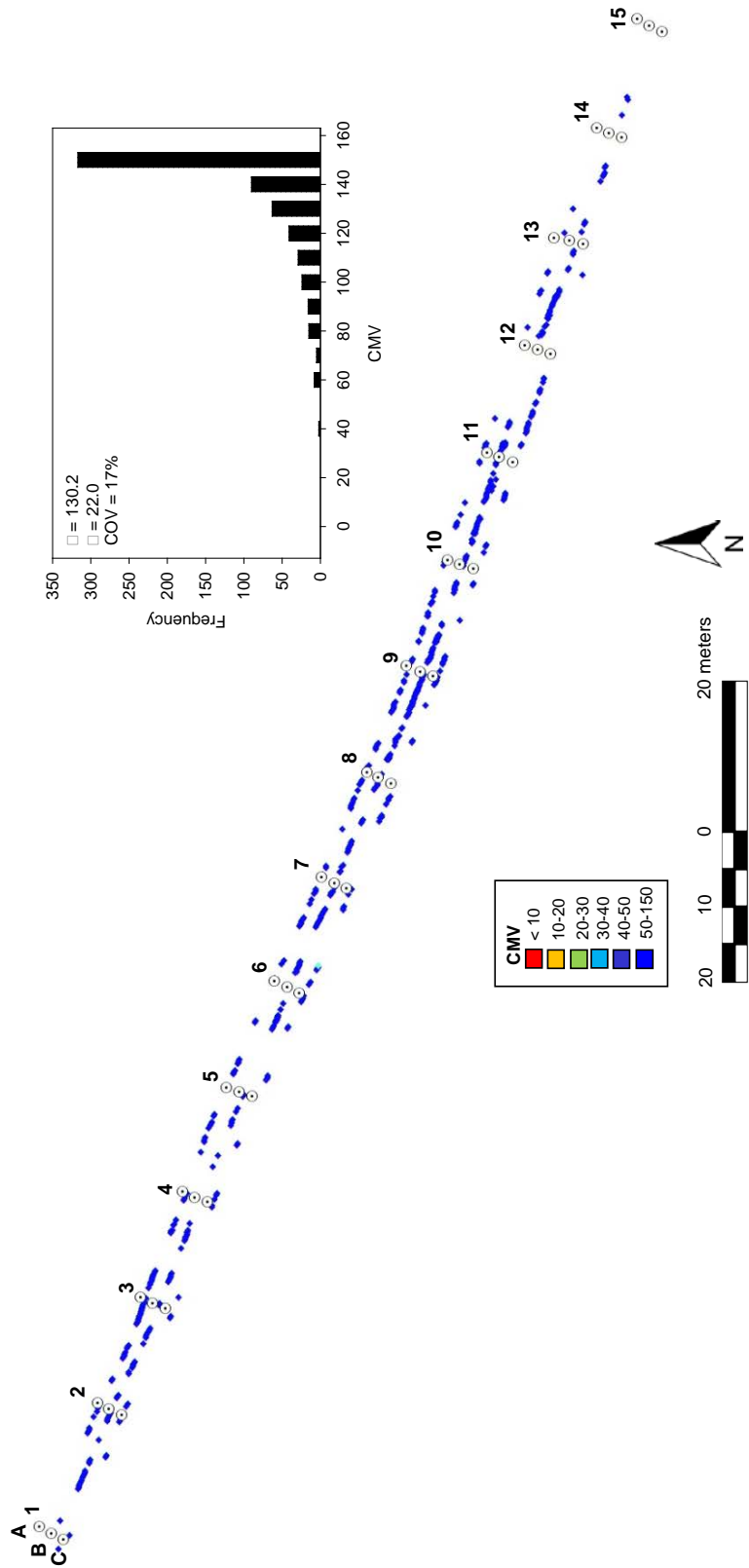
Figure 57. TB 5: Color-coded map of georeferenced CMV map
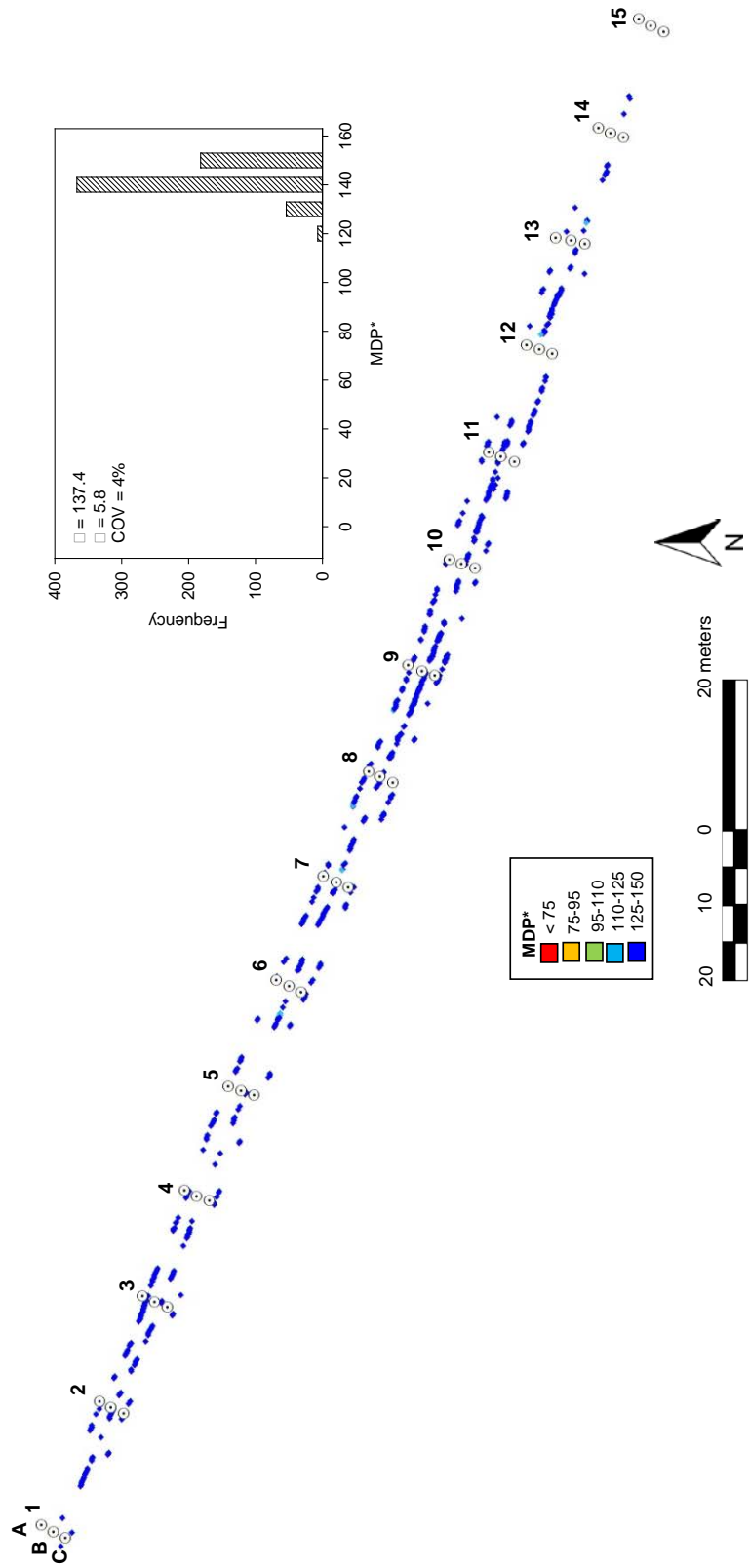
Figure 58. TB 5: Color-coded map of georeferenced MDP* map

65
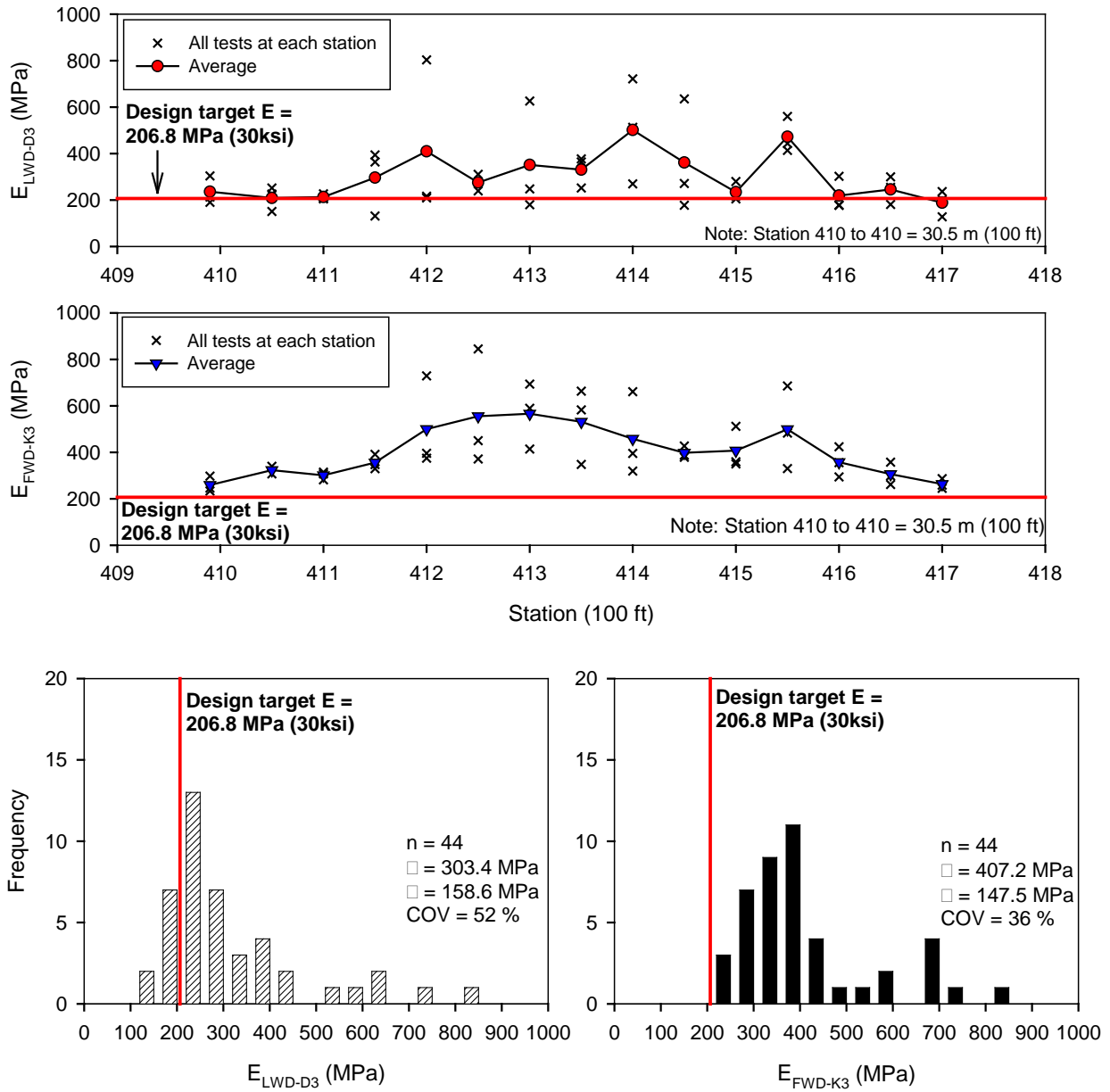
Figure 59. TB 5: Measurements of E_{LWD-D3} (top) and measurements of E_{FWD-K3} (middle) longitudinally along the test section, histogram of E_{LWD-D3} (bottom left), and histogram of E_{FWD-K3} (bottom right) of the measurements

TB6: General Fill Subgrade

The test bed area consisted of general subgrade fill material that was placed and compacted just prior to testing and was located between Sta. 377+00 and 397+00. The material was generally wet during testing. First, the IC roller was used to map the area in three roller lanes and then in situ point testing was conducted at 20 test locations along the middle lane. A picture of the IC

roller performing mapping pass is shown in Figure 60 and local coordinates of test locations along the test bed are shown in Figure 61. In situ testing included NG, DCP, and Zorn LWD.

Figure 60. TB 6: Picture of the test bed area during IC rolling
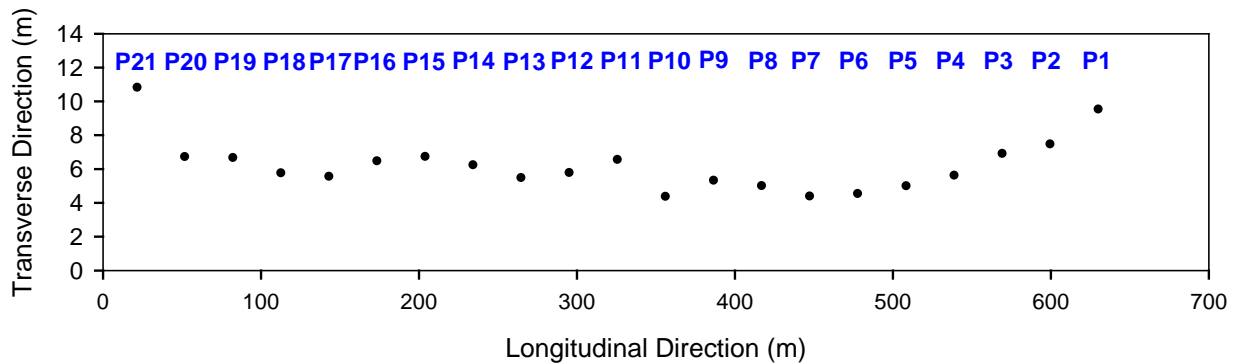

Figure 61. TB 6: Local coordinates of in situ test locations on subgrade

The CMV and MDP* color-coded georeferenced maps are shown in Figure 62 and Figure 63, respectively. A histogram plot of the measurements is also included in the figures. The results

showed an average CMV of about 47 with coefficient of variation (COV) of about 67%, and average MDP* of about 91 with COV of about 18%. The CMV and MDP* values measured on this TB were comparatively lower than measured in TB 2 (subbase) and TB5 (rock cap), as expected.

Results from LWD and NG tests are presented as linear plots with distance in Figure 65 and histograms of each measurement value with univariate statistics are presented in Figure 66.

DCP-CBR profiles are shown in Figure 42 for all test locations. At some test locations, the DCPs were terminated at shallow depths (< 0.5 m) due to refusal with presence of rock in the fill material. CBR values varied between 2 and 100, representing variable conditions in the fill material.

The LWD test results were used to measure the elastic moduli values. It must be noted that the E_{SG} value was assigned to the rock cap layer in the design and not the subgrade layer itself, as the rock cap layer was considered to be subgrade treatment. The design E_{SG} value is shown in Figure 64 for reference only. Results of Zorn LWD testing yielded an average elastic modulus of about 18.1 MPa in this TB with a COV of about 65%.

The NG test measurements were obtained with 304.8 mm (12 in.) measuring depth. In situ relative compaction values ranged from 91–105% of the maximum standard Proctor dry unit weight and in situ moisture values ranged from 3.7% below to 5.6% above standard Proctor optimum moisture content.
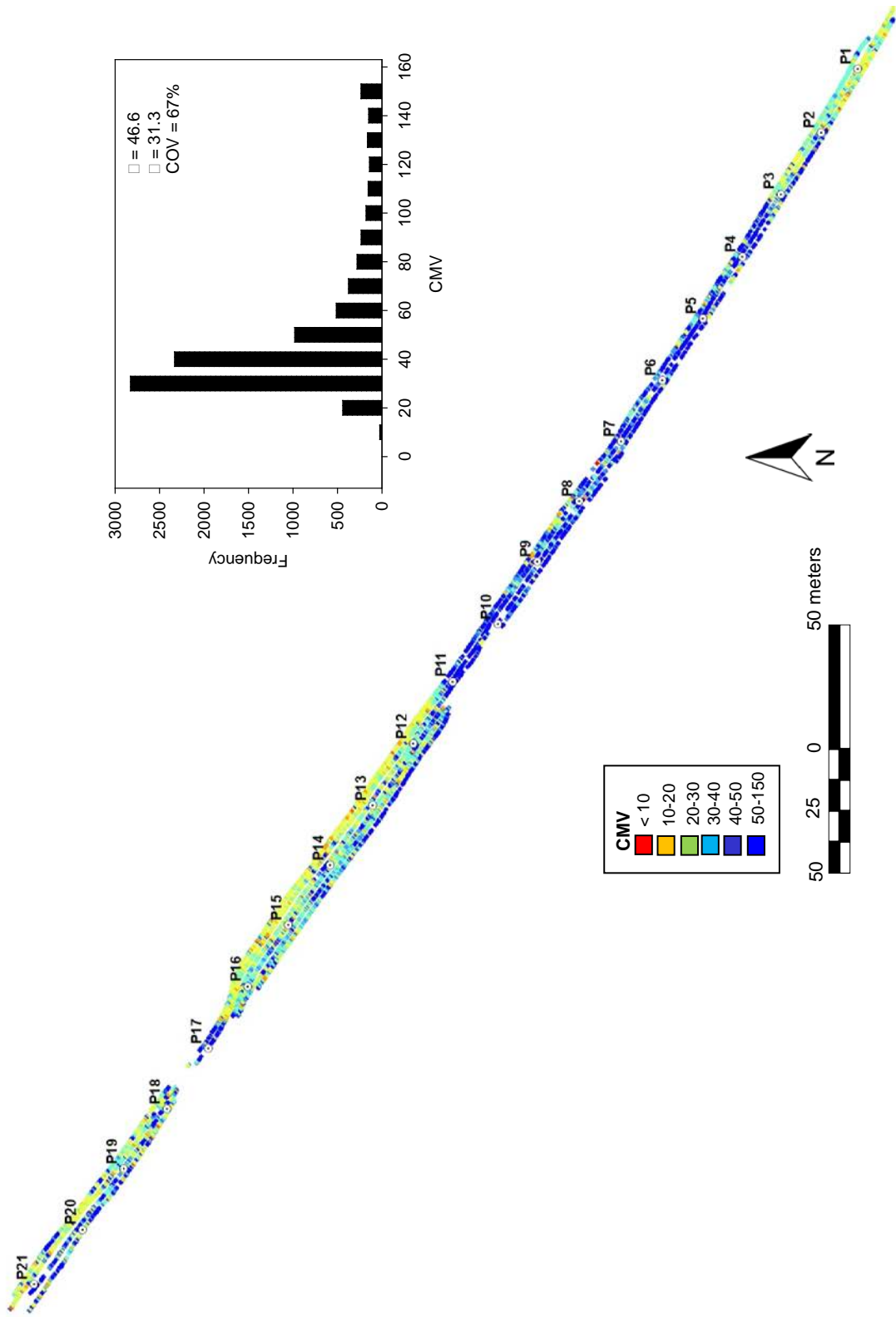
Figure 62. TB 6: Color-coded map of georeferenced CMV map
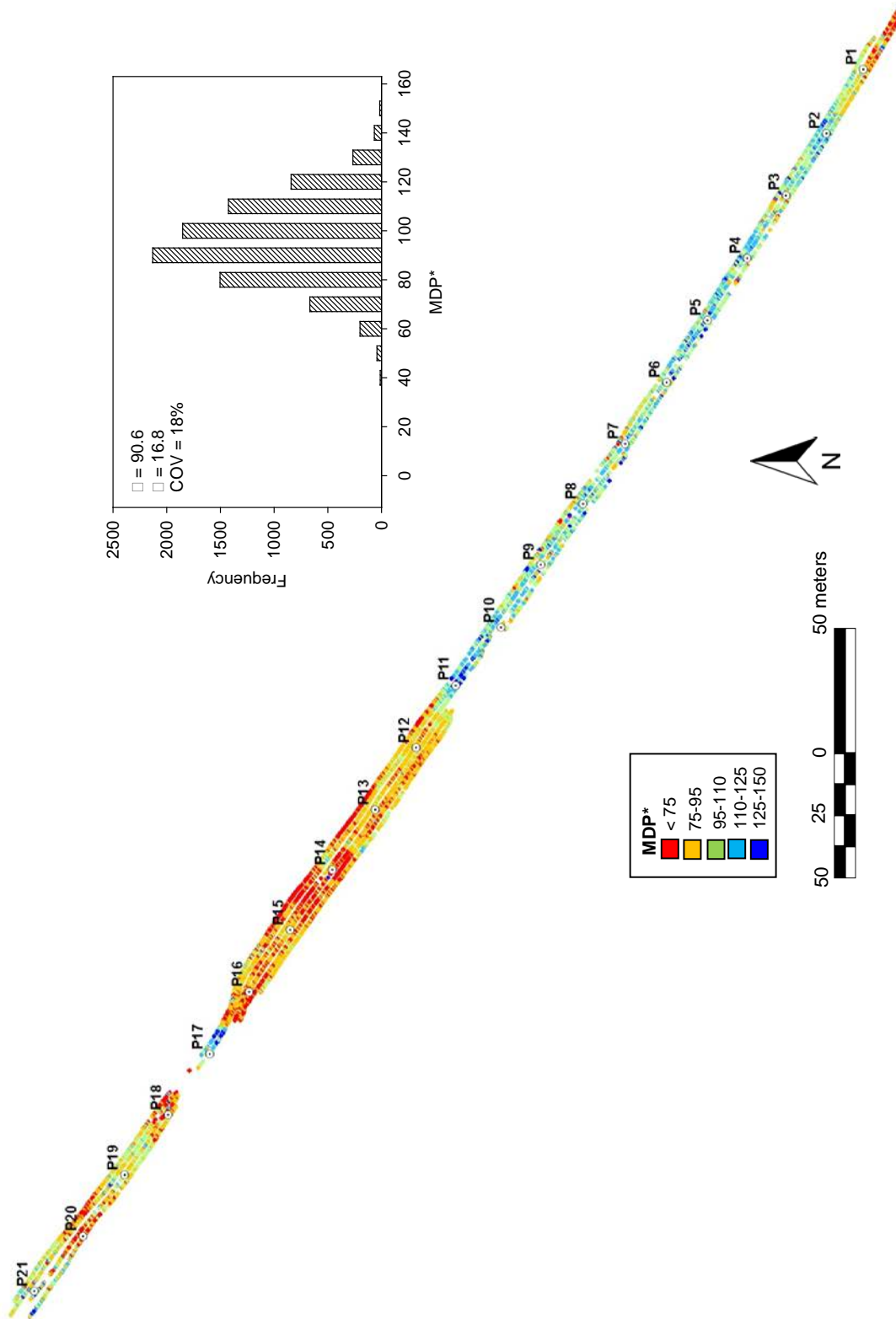
Figure 63. TB 6: Color-coded map of georeferenced MDP* map
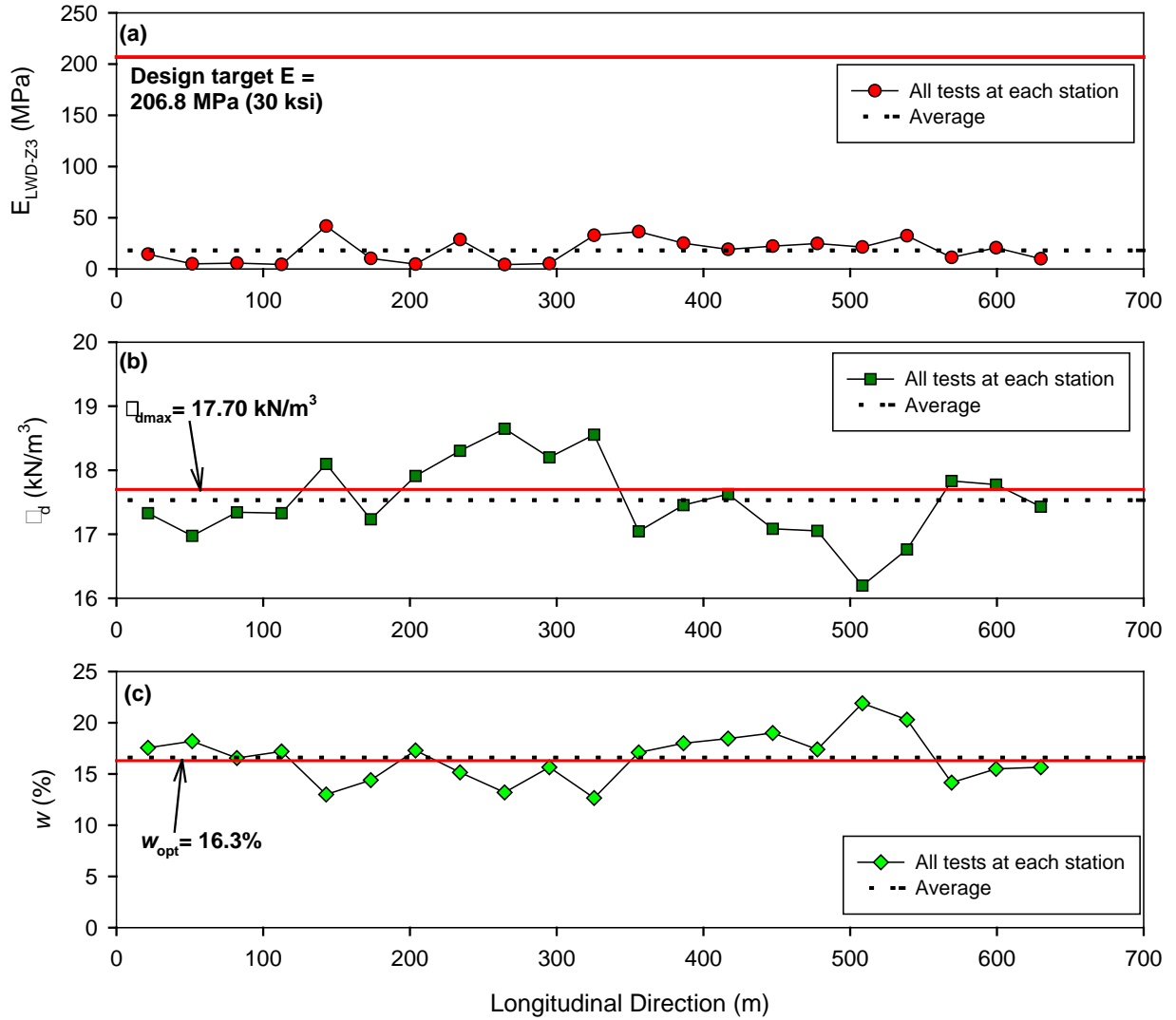
Figure 64. TB 6: In situ test results (a) E$_{LWD-Z3}$, (b) γ$_d$, and (c) *w* along an about 610 m test section in longitudinal direction
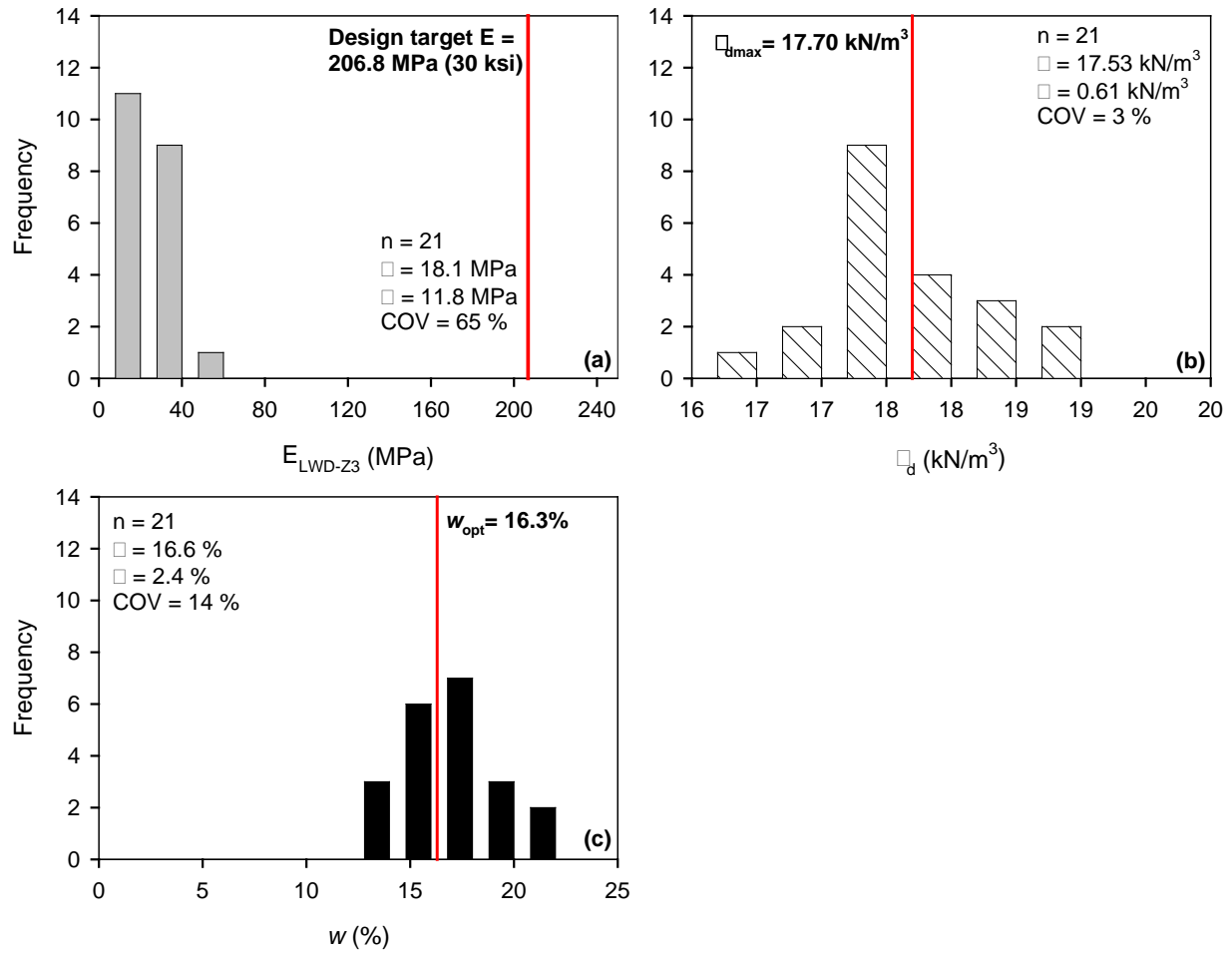
Figure 65. TB 6: Histograms of in situ test measurements (a) E$_{LWD-Z3}$, (b) γ_d, and (c) w
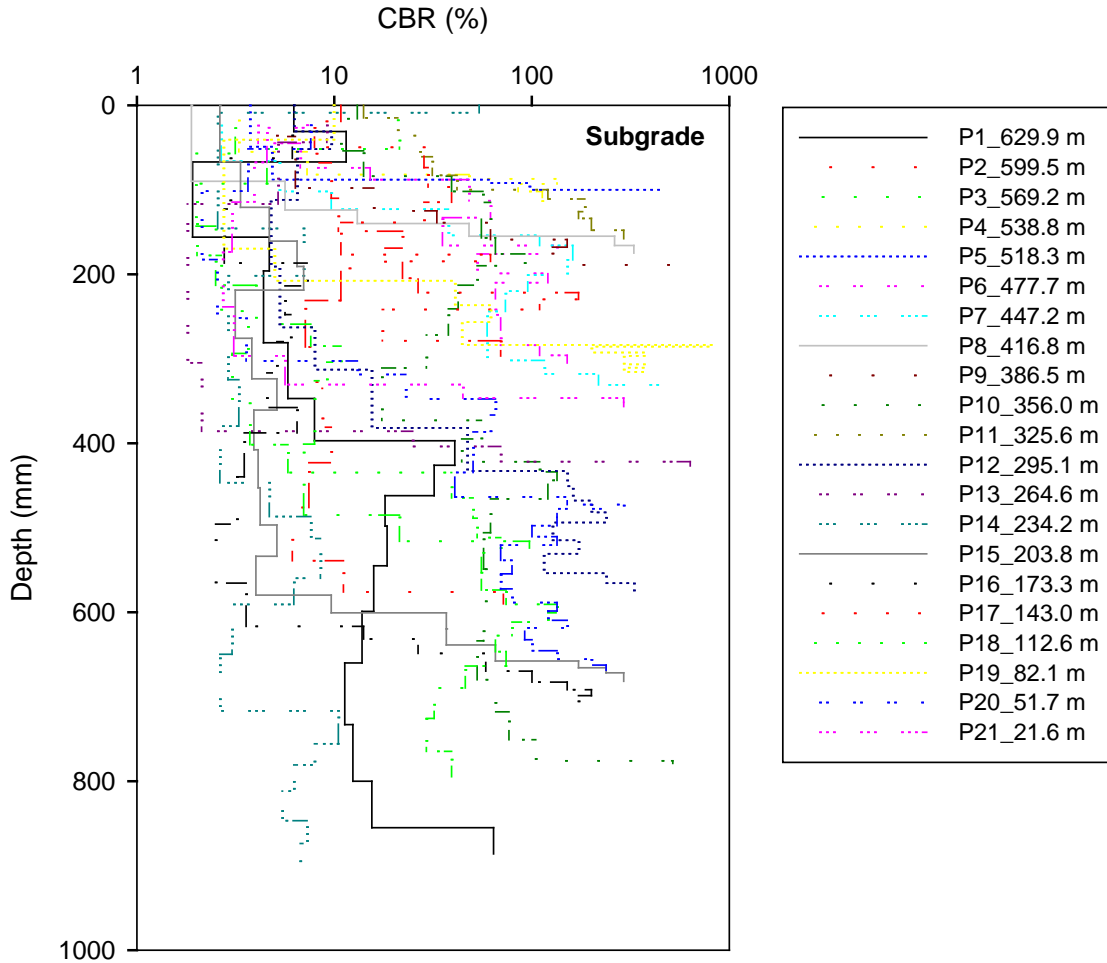
Figure 66. TB 6: DCP-CBR profiles along all four tracks in longitudinal direction

TB7: PCC Pavement Surface

This test bed was located between Sta. 475+00 and 481+00, and FWD tests were conducted on the PCC surface layer (Figure 67) that was placed 2-3 months prior to testing. Testing was conducted in two areas and are referred to in here as TB7A and TB7B.

In TB7A, testing was conducted in a dense grid pattern as shown in Figure 68. Tests were conducted in three testing lines – center of the panel, left edge near centerline longitudinal joint, and right and edge near shoulder longitudinal joint. Tests were conducted near transverse joints and near mid panels. The test grid layout is shown in Figure 68. A total of 90 tests were conducted over a 25 m x 5.5 m area, which included half of the inside lane and the full outside lane.

In TB7B, testing was conducted along the center of the outside lane near middle of each panel over a length of about 180 m. The test layout is shown in Figure 69.

Figure 67. TB 7: Picture of the test area
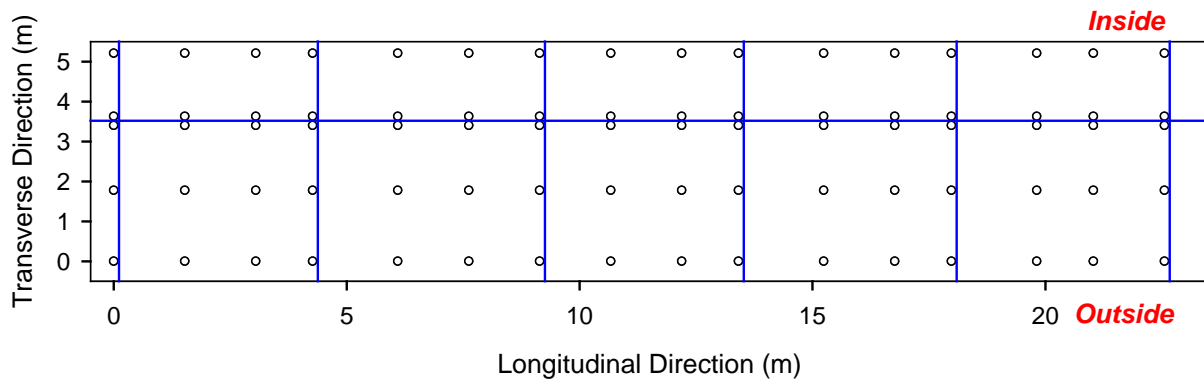
Figure 68. TB 7A: Local coordinates of in situ test locations on PCC [dense testing]
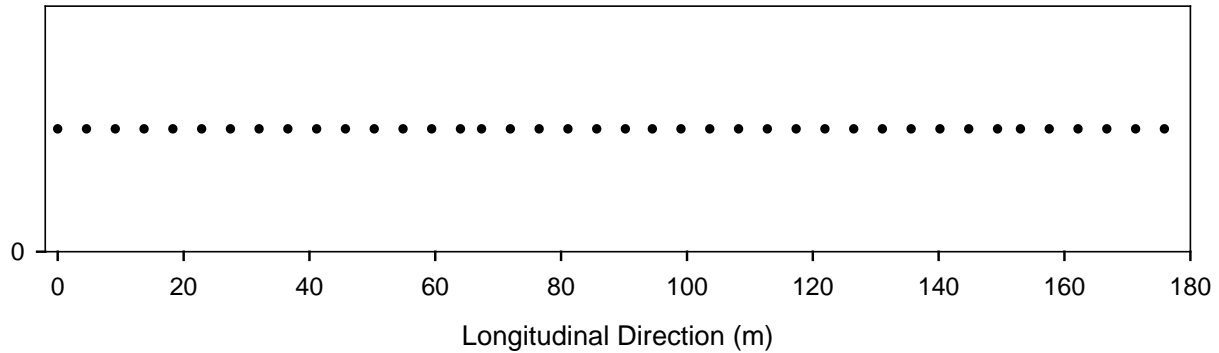
Figure 69. TB 7B: Local coordinates of in situ test locations on PCC [mid panel testing]

The data obtained from TB7A were analyzed using geostatistical analysis to characterize the spatial characteristics of the FWD deflection basin parameters (D_0, SCI, BCI, BDI, Area Factor, and Intercept) and modulus of subgrade reaction ($k_{FWD-Static-Corr}$) measurements. Kriged spatial contour maps, linear plots with actual measurement values along the pavement profile, semi-variograms, and histograms of each in situ point measurement are presented in Figure 70 to Figure 76. The spatial statistical parameters (i.e., scale (sill minus nugget), range, and nugget) are provided in the semivariogram plot of each figure.

Spatial contours of all FWD measurements except D0 and BDI did not show a definite spatial structure in the semi-varaiogram, which indicates that the variability in these measurements values was high over a short distance and requires a much denser spacing to capture the variability.

The results from TB7B are presented as linear plots in Figure 77 and Figure 78, and histograms of the measurements are presented in Figure 79 and Figure 80.

The results from TB7A and TB7B showed average $k_{FWD-Static-Corr}$ of about 75 kPa/mm and 91 kPa/mm. Recent experience with FWD testing on concrete pavements indicated that the $k_{FWD-Static-Corr}$ values are typically representative of the "weaker" layers down to about 2 m below the testing surface (White and Vennapusa 2014). The design k value used in this project is a composite value which is representative of the improvements performed above the "weak" subgrade layer and is therefore not used for comparison with the $k_{FWD-Static-Corr}$ values.
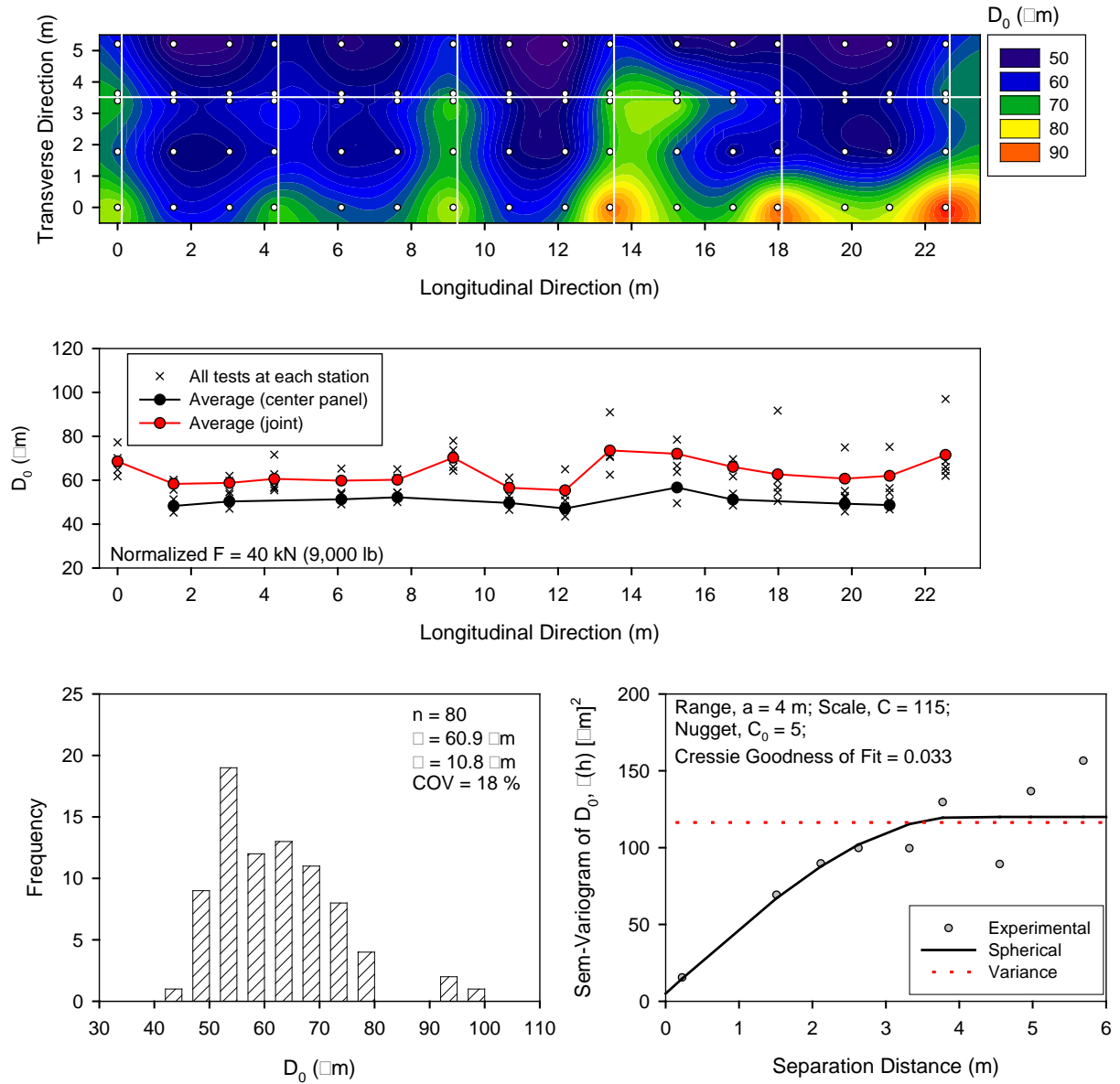
Figure 70. TB 7A: Kriged spatial contour map (top), measurements longitudinally along the test section (middle), histogram (bottom left), and semivariogram (bottom right) of D_0 measurements [dense testing]
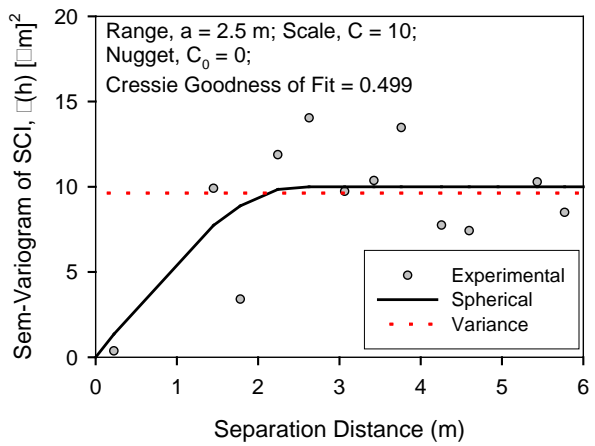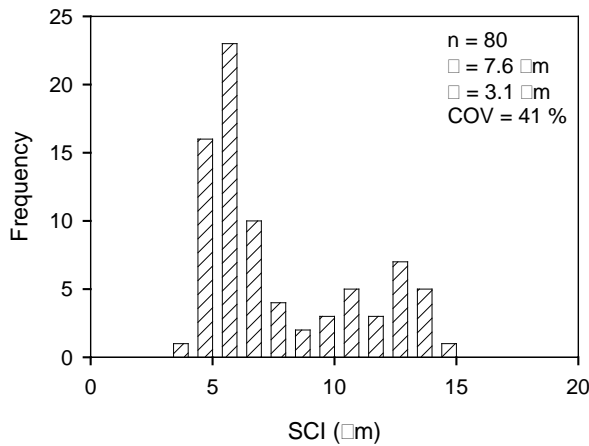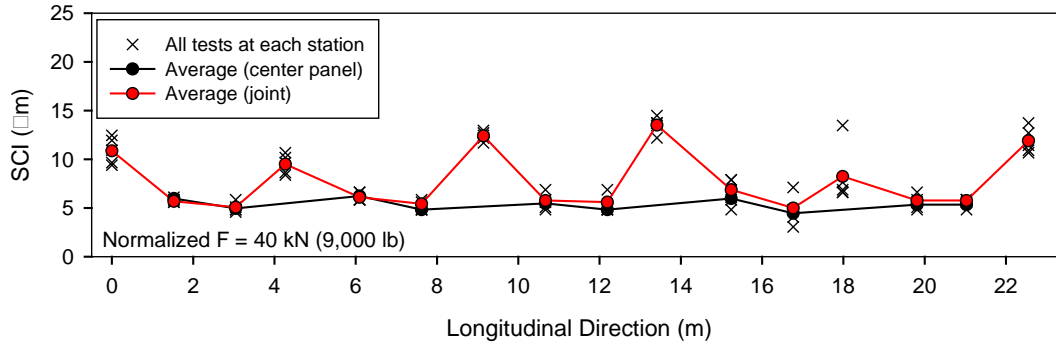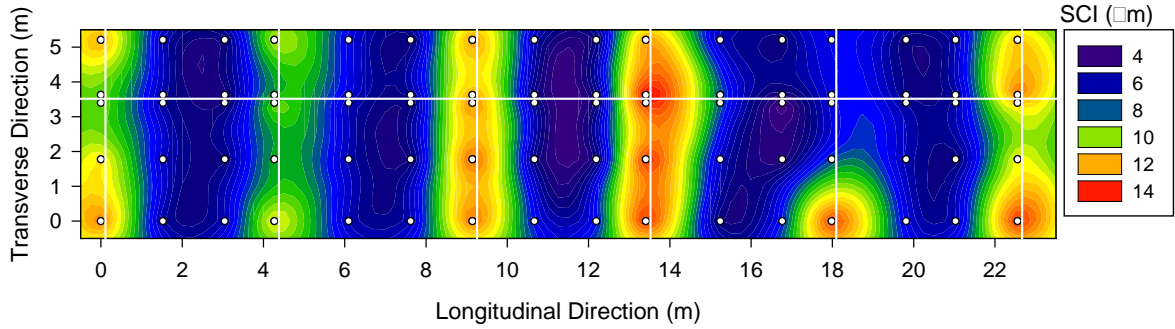
Figure 71. TB 7A: Kriged spatial contour map (top), measurements longitudinally along the test section (middle), histogram (bottom left), and semivariogram (bottom right) of SCI measurements [dense testing]
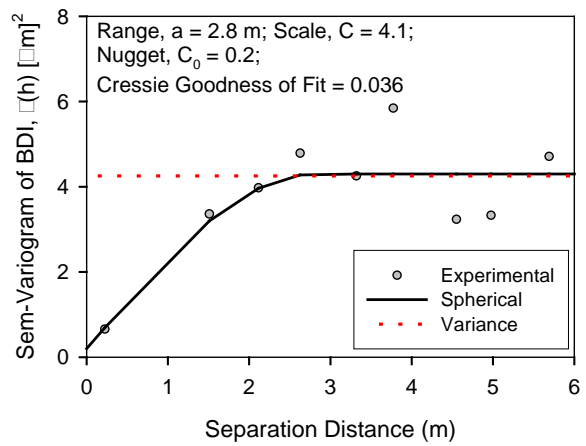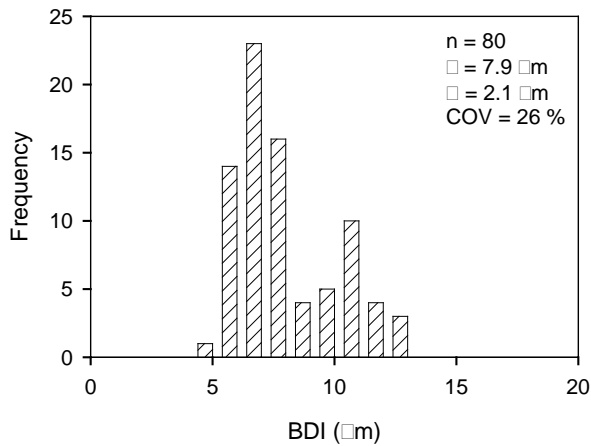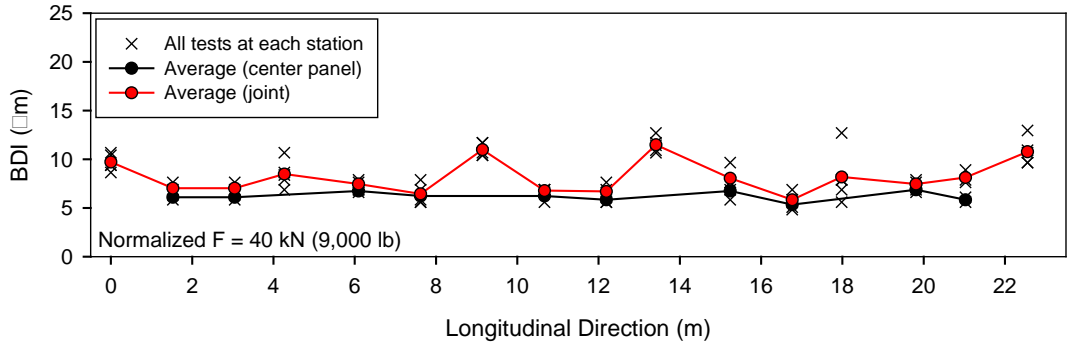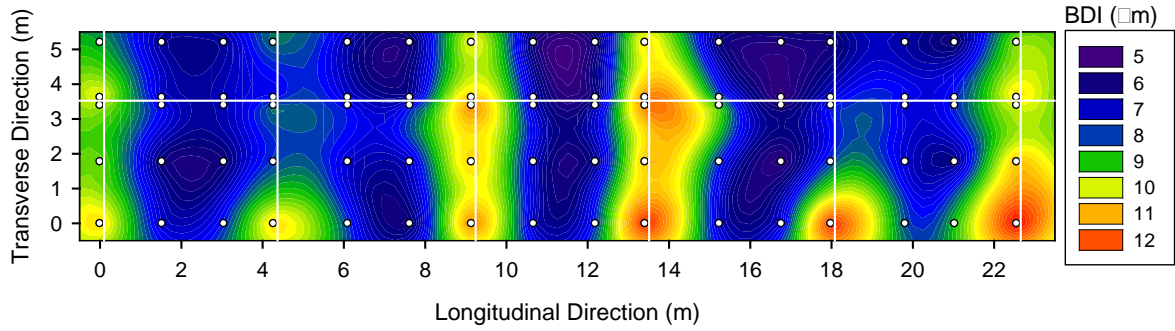
Figure 72. TB 7A: Kriged spatial contour map (top), measurements longitudinally along the test section (middle), histogram (bottom left), and semivariogram (bottom right) of BDI measurements [dense testing]
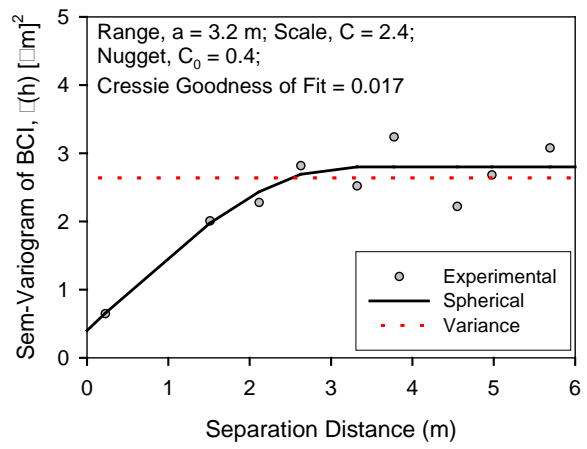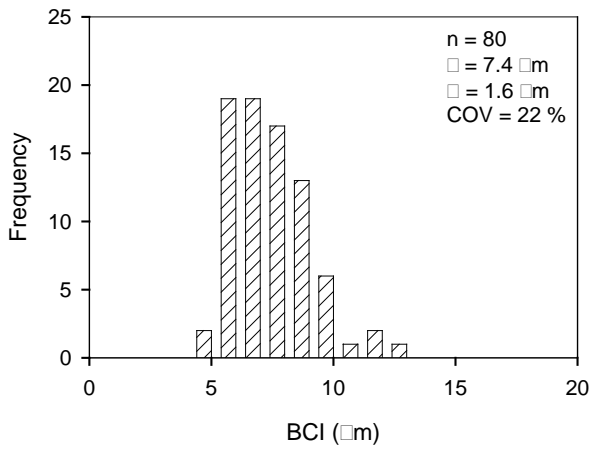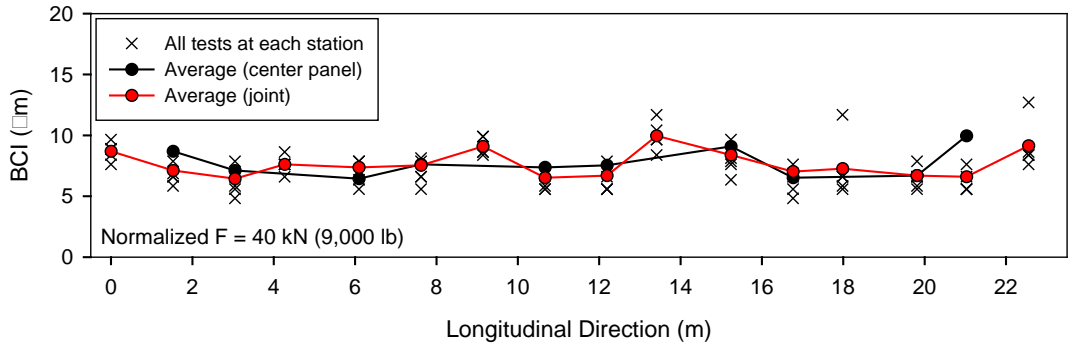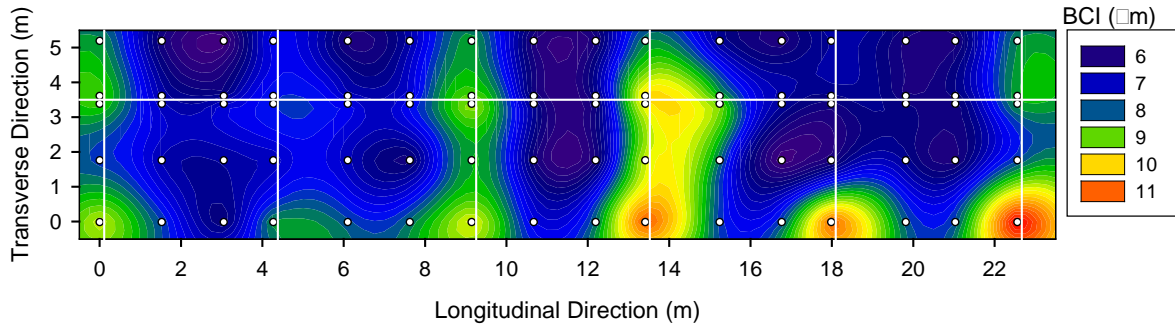
Figure 73. TB 7A: Kriged spatial contour map (top), measurements longitudinally along the test section (middle), histogram (bottom left), and semivariogram (bottom right) of BCI measurements [dense testing]
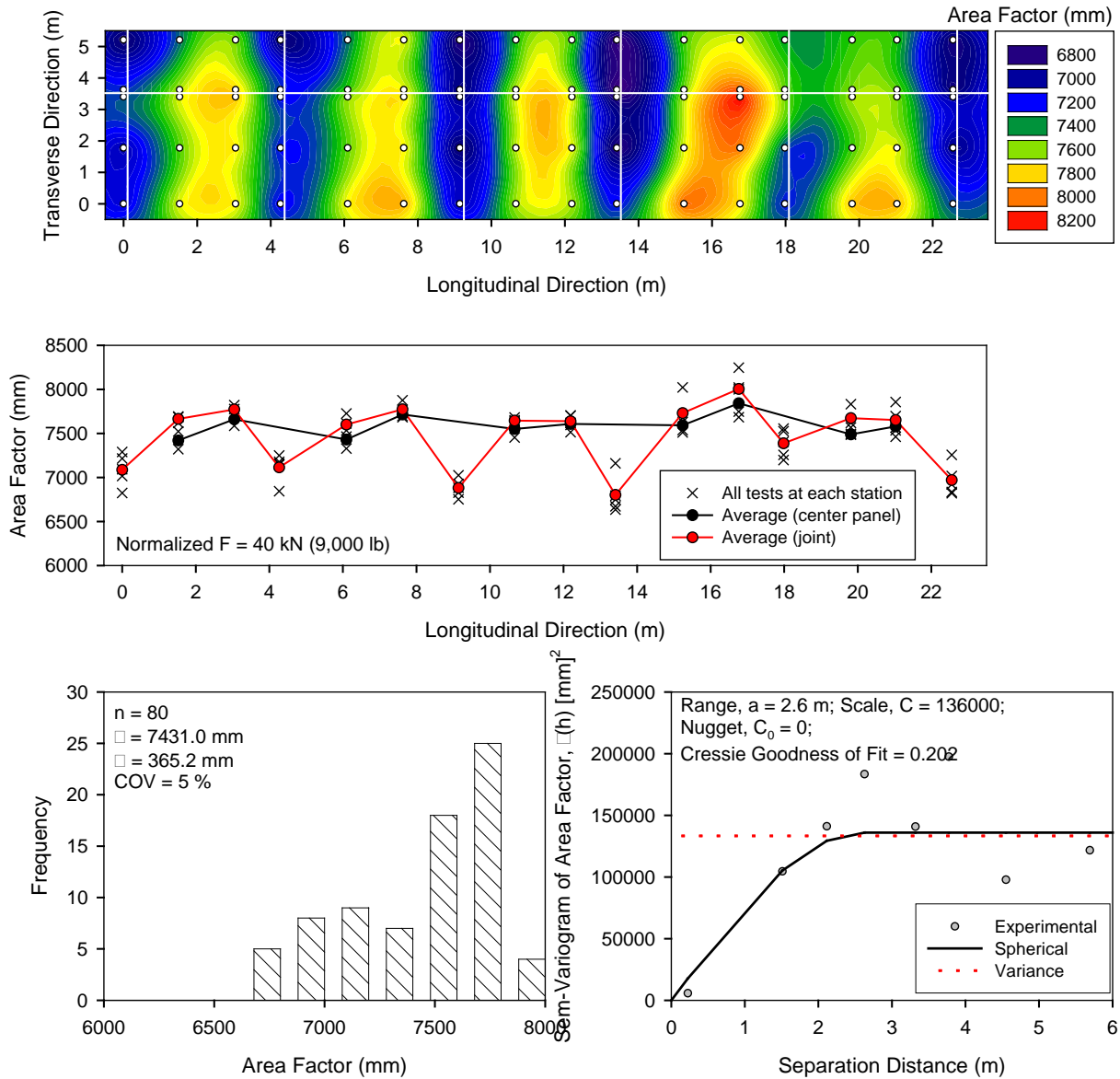
Figure 74. TB 7A: Kriged spatial contour map (top), measurements longitudinally along the test section (middle), histogram (bottom left), and semivariogram (bottom right) of Area Factor measurements [dense testing]
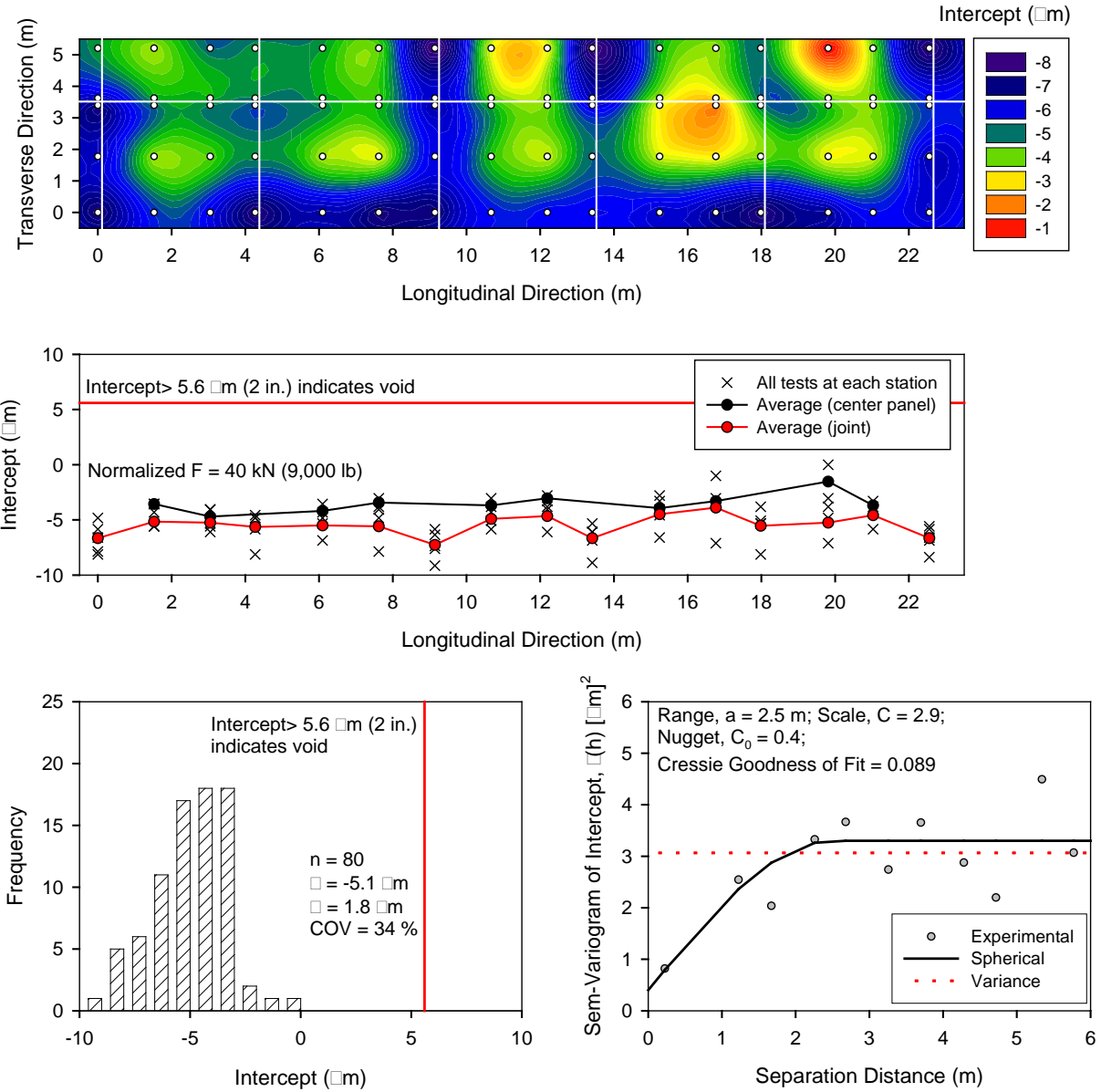
Figure 75. TB 7A: Kriged spatial contour map (top), measurements longitudinally along the test section (middle), histogram (bottom left), and semivariogram (bottom right) of Intercept measurements [dense testing]
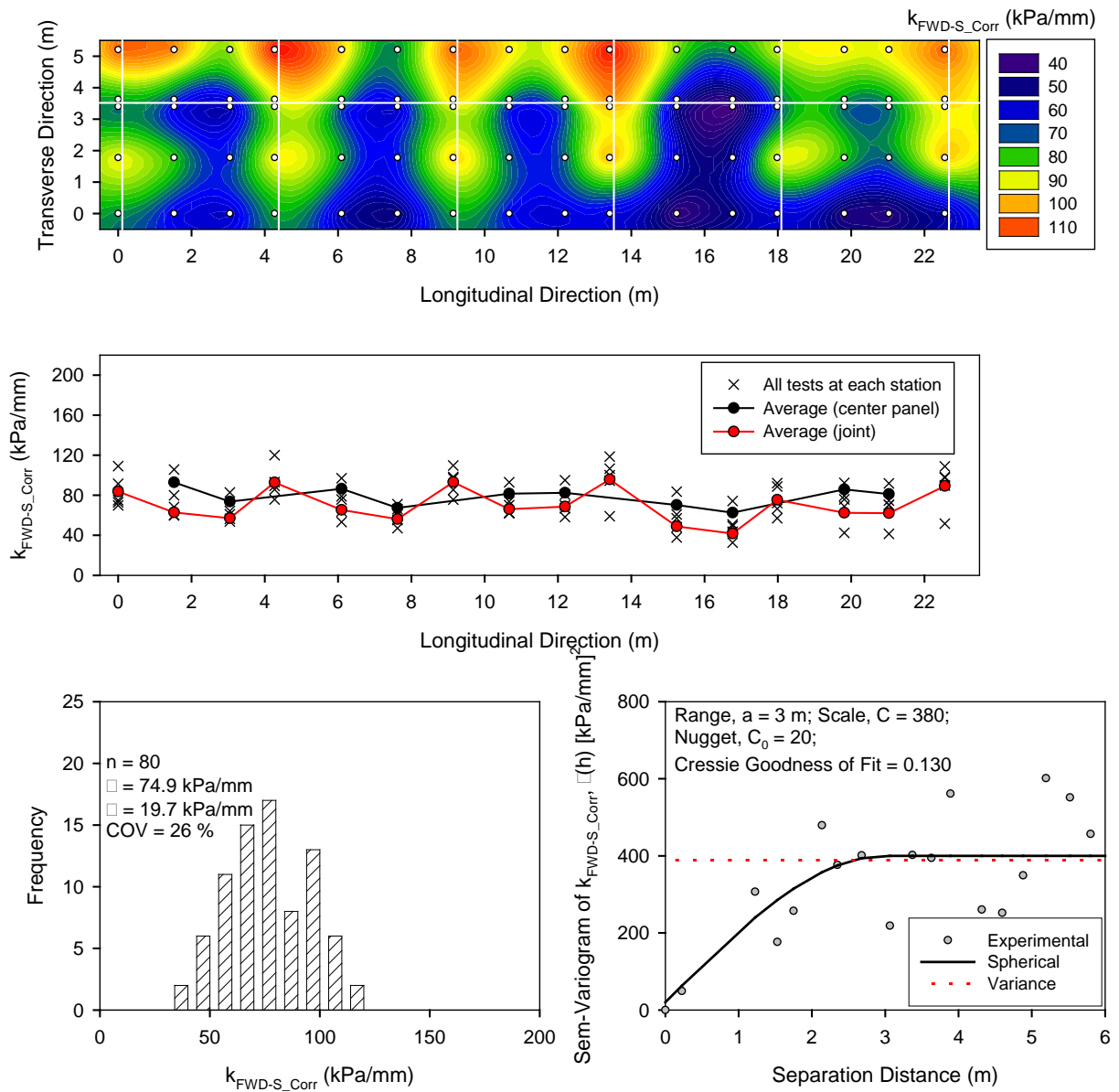
Figure 76. TB 7A: Kriged spatial contour map (top), measurements longitudinally along the test section (middle), histogram (bottom left), and semivariogram (bottom right) of k_FWD-S_Corr measurements [dense testing]
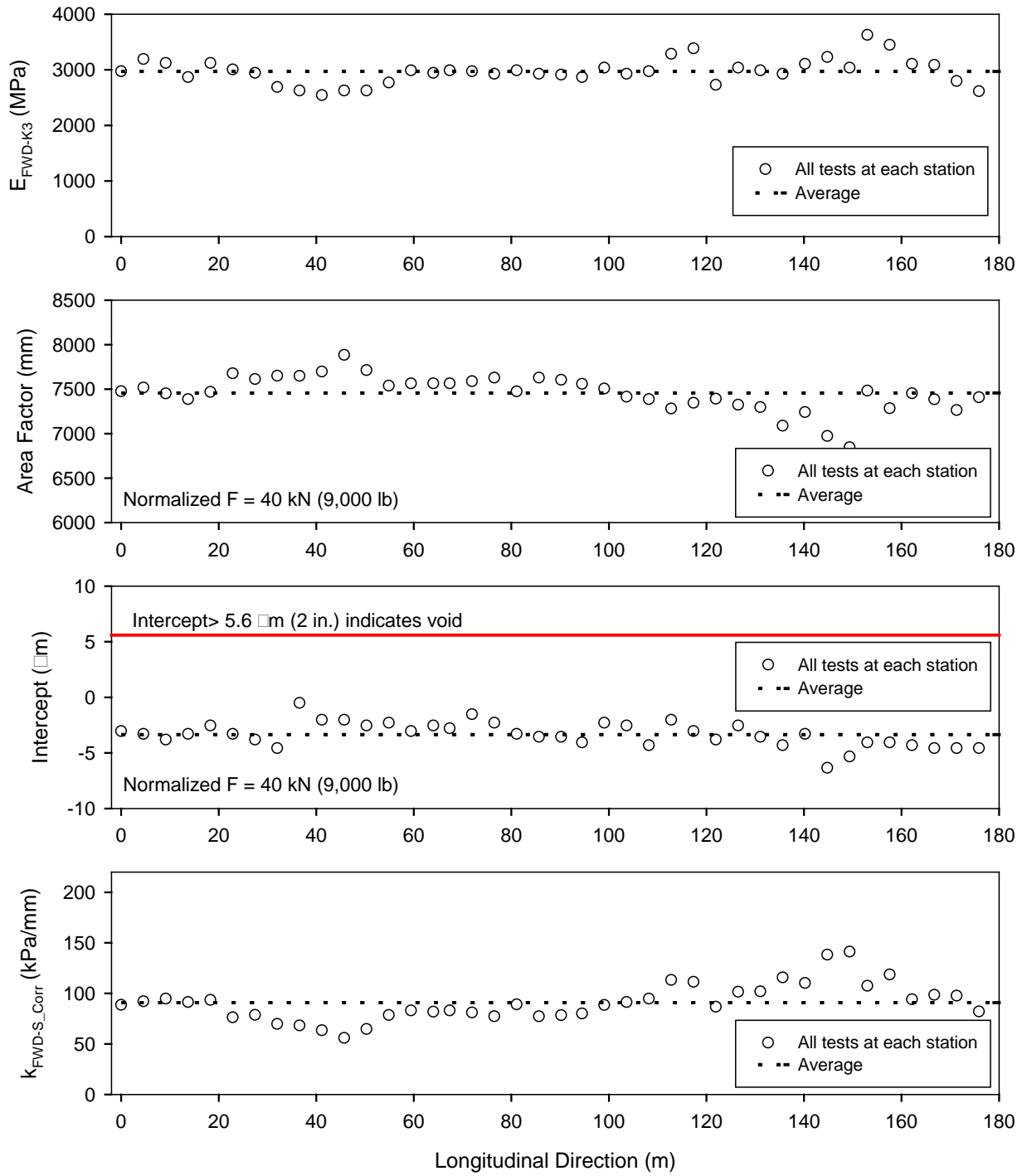
Figure 77. TB 7B: FWD tests results on PCC [mid panel testing]
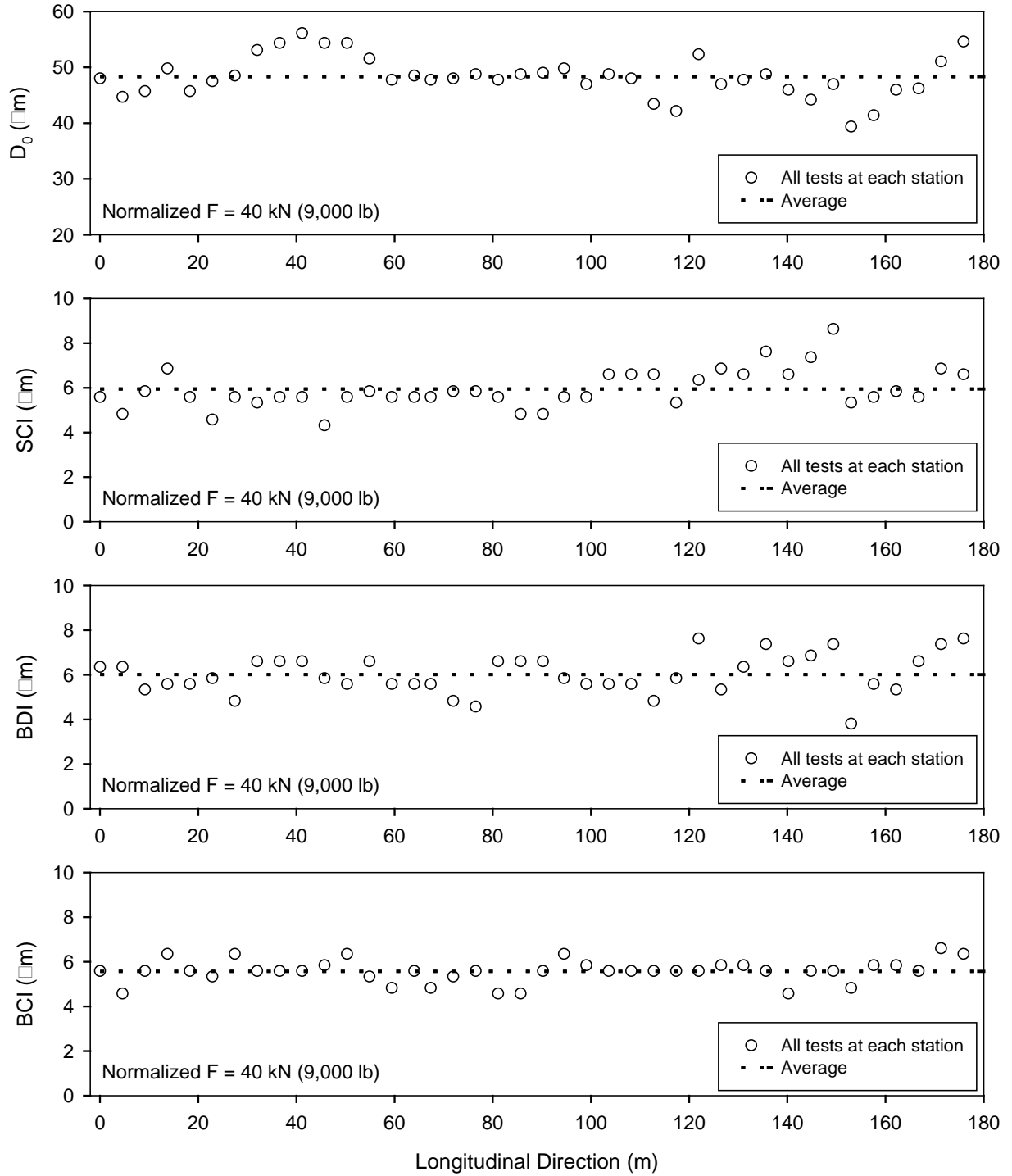
Figure 78. TB 7B: FWD tests results on PCC continue [mid panel testing]
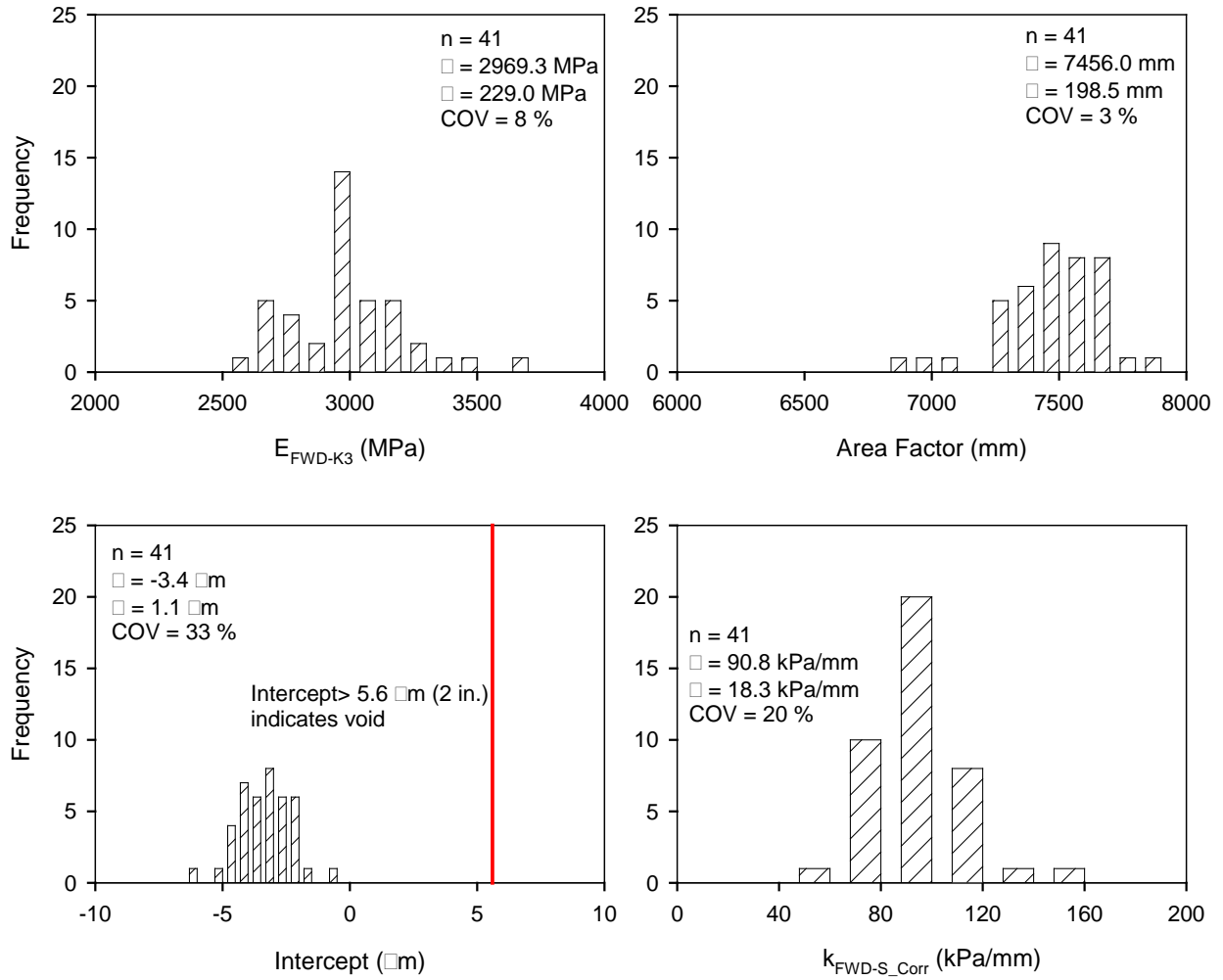
Figure 79. TB 7B: Histograms of FWD test measurements [mid panel testing]
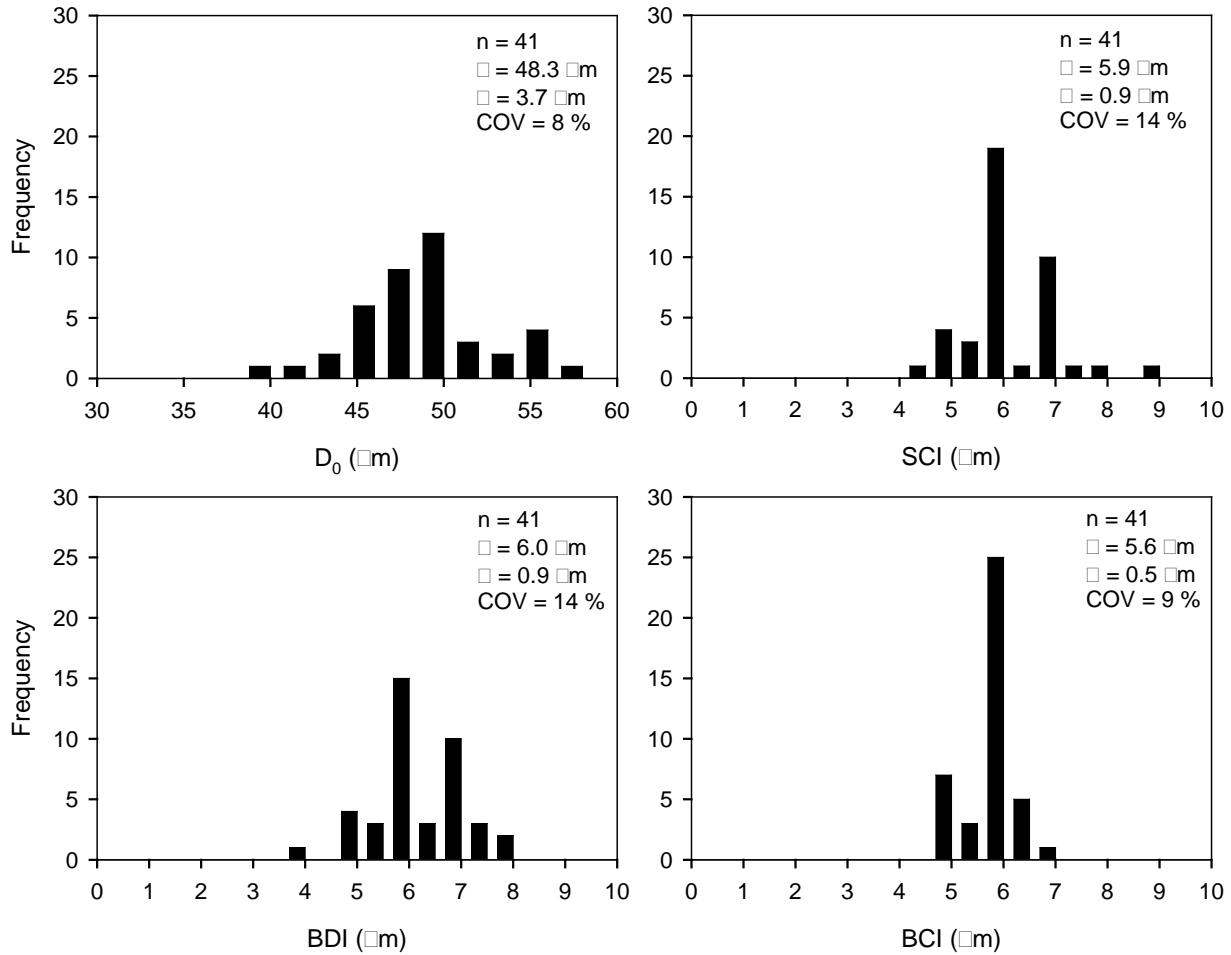
Figure 80. TB 7B: Histograms of FWD test measurements continue [mid panel testing]

Summary of In Situ Measurement Values and Comparison with Design Assumptions

A summary of all in situ measurement values and their univariate statistics are summarized in Table 7 for tests conducted on pavement foundation layers (CTB/ATB, subbase, rock cap, and general fill subgrade).

In the following sections, the average in situ test measurements are compared with design assumed values. A summary of the comparisons between the measured and the design assumed values is provided in Table 8.

Subgrade Resilient Modulus (E_{SG} or M_r)

The E_{SG} value assumed in the design was for the rock cap layer, which is referred to as subgrade treatment in the design. The direct measurements for moduli values on the rock cap layer were obtained from TBs 1, 2, and 5. TBs 1 and 2 consisted of a leveling subbase layer over the rock cap layer, but was considered as one layer, while TB 5 consisted of just the rock cap layer.

86

Average E_{SG} from TBs 1 and 2 from LWD and FWD measurements were 71.5 MPa and 120.2 MPa, which were lower than the design assumed E_{SG} of 206.8 MPa. Average E_{SG} from TB 5 from LWD and FWD measurements were 303.4 and 407.2 MPa, which were higher than the design assumed ESG of 206.8 MPa.

These results indicate that in TBs 1 and 2, the measured values were lower and in TB5 the measured values were higher than the design target value. Possible reasons for lower E_{SG} values in TBs 1 and 2 can be due to weaker general fill material, as evidenced in TB6 with average moduli of 18.1 MPa. It must be noted that LWD and FWD measurements provide a composite response of materials within its measurement influence depth ranging between 1.5 to 2 times the dimeter of the plate (450 to 600 mm depth).

Base Layer Elastic Modulus (E_{SB}):

The E_{SB} values for the CTB and ATB layers were back-calculated from the FWD deflection basin measurements. The average ESB for ATB and CTB were 721 and 4,467 MPa, which are 3.5 to 21.6 times higher than the design assumed E_{SB} of 206.8 MPa. It must be noted that the ATB layer tested in this study was placed one day prior to testing, while the CTB layer was placed several months prior to testing. Additional curing of the ATB material can potentially increase the moduli values of the layer.

Composite Modulus of Subgrade Reaction (k_{comp})

The k_{comp} values were estimated following the AASHTO (1993) procedure and using E_{SB} values back-calculated from FWD measurements for the CTB/ATB layer, E_{SG} values determined from LWD and FWD on the rock cap layer, and the thickness of the CTB/ATB.

For section with ATB, the estimated k_{comp} value ranged between 196.8 kPa/mm (based on LWD measurements for E_{SG}) and 282.3 kPa/mm (based on FWD measurements for E_{SG}) and were about 1.2 to 1.7 times lower than the design target k_{comp} of 340 kPa/mm. Again, it must be noted that additional curing of the ATB material can potentially increase the ESB values and the resulting k_{comp} values.

For section with CTB, the estimated k_{comp} value ranged between 252.4 kPa/mm (based on LWD measurements for E_{SG}) and 367.5 kPa/mm (based on FWD measurements for E_{SG}) and were about 1.3 times lower and 1.1 times higher than the design target k_{comp} of 340 kPa/mm.

Drainage Coefficient (C_d)

The C_d value assumed in design = 1.0, which represents that the quality of drainage is rated as "good". According to AASHTO (1993), if water is removed from the pavement system in one day, the quality of drainage is rated as "good". If water is removed within two hours, the quality of drainage is rated as "excellent".

Based on the pavement geometry (i.e., cross slope, width of the pavement, thickness of the base layer), the measured K_{sat} values from the field, and assuming an effective porosity = 0.3, time for a target 90% of drainage was calculated using "Pavement Drainage Estimator (PDE) Version 1.0)," an Excel-based Visual Basic program developed by Vennapusa (2004). A target of 90% drainage was selected in calculations.

Based on tests conducted on the CTB layer, the time for 90% drainage was estimated as 1.0 day for K_{sat} = 0.2 cm/s (CTB contaminated with fines) to < 1 hour for K_{sat} = 7 cm/s (CTB uncontaminated). Based on tests conducted on the ATB layer the time for 90% drainage was estimated < 1 hour for K_{sat} = 4.6 cm/s. Based on these estimates, the quality of drainage can be rated as "good" to "excellent" and does meet the design requirements.

Table 7. Summary of univariate statistics of in situ test results on pavement foundation layer materials

Measurement	n	μ	σ	COV (%)
TB1 Subbase over rock cap				
γ_d (kN/m^3)	44	21.44	0.50	2
w (%)	44	6.4	1.4	23
E_{LWD-Z3} (MPa)	81	82.9	25.4	31
E_{FWD-K3} (MPa)	80	129.9	38.5	30
TB2 Subbase over rock cap				
γ_d (kN/m^3)	32	22.04	0.70	3
w (%)	32	4.3	0.5	12
E_{LWD-Z3} (MPa)	31	41.6	26.1	63
E_{FWD-K3} (MPa)	32	96.1	57.1	59
K_{sat} (cm/s)	28	0.92	0.79	86
TB3 ATB & Subbase				
E_{FWD-K3} (MPa)	48	190.7	39.5	21
E_{SB} (MPa)	48	721.2	436.7	61
E_{SG} (uncorrected) (MPa)	48	156.8	49.3	31
K_{sat} (cm/s) ATB	99	4.6	1.9	42
K_{sat} (cm/s) Subbase	22	0.16	0.06	40
TB4A CTB				
γ_d (kN/m^3)	42	17.0	1.0	6
w (%)	42	5.5	1.1	21
E_{FWD-K3} (MPa)	41	153.3	43.2	28
E_{SB} (MPa)	41	4466.5	2299.3	51
E_{SG} (uncorrected) (MPa)	41	69.7	16.2	23
$E_{SG\_corrected}$ (MPa)	41	23.0	5.3	23
TB4B CTB				
K_{sat} (cm/s) Area A	49	7.0	3.1	45
K_{sat} (cm/s) Area B (Contaminated with fines)	23	0.20	0.20	101
TB5 Rock cap (Subgrade Treatment)				
E_{LWD-D3} (MPa)	44	303.4	158.6	52
E_{FWD-K3} (MPa)	44	407.2	147.5	36
TB6 General Subgrade Fill				
γ_d (kN/m^3)	21	17.53	0.61	3
w (%)	21	16.6	2.4	14
E_{LWD-Z3} (MPa)	21	18.1	11.8	65

Table 8. Summary of design, in situ measured, and laboratory measured values

Design Parameter	Design Value	In Situ Measurements (Average)
Subgrade M_r or E_{SG} (Rock Cap)	206.8 MPa (30 ksi)	LWD: 71.5 MPa (10.4 ksi)[1] FWD: 120.2 MPa (17.4 ksi)[1] --- LWD: 303.4 MPa (44.0 ksi)[2] FWD: 407.2 MPa (59.1 ksi)[2]
Subbase elastic modulus (E_{SB})	206.8 MPa (30 ksi)	ATB: 721.2 MPa (104.6 ksi)[3] CTB: 4466.5 MPa (647.8 ksi)[3]
Composite modulus of subgrade reaction, (k_{comp})	340 kPa/mm (1250 pci)	*Estimated from Individual Layer Measurements and AASHTO (1993) Procedure:* ATB: 196.8 kPa/mm (725 pci)[4] 282.3 kPa/mm (1040 pci)[5] CTB: 252.4 kPa/mm (930 pci)[4] 367.5 kPa/mm (1354 pci)[5]
C_d	1.0 (*Good*)	1.1 (*Excellent*)

[1]Average of all measurements obtained from TB1 and TB2 (51 mm 2A leveling stone over 457 mm rock cap); [2]Backcalculated from FWD measurements obtained from TB3 (ATB) or TB4A (CTB); [3]Empirically estimated from charts presented in AASHTO (1993) with average of E_{LWD-Z3} measurements from TBs 1 and 2; [4]Empirically estimated from charts presented in AASHTO (1993) with average of E_{FWD-K3} measurements from TBs 1 and 2.

CHAPTER 6. SUMMARY AND CONCLUSIONS

This report presents results and analysis from a field study conducted on SR-22 near Clyde in Indiana County, Pennsylvania. The project consisted of reconstruction of pavement foundation layers (subbase and subgrade) of the east and west bound lanes of the highway. The total length of the reconstruction project was about 7.74 km (4.81 miles).

The pavement foundation layers consisted of a minimum 457.2 mm (18 in.) thick rock cap that was placed and compacted on the subgrade and is referred to as subgrade treatment in the project plans. The subgrade beneath the rock cap consisted of general embankment fill consisted of rocky subgrade material obtained from cuts. A geosynthetic separation layer was installed at the subgrade rockcap interface. A 50.8 mm (2 in.) thick Class 2A levelling stone consisting of crushed limestone material was placed as granular leveling course layer over the rock cap. A minimum 76.2 mm (3 in.) thick asphalt treated base (ATB) or cement treated base (CTB) layer was installed over the granular subbase layer. A 254 mm (10 in.) thick new jointed PCC layer was installed over the CTB/ATB layer. The pavement section was designed in accordance with the *AASHTO design guide for design of pavement structures* (AASHTO 1993) rigid pavement design.

Field testing was conducted on seven test beds (TBs). Two test beds consisted of levelling stone subbase layer at the surface, and one test bed each consisted of PCC, CTB, ATB, rock cap layer, and general subgrade fill at the testing surface. Field testing involved FWD, Zorn and Dynatest LWD, NG, DCP, and APT point testing and IC measurements. The length of the test beds varied between 15 m to 620 m. Testing was conducted along the center line and along left and right of the center line with test point spacing of about 5 to 10 m. In addition, dense grid testing with test spacing between 1 and 4 m was also conducted to capture spatial variability of the measurement values over a small area. Geostatistical semivariogram analysis was performed to analyze the point test data from dense grid pattern testing to characterize and quantify spatial non-uniformity of the PCC surface and foundation layer properties.

Comparing measured properties from laboratory and in situ testing with the design assumed values revealed the following:

- Average subgrade layer moduli (ESG) was determined based testing on the rock cap layer from three TBs. Average E_{SG} from TBs 1 and 2 from LWD and FWD testing was 71.5 MPa and 120.2 MPa, respectively, which were lower than the design assumed E_{SG} of 206.8 MPa. Average E_{SG} from TB 5 from LWD and FWD measurements were 303.4 and 407.2 MPa, which were higher than the design assumed E_{SG} of 206.8 MPa. Possible reasons for lower E_{SG} values in TBs 1 and 2 can be due to weaker general fill material, as evidenced in TB6 with average moduli of 18.1 MPa. It must be noted that LWD and FWD measurements provide a composite response of materials within its measurement influence depth ranging between 1.5 to 2 times the dimeter of the plate (450 to 600 mm depth).

91

- Average subbase layer moduli (E_{SB}) values for the CTB and ATB layers were 721 and 4,467 MPa, which are 3.5 to 21.6 times higher than the design assumed E_{SB} of 206.8 MPa. It must be noted that the ATB layer tested in this study was placed one day prior to testing, while the CTB layer was placed several months prior to testing. Additional curing of the ATB material can potentially increase the moduli values of the layer.

- For section with ATB, the composite modulus of subgrade reaction (k_{comp}) values ranged between 196.8 kPa/mm (based on LWD measurements for E_{SG}) and 282.3 kPa/mm (based on FWD measurements for E_{SG}) and were about 1.2 to 1.7 times lower than the design target k_{comp} of 340 kPa/mm. Again, it must be noted that additional curing of the ATB material can potentially increase the E_{SB} values and the resulting k_{comp} values.

- For section with CTB, the estimated k_{comp} value ranged between 252.4 kPa/mm (based on LWD measurements for E_{SG}) and 367.5 kPa/mm (based on FWD measurements for E_{SG}) and were about 1.3 times lower and 1.1 times higher than the design target k_{comp} of 340 kPa/mm.

- The drainage coefficient (C_d) value was assumed in the design as 1.0, which represents that the quality of drainage is rated as "good". Based on the pavement geometry (i.e., cross slope, width of the pavement, thickness of the base layer), the measured K_{sat} values from the field, and assuming an effective porosity = 0.3, the time for a target 90% drainage was calculated. Based on APT tests conducted on the CTB layer, the time for 90% drainage was estimated as 1.0 day for $K_{sat} = 0.2$ cm/s (CTB contaminated with fines) to < 1 hour for $K_{sat} = 7$ cm/s (CTB uncontaminated). Based on tests conducted on the ATB layer the time for 90% drainage was estimated < 1 hour for $K_{sat} = 4.6$ cm/s. Based on these estimates, the quality of drainage can be rated as "good" to "excellent" and does meet the design requirements.

REFERENCES

AASHTO T-307. (1999). *Standard method of test for determining the resilient modulus of soils and aggregate materials*, American Association of State Highway and Transportation Officials AASHTO, Washington, DC.

AASHTO. (1993). *AASHTO Design Guide for Design of Pavement Structures*. American Association of State Highway and Transportation Officials, Washington D.C.

Andrei, D., M. W. Witczak, C. W. Schwartz, and J. Uzan. (2004). Harmonized resilient modulus test method for unbound pavement materials. *Transportation Research Record: Journal of the Transportation Research Board No. 1874*. Transportation Research Board, Washington, DC, 29-37.

ASTM C39/C39M-12. (2012). *Standard test method of compressive strength of cylindrical concrete specimens*. ASTM International, West Conshohocken, PA.

ASTM C117-04. (2010). *Standard test method for materials finer than 75μm (No. 200) sieve in mineral aggregates by washing*. American Standards for Testing Methods (ASTM), West Conshohocken, PA.

ASTM C136-06. (2010). *Standard test method for sieve analysis of fine and coarse aggregates*. ASTM International, West Conshohocken, PA.

ASTM D422-63. (2010). *Standard test method for particle-size analysis of soils*. ASTM International, West Conshohocken, PA.

ASTM D559-03. (2010). *Wetting and drying compacted soil-cement mixtures*. ASTM International, West Conshohocken, PA.

ASTM D560-03. (2010). *Freezing and thawing compacted soil-cement mixtures*. ASTM International, West Conshohocken, PA.

ASTM D698-07. (2010). *Standard test method for laboratory compaction characteristics of soil using standard effort 12,400 ft-lbf/ft^3 600 kN-m/m^3*. ASTM International, West Conshohocken, PA.

ASTM D854-14. (2014). *Standard test methods for specific gravity of soil solids by water pycnometer*. ASTM International, West Conshohocken, PA.

ASTM D1557-07. (2010). *Standard test method for laboratory compaction characteristics of soil using modified effort 56,000 ft-lbf/ft^3 2,700 kN-m/m^3*. ASTM International, West Conshohocken, PA.

ASTM D1883-07. (2010). *Standard test method for CBR (California Bearing Ratio) of laboratory-compacted soils*. ASTM International, West Conshohocken, PA.

ASTM D2487-10. (2010). *Standard test method for classification of soil for engineering purposes unified soil classification system*. ASTM International, West Conshohocken, PA.

ASTM D3282-09. (2010). *Standard test method for classification of soils and soil-aggregate mixtures for highway construction purposes*. ASTM International, West Conshohocken, PA.

ASTM D4253-00. (2010). *Standard test methods for maximum index density and unit weight of soils using a vibratory table*. ASTM International, West Conshohocken, PA.

ASTM D4254-00. (2010). *Standard test methods for minimum index density and unit weight of soils and calculation of relative density*. ASTM International, West Conshohocken, PA.

ASTM D4318-10. (2010). *Standard test methods for liquid limit, plastic limit, and plasticity index of soils*. ASTM International, West Conshohocken, PA.

ASTM D4694-09. (2010). *Standard test method for deflections with a falling-weight-type impulse load device*. American Standards for Testing Methods (ASTM), West Conshohocken, PA.

ASTM D5918-06. (2010). *Standard test methods for frost heave and thaw weakening susceptibility of soils*. American Standards for Testing Methods (ASTM), West Conshohocken, PA.

ASTM D6951-03. (2010). *Standard test method for use of the dynamic cone penetrometer in shallow pavement applications*. ASTM International, West Conshohocken, PA.

ASTM D6938-10. *Standard test method for in-place density and water content of soil and soil-aggregate by nuclear methods shallow depth*. ASTM International, West Conshohocken, PA.

Barenberg, E. J., and Petros, K. A. (1991). Evaluation of Concrete Pavements Using NDT Results, Illinois Highway Research Project IHR-512, University of Illinois and Illinois Department of Transportation, Report No. UILU-ENG-91-2006, IL.

Brandl, H., and D. Adam. (1997). "Sophisticated continuous compaction control of soils and granular materials." Proceedings of the 14th International Conference of Soil Mechanics and Foundation Engineering. Hamburg, Germany, 1-6.

Clark, I. and W. Harper. 2002. *Practical Geostatistics 2000*. 3rd reprint, Ecosse North America LLC, Columbus, OH.

Darter, M. I., Hall, K. T., and Kuo, C-M. (1995). Support under Portland Cement Concrete Pavements, NCHRP Report 372. Transportation Research Board, Washington, D.C.

ERES Consultants Inc. (1982). Techniques for Pavement Rehabilitation: A Training Course. U.S. Department of Transportation, FHWA, Washington, D.C.Floss, R., G. Bräu, M. Gahbauer, N. Gruber, and J. Obermayer. 1991). Dynamische Verdichtungsprüfung bei Erd-und Straßenbauten. *Prüfamt für Grundbau, Boden-und Felsmechanik Technische Universität München*, Heft 612, München, Germany in German).

Hoffman, M. S., and Thompson, M. R. (1981). Mechanistic Interpretation of Nondestructive Pavement Testing Deflections. Transportation Engineering Series No. 32, Illinois cooperative Highway and Transportation Research Series No. 190. University of Illinois at Urbana-Champaign, Champaign, IL.

Horak, E. (1987). "Aspects of deflection basin parameters used in a mechanistic rehabilitation design procedure for flexible pavements in South Africa." University of Pretoria, South Africa.

Ioannides, A. M. (1990). "Dimensional analysis in NDT rigid pavement evaluation." Transportation Engineering Journal, ASCE, Vol. 116, No. TE1.

Isaaks, E. H. and R. M. Srivastava. (1989). *An Introduction to Applied Geostatistics*. Oxford University Press, New York.

Janssen, D. J., and Snyder, M. B. (2000). "Temperature-moment concept for evaluating pavement temperature data." *Journal of Infrastructure Systems*, 6(2), 81–83.

Kilareski, W. P., and Anani, B. A. (1982). "Evaluation of in situ moduli and pavement life from deflection basins." *Presented at the 5th International Conference of Asphalt Pavements*, University of Michigan, Ann Arbor, MI.

NCHRP 1-28A. (2002). *Recommended standard method for routine resilient modulus testing of unbound granular base/subgrade materials and subgrade soils–NCHRP protocol 1-28A,* National Cooperative Highway Research Program.

Quintus, V. H. L., and A. L. Simpson. (2002). *Backcalculation of Layer Parameters for LTPP Test Sections, Volume II: Layered Elastic Analysis for Flexible and Rigid Pavements, Research Report, Long-Term Pavement Performance Program*, Report No. FHWA-RD-01-113, Federal Highway Administration, Washington, DC, October 2002.

Samaras, A. A., R. Lamm, and J. Treiterer. (1991). Application of continuous dynamic compaction control for earthworks in railroad construction. *Transportation Research Record: Journal of the Transportation Research Board.* No. 1309, Transportation Research Board of the National Academies, Washington, DC, 42-46.

Sandström, Å. (1994). *Numerical simulation of a vibratory roller on cohesionless soil*. Internal Report, Geodynamik, Stockholm, Sweden.

Sandström Å., and C. B. Pettersson. (2004). Intelligent systems for QA/QC in soil compaction, *Proceedings of the TRB 2004 Annual Meeting* (CD-ROM), Transportation Research Board, Washington, D.C.

Schmalzer, P. N. (2006). LTPP Manual for Falling Weight Deflectometer Measurements, Version 4.1. Final Report, FHWA-HRT-06-132. Federal Highway Administration.

Smith, K. D., Wade, M. J., Bruinsma, J. E., Chatti, K., Vandenbossche, J. M., Yu, H. T., Hoerner, T. E., Tayabji, S. D. (2007). Using Falling Weight Deflectometer Data with Mechanistic-Empirical Design and Analysis, Draft Interim Report, DTFH61-06-C-0046, Federal Highway Administration, Washington, D.C.

Substad, R. N. (2002). "LTPP data analysis: Feasibility of using FWD deflection data to characterize pavement construction quality." NCHRP Web Document 52, Project No. 20-50(9), National Cooperative Highway Research Program, Transportation Research Board of the National Academies, Washington, D.C.

Thompson, M., and D. White. (2008). "Estimating compaction of cohesive soils from machine drive power." *Journal of Geotechnical and Geoenvironmental Engineering*, ASCE, 134(12), 1771–1777.

Trimble Navigation Ltd. (2013). Trimble S3 Total Station Datasheet. Retrieved December 12, 2013, < http://trl.trimble.com/docushare/dsweb/Get/Document-469042/022543-492A_TrimbleS3_DS_0110_sec.pdf > (Date accessed 8/6/2015).

Ullidtz, P. (1987). *Pavement analysis. Developments in civil engineering*, 19. 318 p. Elsevier, Amsterdam.

Vandenbossche, J. M. (2005). Effects of slab temperature profiles on the use of falling weight deflectometer data to monitor joint performance and detect voids. *Transportation Research Record: Journal of the Transportation Research Board*, 2005, Washington, D.C., 75–85.

Vennapusa, P. (2004). *Determination of the Optimum Base Characteristics for Pavements*. Master's Thesis, Department of Civil Construction and Environmental Engineering, Iowa State University, Ames, Iowa.

Vennapusa, P., and D. J. White. (2009). Comparison of light weight deflectometer measurements for pavement foundation materials. *Geotechnical Testing Journal*, ASTM, 323, 239–251.

Vennapusa, P., D. J. White, and M. Morris. (2010). Geostatistical analysis of spatial referenced roller-integrated compaction measurements. *Journal of Geotechnical and Geoenvironmental Engineering*, ASCE, 1366, 813–822.

Vennapusa, P., D. J. White, and H. Gieselman. (2009). Influence of support conditions on roller-integrated machine drive power measurements for granular base. International Foundation Congress and Equipment Exposition 2009 (IFCEE 09). March 15-19, Orlando, FL.

White, D.J., Vennapusa, P. (2014). "Optimizing pavement base, subbase, and subgrade layers for cost and performance of local roads." *Final Field Data Report IHRB Project TR-640,* Iowa State University, Ames, Iowa.

White, D. J., and M. Thompson. (2008). Relationships between in situ and roller-integrated compaction measurements for granular soils. *Journal of Geotechnical and Geoenvironmental Engineering*, ASCE, 134(2), 1763-1770.

White, D., P. Vennapusa, and L. Zhao. (2014). Verification and repeatability analysis of the in situ air permeameter test. *Geotechnical Testing Journal*, 37(2), DOI: 10.1520/GTJ20130111.

White, D. J., E. Jaselskis, V. Schaefer, and T. Cackler. (2005). Real-time compaction monitoring in cohesive soils from machine response. *Transportation Research Record: Journal of the Transportation Research Board No. 1936*, Washington DC, 173–180.

Witczak, M. W. and J. Uzan. (1988). *The universal airport design system–Report I of IV: Granular material characterization*. Department of Civil Engineering, University of Maryland, College Park, MD.

Zorn, G. (2003). *Operating Manual: Light Drop-weight Tester ZFG2000*, Zorn Stendal, Germany.

APPENDIX: 1993 AASHTO RIGID PAVEMENT DESIGN CRITERIA

1993 AASHTO Pavement Design

DARWin Pavement Design and Analysis System

A Proprietary AASHTOWare
Computer Software Product

Rigid Structural Design Module

SR 0022 Section 494 (CLYDE)   ECMS NO. 25833
West & East Wheatfield Township
Indiana County
STA. 311+00.00 TO 577+00.00 LENGTH 25,600 FT 4.848 MI.
SEG./OFF. 0160/0315 TO 0270/1350

Construction Season 2008 to 2009

Rigid Structural Design

Pavement Type	JPCP
18-kip ESALs Over Initial Performance Period	12,822,405
Initial Serviceability	4.5
Terminal Serviceability	3
28-day Mean PCC Modulus of Rupture	631 psi
28-day Mean Elastic Modulus of Slab	4,000,000 psi
Mean Effective k-value	526 psi/in
Reliability Level	95 %
Overall Standard Deviation	0.35
Load Transfer Coefficient, J	2.7
Overall Drainage Coefficient, Cd	1
Calculated Design Thickness	9.91 in

Effective Modulus of Subgrade Reaction

Period	Description	Roadbed Soil Resilient Modulus (psi)	Base Elastic Modulus (psi)
1	summer	30,000	30,000
2	fall	30,000	30,000
3	winter	30,000	50,000
4	spring	30,000	15,000

Base Type	3" min. ATPBC on 18" Rock Cap (sandstone)
Base Thickness	18 in
Depth to Bedrock	15 ft
Projected Slab Thickness	10 in
Loss of Support Category	0.75
Effective Modulus of Subgrade Reaction	526 psi/in

Rigorous ESAL Calculation

Performance Period (years)	20
Two-Way Traffic (ADT)	11,540

Page 1

97